REPORT CDOT-2022-11 Dec 2022

Development of Tub Girders for Prestressed Concrete Bridges Complying with LRFD

APPLIED RESEARCH & INNOVATION BRANCH

Yail Jimmy Kim

COLORADO
Department of Transportation

The contents of this report reflect the views of the author(s), who is(are) responsible for the facts and accuracy of the data presented herein. The contents do not necessarily reflect the official views of the Colorado Department of Transportation or the Federal Highway Administration. This report does not constitute a standard, specification, or regulation.

Technical Report Documentation Page

1. Report No.	2. Government Accession No.	3. Recipient's Catalog No.
CDOT-2022-11		

4. Title and Subtitle	5. Report Date
Development of Tub Girders for Prestressed Concrete Bridges Complying with LRFD	Dec. 2022
	6. Performing Organization Code
7. Author(s)	8. Performing Organization Report No.
Yail Jimmy Kim	CDOT-2022-11
9. Performing Organization Name and Address	10. Work Unit No. (TRAIS)
University of Colorado Denver 1200 Larimer St., Denver, CO 80217	11. Contract or Grant No.
12. Sponsoring Agency Name and Address	13. Type of Report and Period Covered
Colorado Department of Transportation - Research 2829 W. Howard Pl. Denver, CO 80204	14. Sponsoring Agency Code

15. Supplementary Notes

Prepared in cooperation with the US Department of Transportation, Federal Highway Administration

16. Abstract

This report presents the development of tub girders for prestressed concrete bridges complying with the Load and Resistance Factor Design (LRFD) method. In addition, the use of 0.7 in. strands is elaborated for the B618-U girders of the Colorado Department of Transportation. In the first part of the report as regards a state-of-the-art review, technical parameters are categorized in accordance with physical characteristics and corresponding contents are examined. The second part of the report suggests a new tub girder series. After understanding the performance of tub girders selected from six transportation agencies in the nation, an optimization algorithm is employed to generate efficient prototype sections. Afterward, detailed investigations are conducted to appraise various practical aspects. A simplified version of the prototype sections is also delineated for regional precasters. A comparative study is carried out to evaluate the geometric stability and production costs of the prototype, simplified, and existing B618-U girders.

Implementation

A new tub girder series is proposed to improve structural efficiency and the potential implementation of 0.7 in. strands is discussed for bridge construction in Colorado.

17. Keywords	18. Distribution Statement
bridges; development; load and resistance factor design; prestressed concrete; review; structural efficiency; tub girder	This document is available on CDOT's website http://www.coloradodot.info/programs/research/pdfs

19. Security Classif. (of this report)	20. Security Classif. (of this page)	21. No. of Pages	22. Price
Unclassified	Unclassified		

ACKNOWLEDGMENTS

The research team would like to acknowledge valuable guidance and thought-provoking comments provided by the study panel members: Trever Wang (Staff Bridge, CDOT), Brandon Field (Staff Bridge, CDOT), Andrew Pott (Staff Bridge, CDOT), Jacob O'Brien (Staff Bridge, CDOT), and Spencer Tucker (Federal Highway Administration). The research team is also grateful to Thien Tran (Applied Research and Innovation Branch, CDOT) for his comprehensive support and administrative assistance.

Executive Summary

This report presents three major aspects that are related to the development of tub girders for prestressed concrete bridges complying with the Load and Resistance Factor Design (LRFD) method: i) a literature review, ii) an assessment of existing and proposed girders, and iii) parametric investigations. In addition, the use of 0.7 in. strands is elaborated for the B618-U girders of the Colorado Department of Transportation. The first part of the report deals with a state-of-the-art review of prestressed concrete tub girders for bridge structures. Technical parameters are categorized in accordance with physical characteristics and corresponding contents are examined. Unlike the case of box girders, the open-section tub girders demand secondary structural elements to improve stability. As far as application is concerned, pre- and post-tensioning methods are taken into account with a focus on the implications of geometric variables, on-site splice, and applied forces. The applicability of existing design provisions is evaluated in the context of live load distributions and end zone cracking. While the strand size of 0.5 in. and 0.6 in. is dominant in the United States, research has commenced on the use of 0.7 in. strands to accommodate a high level of prestressing force. The effectiveness of precast decking panels is elaborated against conventional cast-in-place decks, and the extension of overhangs is discussed. The second part of the report explores the development of a new tub girder series for Colorado, conforming to the articles of the American Association of State Highway and Transportation Officials (AASHTO) Load and Resistance Factor Design (LRFD) Bridge Design Specifications (BDS). Although the B618-U girders developed by the Colorado Department of Transportation in the 1990s have been successfully used for decades, the need for an upgrade is essential to satisfy the requirements of contemporary bridge design and construction. After examining the performance of tub girders selected from six transportation agencies in the nation, an optimization algorithm is employed to generate efficient prototype sections. Then, detailed investigations are conducted to examine various practical aspects concerning the serviceability and ultimate limit states of AASHTO LRFD BDS. Parametric analysis with five bridge superstructures that accommodate up to four traffic lanes demonstrates the applicability of the prototype girders. A simplified version of the prototype sections is also delineated for regional precasters. Furthermore, a comparative study is carried out to evaluate the geometric stability and production costs of the prototype, simplified, and existing B618-U girders.

Implementable Outcomes: The research suggests a new tub girder series demonstrating better performance relative to the existing B618-U girders, particularly with improved structural efficiency. Considering practical implementation, a variable web thickness ranging from 5 in. to 10 in. is provided so that both pre- and post-tensioning applications are covered. Additionally, the use of 0.7 in. strands is dealt with for CDOT to prepare a transition of prestressed concrete technologies in Colorado.

Keywords: bridges; development; load and resistance factor design; prestressed concrete; review; structural efficiency; tub girder

List of Tables

List of Figures

Table of Contents

1. Literature Review

1.1. Introduction

Prestressed concrete girders are one of the primary structural components in highway bridges. Benefits of using precast members include accelerated construction time, favorable life-cycle expense, affordable maintenance and repair, quality control, aesthetics, and minimal disruption to traffic (Nawy 2006; Baker et al. 2018). From a functionality perspective, such bridge configurations enable a long span with durable performance and improved serviceability relative to conventional reinforced concrete members.

Prestressed girders were initially constructed in an I-shape; however, the requirements for many girders and aesthetically unpleasant layouts brought about the development of a new girder type (Ralls et al. 1993). Furthermore, state Departments of Transportation (DOTs) preferred to reduce the number of girders for economic reasons and, as a result, tub girders (also known as U-shaped girders) became a strong alternative, as schematically explained in Fig. 1; because one tub girder can replace two I-beams, cost-saving is expected (e.g., fabrication, formwork, in-situ labor, and transport).

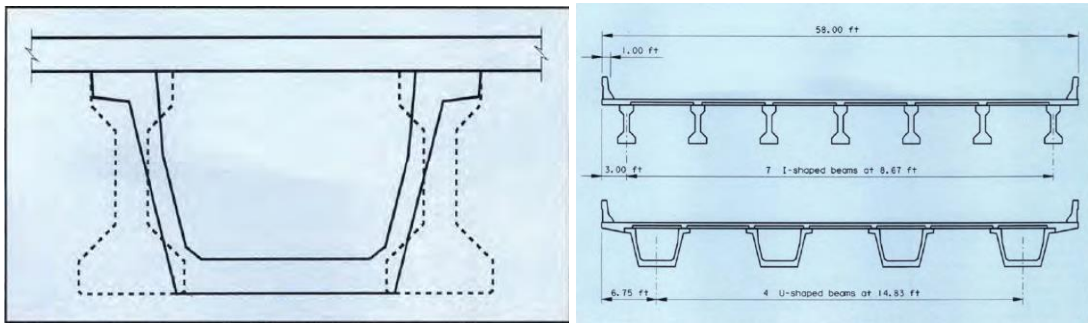

Fig. 1. Conceptual placement of prestressed concrete girders (Ralls et al. 1993)

Since the construction of the I-270 Bridge over I-76 in the 1990's, tub girders became a major girder type in Colorado (Saindon and McMullen 2010). Local precasters can fabricate and produce various sizes of tub girders at competitive cost. From 1995 to 2000, the Colorado Department of Transportation (CDOT) spent resources to develop the B618-U series for pretensioning and post-tensioning applications with a web thickness of 5 in. and 7.5 in., respectively. The B618-U girders, varying from 48 in. to 96 in. in depth, offer many advantages against closed-box girders in terms of fabrication process, flexible use of top flanges, and shipping weight.

Despite the above-mentioned competency, CDOT's tub girders are outdated. Given the noticeable advances in modern technologies, it is doubtful whether Colorado's bridge design is optimally conducted. In other words, structurally inefficient sections may be chosen at the design stage, which necessitate additional dollars. This research aims to develop a new LRFD-based tub girder series for bridge construction in Colorado with improved constructability, structural performance, and cost-effectiveness.

To better understand the state of the art of tub girders, a comprehensive literature review is conducted with an emphasis on geometric configurations and strand details, assessments on existing girders, prestressing methods, splice, decking, overhangs, live load distributions, and end-zone behavior.

1.2. Geometric Configuration of Tub Girders

It is recognized that geometric details control the performance of constructed girders. To provide adequate flexural and shear capacities, several factors need to be considered (e.g., girder height, web thickness, and number of prestressing strands). A tub girder is generally composed of a bottom flange and inclined webs plus short top flanges (Fig. 2). Tub girders need drainage holes to allow for the flow of internal water and cast-in-place concrete for a closure should have a compressive strength of 5 ksi or higher (Baker et al. 2018).

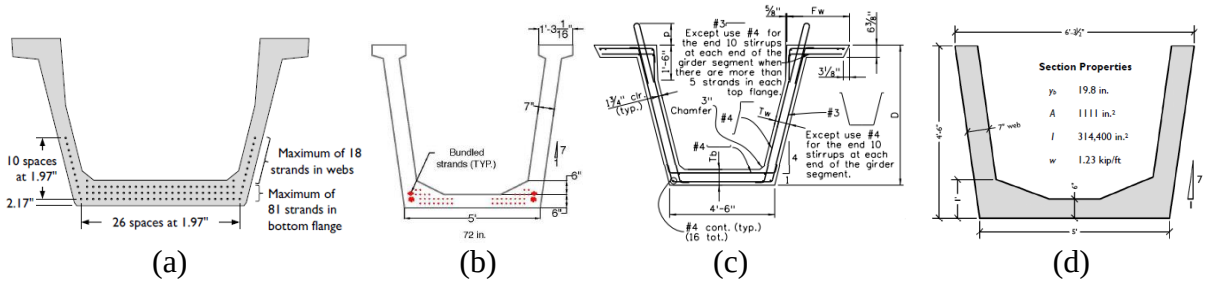

Fig. 2. Selected tub girder sections: (a) Texas U54; (b) Washington UF72G5; (c) Colorado B618-U; (d) Washington trapezoidal

Tub girders save forming costs, compared with closed box girders, and segmental construction can be implemented for both pretensioned and post-tensioned superstructures at variable web thickness (5 in. to 10 in.). Typically, the web thickness of a tub girder is determined by shear and prestressing forces (Saindon and McMullen 2010). It is also expected that a reduction in web thickness increases the girder depth to compensate for its flexural rigidity. Multiple diaphragms may be placed at both ends and the middle of a tub girder (Huang and Shahway 2005), as shown in Fig. 3, to resist local torsion and relieve stress concentrations. One large or two small neoprene pads can be placed underneath a tub girder at the location of piers.

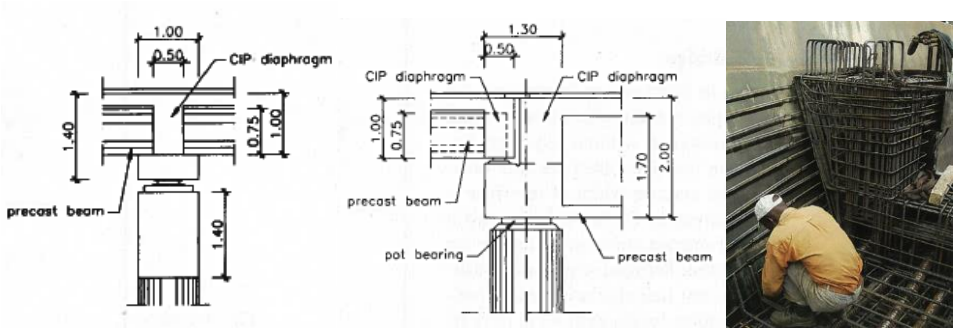

Fig. 3. Cast-in-place diaphragms for tub-girders and reinforcing details (Cruz and Wisniewski 2004)

The use of end blocks lowers tensile stress in the transverse direction (Sarles and Itani 1984), which is beneficial in reducing the likelihood of premature cracking; however, the blocks generate curing heat and delayed ettringite formation (Dunkman 2009). For skewed tub girders, a couple of end block options are available (Fig. 4)

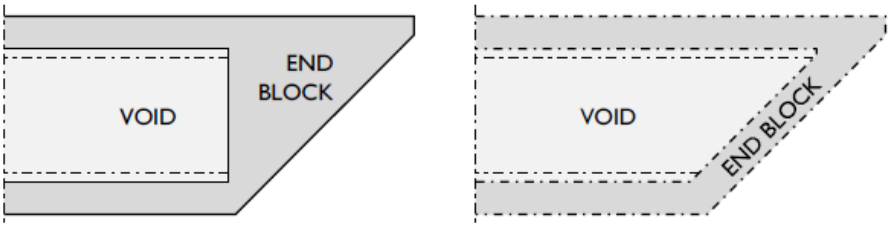

Fig. 4. End block options for tub girders (TxDOT 2006)

The prestressed concrete community adopts the following structural efficiency factor (Eq. 1) and efficiency ratio (Eq. 2) to evaluate the geometry of a girder section (Rabbat and Russell 1982):

$$\rho = \frac{r^2}{y_t y_b} \tag{1}$$

$$\alpha = \frac{3.46 S_b}{Ah} \tag{2}$$

where ρ and α are the structural efficiency factor and ratio, respectively; r is the radius of gyration of the girder; y_t and y_b are the distances from the centroid of the girder section to the top and bottom fibers, respectively; S_b is the section modulus for the bottom fiber; and A and h are the cross-sectional area and depth of the girder, respectively.

The B618-U girders employed in Colorado have variable depths (48, 60, 72, 84, and 96 in.) with web thicknesses of 5, 7.5, and 10 in. and bottom flange thicknesses of 6.35 and 8.1 in. In practice, a bridge system with twin tub girders is often constructed at a deck width varying from 33 ft to 47 ft with a girder spacing between 12 ft and 26 ft on center (Saindon and McMullen 2010).

The geometry of tub girders is relevant for handling and erection, whereas, when curved girders are transported and erected, stability may be of concern due to a lack of torsional resistance. Installing steel bracings or diaphragms can help increase the torsional stiffness of the open section (Alawneh et al. 2016); particularly, end blocks enhance force distributions (Dunkman 2009).

1.3. Tub Girders Employed in the Nation

Shown in Fig. 5 are assorted tub girder sections used in the nation. These girders possess a typical depth of 40 in. to 96 in. with a variety of upper flange sizes. Both pretensioning and post-tensioning applications are available.

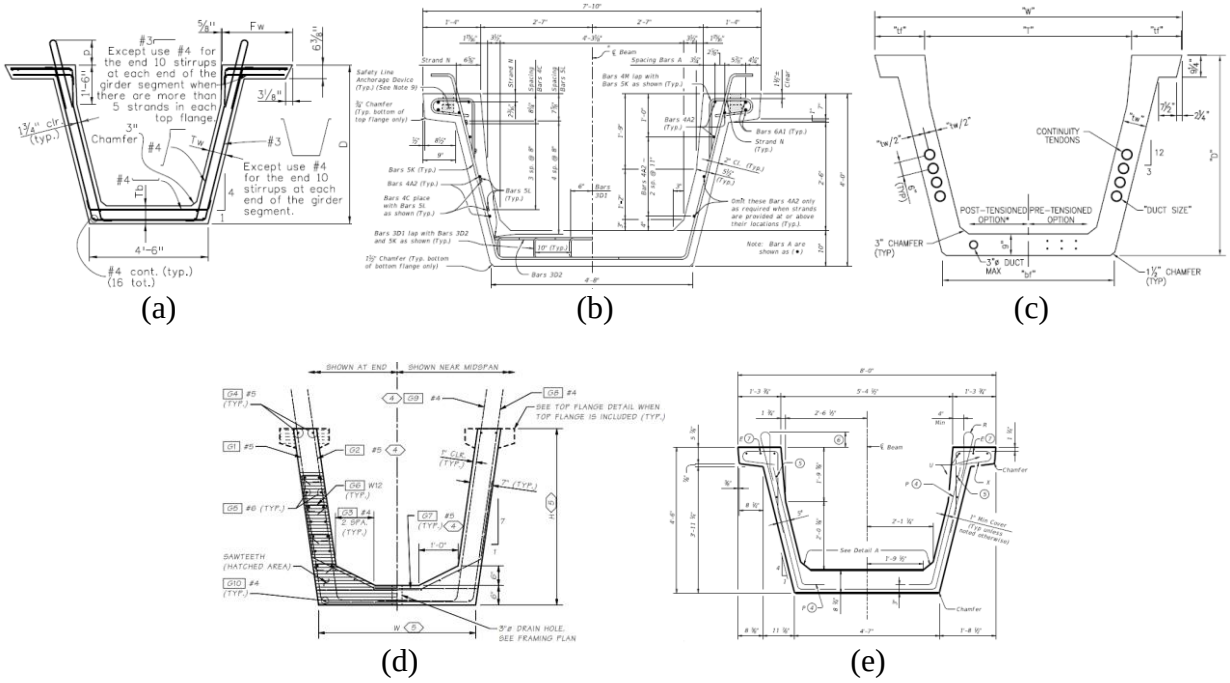

Fig. 5. Prestressed concrete tub girders: (a) Colorado; (b) Florida; (c) PCI; (d) Washington; (e) Texas

Table 1 enumerates the sectional properties of selected tub girders. Even though the cross-sectional area and moment of inertia of the girders noticeably change with depth, their radii of gyration are relatively stable ($16.32 \leq r \leq 32.65$). This fact implies that optimal properties exist in tub girders and structurally efficient sections can be proposed in compliance with AASHTO LRFD BDS (AASHTO 2020).

Table 1. Properties of tub girders

State/ agency	ID	Depth (in.)	Area (in.^{2})	Inertia (in.^{4})	y_t (in.)	y_b (in.)	S_t (in.^{3})	S_b (in.^{3})	R (in.)
CA	UB 1400	55	1,339	460,080	31	24	14,832	19,098	18.54
	UB 1550	61	1,435	604,231	34	27	17,699	22,479	20.52
	UB 1700	67	1,531	773,127	37	30	20,772	26,022	22.47
	UB 1850	73	1,627	968,691	40	33	24,055	29,751	24.40
	UB 2000	79	1,723	1,192,605	43	35	27,511	33,708	26.31
	UB 2150	85	1,819	1,446,551	46	38	31,176	37,818	28.20
CO	U48	48	1,399	409,606	24	24	16,974	17,161	17.11
	U60	60	1,584	726,035	30	30	24,055	24,349	21.41
	U72	72	1,770	1,157,722	36	36	31,964	32,356	25.58
	U84	84	1,955	1,716,209	42	42	40,621	41,106	29.63
FL	FU48	48	1,206	321,222	29	19	11,259	16,498	16.32
	FU54	54	1,275	439,370	32	22	13,735	19,962	18.56
	FU63	63	1,377	659,103	37	26	17,775	25,428	21.88
	FU72	72	1,479	933,707	42	30	22,184	31,217	25.13
PCI	PCI72_9	72	2,032	1,242,461	40	32	31,132	38,718	24.73
	PCI84_9	84	2,260	1,862,691	46	38	40,327	49,265	28.71
	PCI96_9	96	2,482	2,645,338	52	44	50,474	60,687	32.65
	PCI72_10	72	2,185	1,312,653	40	32	33,223	40,402	24.51
	PCI84_10	84	2,432	1,972,138	46	38	43,116	51,546	28.48
	PCI96_10	96	2,680	2,806,535	52	44	54,045	63,684	32.36
TX	U 40	40	980	183,107	24	16	7,723	11,240	13.67
	U 54	54	1,120	403,020	32	22	12,734	18,032	18.97
	U72_9	72	2,037	1,242,461	40	32	31,132	38,718	24.70
	U84_9	84	2,260	1,862,691	46	38	40,327	49,265	28.71
	U96_9	96	2,482	2,645,338	52	44	50,474	60,687	32.65
	U72_10	72	2,185	1,312,653	40	32	33,223	40,402	24.51
	U84_10	84	2,432	1,972,138	46	38	43,116	51,546	28.48
	U96_10	96	2,680	2,806,535	52	44	54,045	63,684	32.36
WA	U54_4	54	1,039	292,423	33	21	8,853	13,945	16.78
	U66_4	66	1,209	516,677	40	26	13,064	19,534	20.68
	U78_4	78	1,378	827,453	46	32	18,012	25,810	24.50
	U54_5	54	1,111	314,382	35	19	9,110	16,130	16.82
	U66_5	66	1,281	554,262	41	25	13,562	22,056	20.80
	U78_5	78	1,450	885,451	47	31	18,688	28,918	24.71

y_t and y_b = distances from neutral axis of girder to top and bottom, respectively; S_t and S_b = section moduli for top and bottom components, respectively; r = radius of gyration

Given that precast girders have standard sections in contrast to cast-in-place girders, design aids are charted to estimate achievable spans with girder spacing (Fig. 6). Information on expected costs can also be developed. It should, however, be noted that these aids are intended for the convenience of preliminary design and, hence, practitioners need to check all details associated with actual practice.

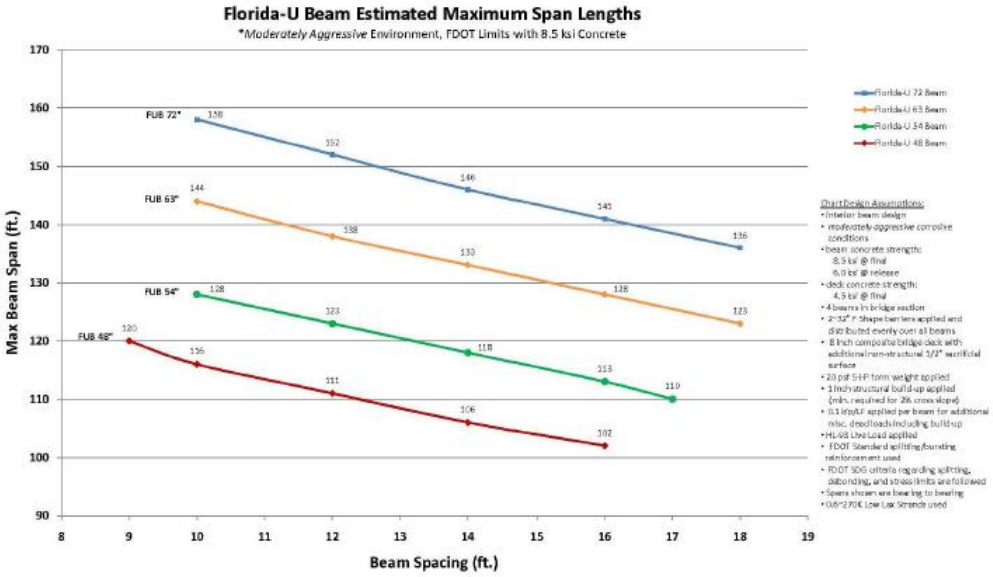

Fig. 6. Design aid for tub girder bridges (FDOT 2020)

1.4. Reinforcing and Strand Details in Tub Girders

Similar to other prestressed concrete girders, 0.5 in. and 0.6 in. strands are broadly used for tub girders at typical spacings of 2 in. Prestressing forces are released by either flame-cutting or gradual jack-down. The transferred forces bring about elastic shortening and end zone cracking in pretensioned tub girders. Compared with flame-cutting, the gradual jack-down method, performed by releasing a hydraulic pressure, mitigates the occurrence of concrete cracking (Tadros et al. 2010). In addition to the conventional placement of steel strands in the tensile side of a tub girder that requires a transfer length of 60 times the diameter (AASHTO 2020), four to six strands may be positioned in the compression zone of the girder when required (Ralls et al. 1993). Debonding of prestressing steel can reduce stress in the transverse bars (Hovell et al. 2013). Cast-in-place diaphragms should be adequately reinforced to avoid premature cracking, which is beneficial in maintaining the integrity of spliced girders, and the location of the diaphragms needs to be at least 3 ft away from concrete closures (Baker et al. 2018).

Steel strands with a diameter of 0.7 in. are used in tunnel construction, whereas these are not yet widely adopted for highway bridges. Figure 7 compares the size and cross-sectional area of 0.7-in. prestressing strands with those of conventional strands. Field demonstration projects were recently reported using 0.7 in. strands alongside preliminary assessments (Morcous et al. 2014).

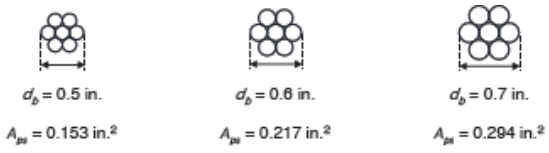

Fig. 7. Comparison of prestressing strands (Salazar et al. 2017)

Because the size of steel strands affects prestressing details, existing design provisions may not be applicable to members with 0.7 in. strands and currently limited information is available. Expected benefits of using such large diameter strands include reduced number of strands, affordable cost, enhanced construction convenience, efficient fabrication, and increased span length (Morcous et al. 2014; Dang et al. 2016; Salazar et al. 2017). ASTM A416 (ASTM 2018) specifies that 0.7 in. strands have a nominal area of A_p = 0.294 in.^{2} and a weight of w_p = 1.0 lb/ft, which are greater than those of 0.5 in. and 0.6 in. strands (A_p = 0.153 in.^{2} and 0.217 in.^{2} with w_p

= 0.52 lb/ft and 0.74 lb/ft, respectively). If the conventional spacing of 2 in. is maintained in a pretensioned girder with 0.7 in. strands, resultant stresses may be overlapped (Fig. 8) and premature cracking can take place (Dang et al. 2016).

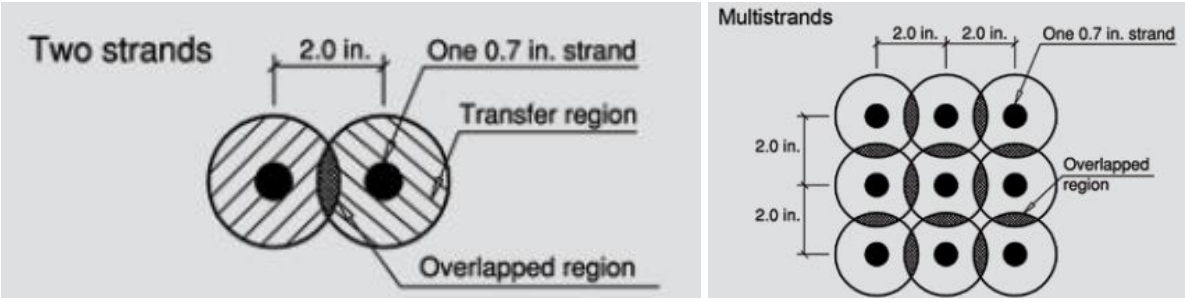

Fig. 8. Overlapped stresses at strand spacings of 2 in. (Dang et al. 2016)

If the diameter of strands is changed from 0.6 in. to 0.7 in., several aspects of tub girders need to be examined (e.g., achievable span length, girder depth and spacing, and bond characteristics). The configuration of tub girders dominates the effectiveness of 0.7 in. strands: the Washington girders were more efficient with 0.7-in. strands relative to the Texas girders (Ball 2019). By adopting 0.7 in. strands in a tub girder, its overall depth can be reduced, thereby lowering the self-weight of the superstructure with an increased span length. It should, however, be noted that the use of 0.7 in. strands may not significantly extend the achievable span length of tub girders (Salazar et al. 2017). The number of 0.7 in. strands can be increased in a tub girder until its stress exceed the serviceability limits stipulated in AASHTO LRFD BDS (AASHTO 2020). If necessary, partial debonding may be considered or the strands may be harped. The provisions of ACI 318 (ACI 2019) and AASHTO LRFD BDS (AASHTO 2020) cannot be used for the prediction of transfer length in a beam with 0.7 in. strands (Dang et al. 2016). Further research is recommended in regard to the application of 0.7 in. strands (e.g., bond behavior, transfer length, spacing requirements, partial debonding, harping, and splitting cracks). Precasters also need to examine their jacking apparatus and harping devices in order to hold down the relatively stiff strands.

1.5. Pretensioning and Post-Tensioning Methods

Prestressing methods for precast tub girders involve both pre- and post-tensioning with straight and harped strands. Regarding implementation costs, pretensioning has economic advantage over post-tensioning (Noisternig and Jungwirth 1996). Pretensioning is performed in a stressing bed comprising abutments, a jacking apparatus, hold-downs, and steel strands. Steam curing accelerates the hydration of concrete and casting operations. Post-tensioning is conducted to achieve continuity between tub girders (Cruz and Wisniewski 2004) before and after casting deck concrete using special equipment. Figure 9 demonstrates jacking procedures for tensioning bridge girders:

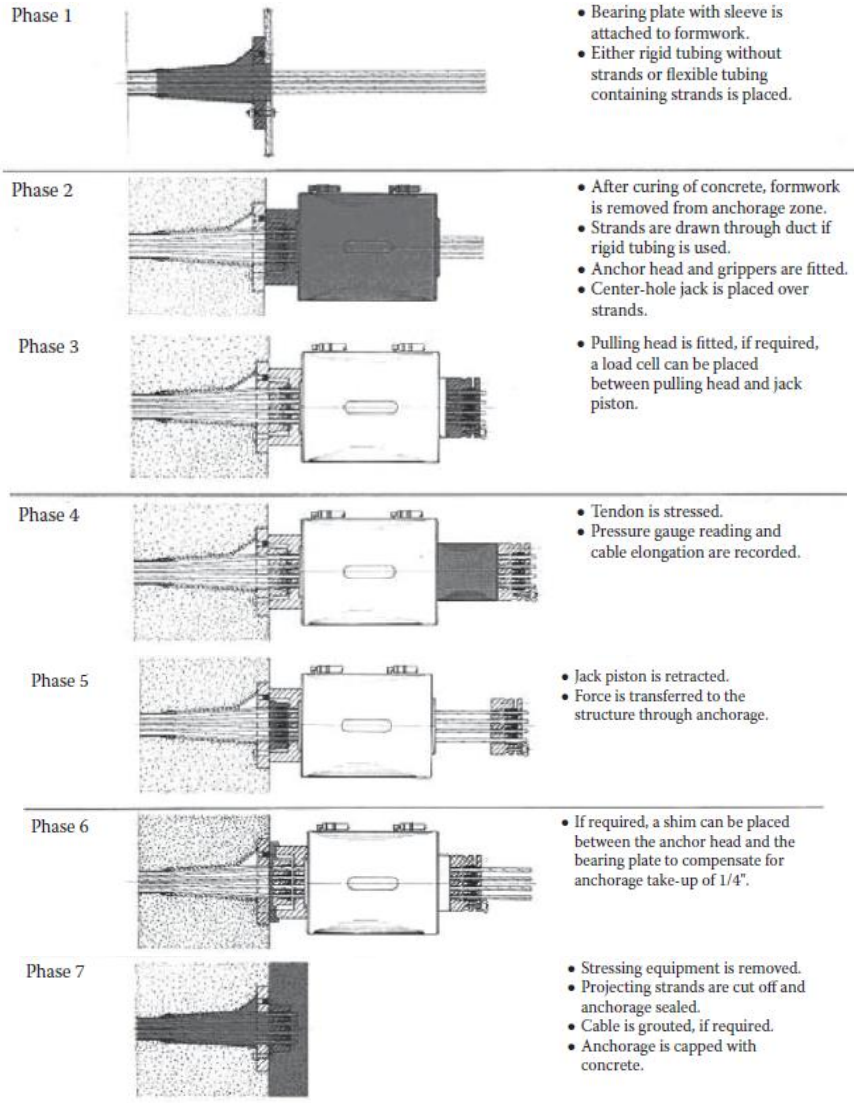

Fig. 9. Jacking procedure for post-tensioned girders (Duan and Chen 2014)

Multiple tub girders may be post-tensioned and spliced to establish full continuity, dependent upon the number of spans and intermediate supports (Ma and Low 2014). The benefits of post-tensioned splices are found in the reduced number of piers and joints, favorable maintenance expense, enhanced serviceability, shallow superstructure geometries, and increased girder spacing (Ma and Low 2014). The following parameters are recommended to be checked at the design stage: concrete properties, prestressing forces, and long-term deformations. The sequence of post-tensioning spliced girders is sketched in Fig. 10:

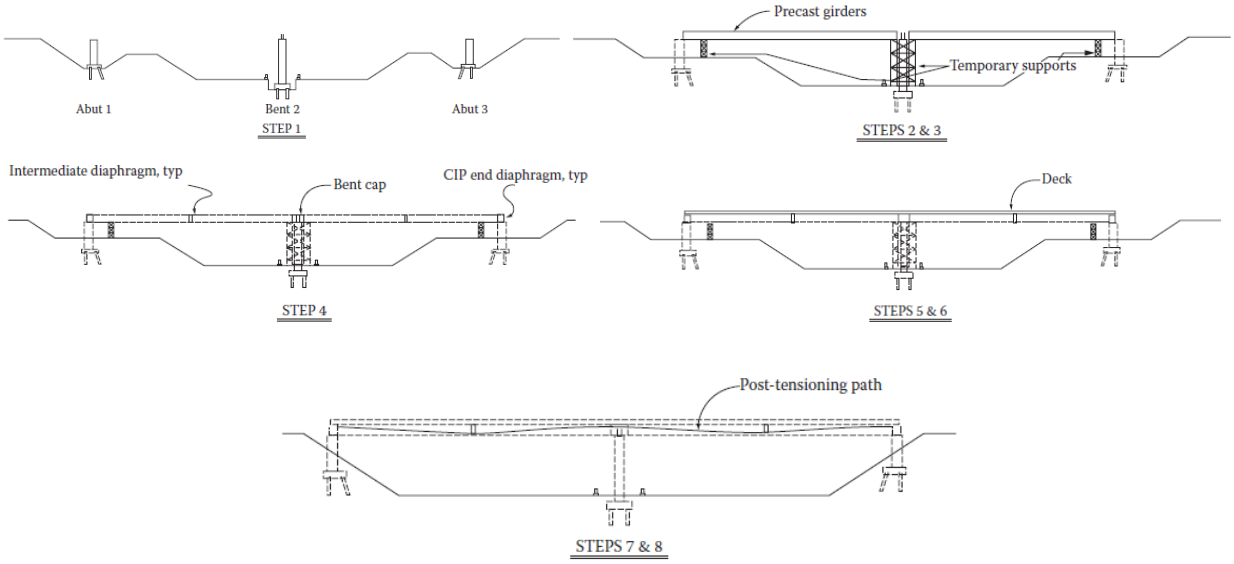

Fig. 10. Post-tensioning spliced girders (Ma and Low 2014)

To determine a post-tensioning option, several factors need to be considered (Lounis et al. 1997): span length, girder spacing, self-weight, maintenance, lateral stability, and life cycle costs. When a girder section is not large enough to accommodate prestressing forces, partial-length post-tensioning is conducted rather than full-length tensioning (Ficenec et al. 1993). Pursuant to AASHTO LRFD BDS (AASHTO 2020), short- and long-term prestress losses are calculated: anchor set, friction, elastic shortening, relaxation, creep, and shrinkage.

1.6. Splice of Girders

Like other superstructure members, multiple pieces of tub girders are erected and spliced (Fig. 11). The diaphragms of tub girders are often positioned at splice locations.

Fig. 11. Spliced precast tub girders (Theryo 2014)

Even if the length of precast girders is typically limited to 150 ft on account of handling challenges (a girder weight of 85 to 120 tons is acceptable for shipping, McMullen et al. 2008), the design and construction of long-span bridges at affordable cost have been of interest. By connecting multiple prestressed concrete girders on site, such an intended plan is accomplished and the serviceability of the superstructure is enhanced; scilicet, after splicing the girders, the superstructure system becomes more effective in carrying live loads with reduced deflections and stresses. In addition, a number of advantages are expected from spliced girders in comparison with segmental girders: moment redistribution, reduced maintenance, favorable labor, and cost savings (Hueste et al. 2012). From a functionality standpoint, the location and methods of splicing are considered important. Connection details should thus be examined to select suitable splicing techniques, including efficient strand profiles, hardware usage, tensioning method, and contractor's specialty (Ficenec et al. 1993). Various splice types were proposed and implemented for prestressed concrete girders (Fig. 12).

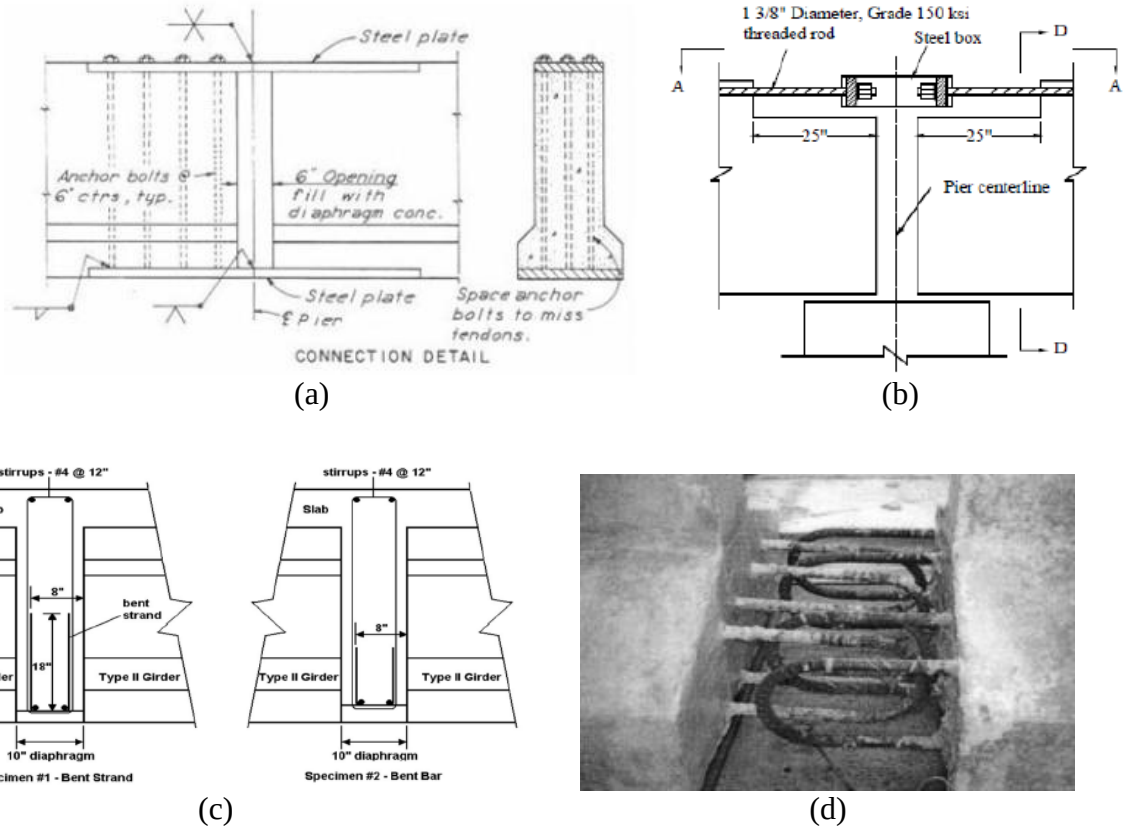

Fig. 12. Splice methods for continuity of pretensioned girders: (a) bolted plates (Bishop 1962); (b) threaded rods (Sun 2004); (c) positive moment connection (Miller et al. 2004); (d) bent bars (Newhouse et al. 2005)

Girder-splicing may be conducted on piers or in span, depending upon structural need. The former is common and economical, whereas the latter is effective in increasing span length. To facilitate splicing in the field, prestressing strands and steel reinforcing bars are extended from the ends of pretensioned girders. For the case of post-tensioning, strands are passed through hardened splice diaphragms and tensioned; then, the ducts are grouted. Shown in Fig. 13 are the view of a local splice connecting two prestressed concrete girders (Fig. 13(a)) and post-tensioning schemes in bridge superstructures (Figs. 13(b) to (d)).

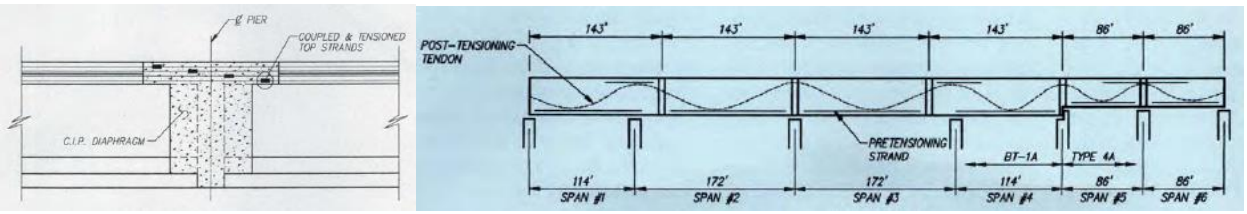

(a) (b)

(c) (d)

Fig. 13. Splice of prestressed concrete girders: (a) overpass splice joint (Ficenec et al. 1993); (b) post-tensioning scheme (Ficenec et al. 1993); (c) tendon layout (Caroland et al. 1992); (d) post-tensioning through girder end block (Caroland et al. 1992)

Temporary supports are necessary when erecting and splicing prestressed concrete girders (e.g., shoring towers and cross bracings, Fig. 14).

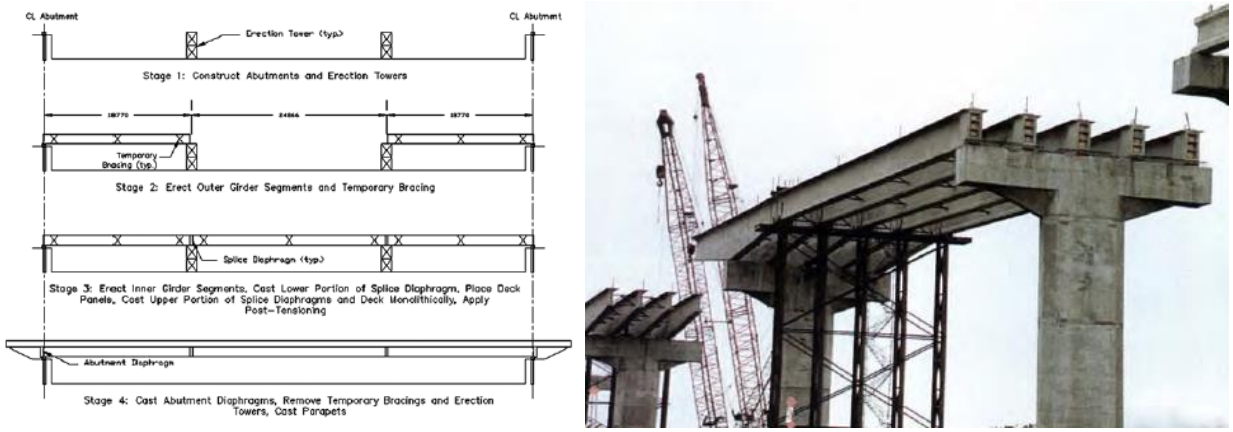

(a) (b)

Fig. 14. Multistage splicing of prestressed concrete bridges: (a) 4500 South Street in Utah (Pantelides et al. 2007); (b) Highland View Bridge in Florida (Janssen and Spaans 1994)

Figure 15(a) graphs prestress losses measured from the Interstate 15 Bridge over 4500 South Street in Salt Lake City, Utah, for two months (Pantelides et al. 2007). The losses were gradual with time and relatively large magnitudes were recorded before grouting ducts and after placing diaphragms. These observations indicate that care should be exercised to preserve prestressing forces when in-situ splicing is conducted. The failure of spliced tub girders at a pier location is pictured in Fig. 15(b), where extensive cracking occurred with inelastic deformations (Holombo et al. 2000). Damage localization was conspicuous in the splice diaphragm and the girders did not exhibit visible cracks, corroborating the critical region of the spliced tub girder system.

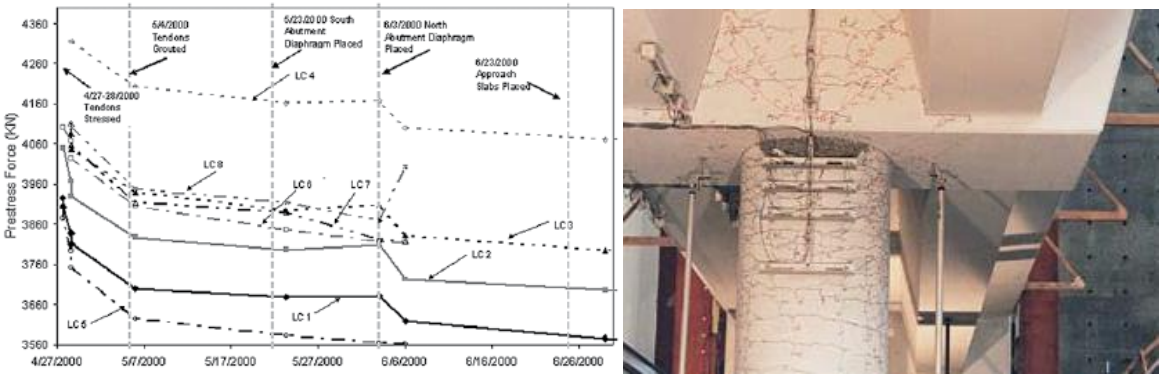

(a) (b)

Fig. 15. Behavior of spliced girders: (a) prestress loss (Pantelides et al. 2007); (b) failure mode (Holombo et al. 2000)

Splice connections may be prestressed outside support locations in order to achieve a long-span superstructure (Fig. 16). Fully prestressed splices are tensioned with either strands or bars, and the space between the adjacent girders is grouted (Fig. 16(a)). Partially prestressed splices contain hooked bars, also known as 180-U bars, in addition to prestressing strands (Fig. 16(b)).

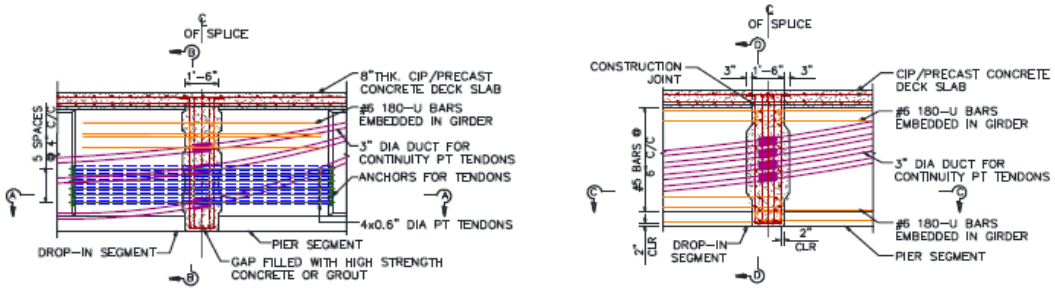

(a) (b)

Fig. 16. Prestressed splice connections (Hueste et al. 2012): (a) fully prestressed splice; (b) partially prestressed splice

1.7. Full- and Partial-Depth Decks for Prestressed Girders

Deck slabs are an important element in a bridge, transferring live loads to the supporting girders. Decks can be cast either in the field or in a plant (cast-in-place and precast, respectively, Fig. 17). Cast-in-place decks are common; however, its construction is slow, which can be addressed by the use of precast decks. Cost-savings are also achieved in the case of precast decks.

(a) (b)

Fig. 17. Deck construction (Shen 2014): (a) cast in place; (b) assembly of precast panels

Precast concrete panels are often used to cover tub girders, so that the load-bearing system can act like a closed box superstructure showing composite action (Fig. 18). It should be noted that stay-in-place metallic decking is often used to accommodate deck slabs between tub girders (Huang and Shahway 2005).

(a) (b) (c)

Fig. 18. Precast decks with tub girders: (a) before placing (Reese and Nickas 2010); (b) after placing (Reese and Nickas 2010); (c) connectors for composite action (Hovell et al. 2013)

The application of precast decks is categorized into full- and partial-depth panels. Unlike the full-depth panels covering the entire deck area, partial-depth panels function as a stay-in-place element to be covered by cast-in-place concrete. Care should be taken at the location of connections between partial-depth panels, where excessive deflections may be associated (Shen

2014). Post-tensioning is available for full-depth precast decks in the transverse and longitudinal directions (Fig. 19).

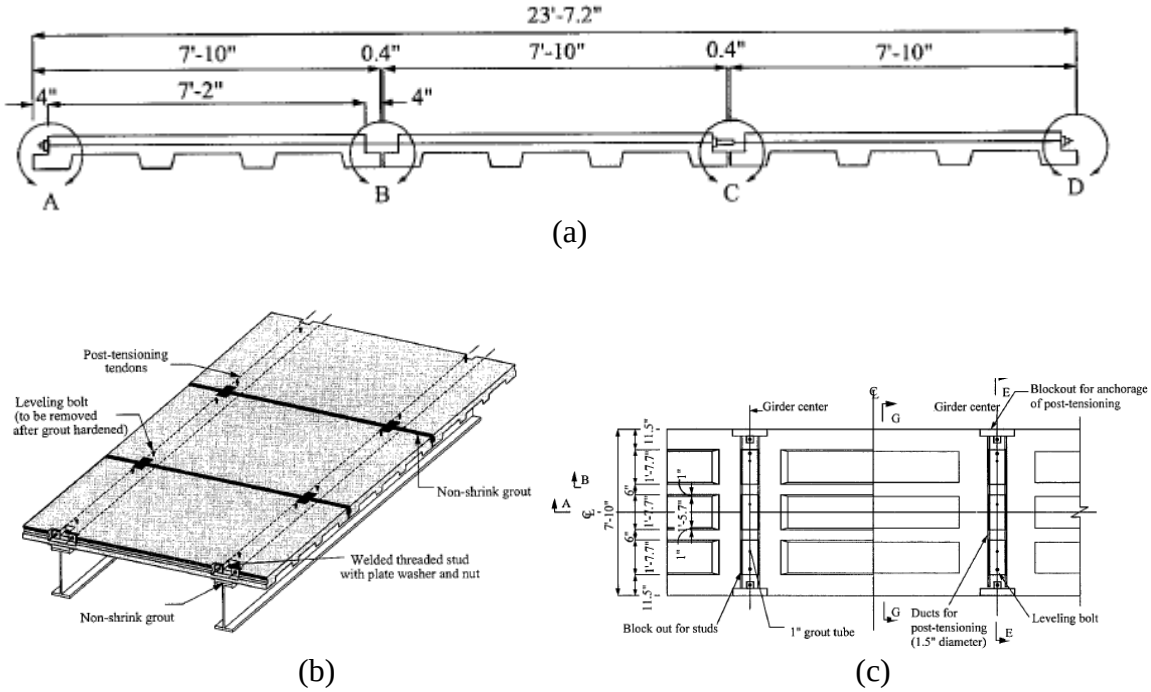

Fig. 19. Prestressing of full-depth decks (Tadros and Baishya 1998): (a) longitudinal post-tensioning; (b) schematic of post-tensioning; (c) transverse post-tensioning

1.8. Overhangs, Shoulders, and Drainage

Bridge overhangs extend the functional width of a deck beyond exterior girders and resist dead (deck, barrier, and railing) and live (vehicle, pedestrian, and barrier impact force) loads. Further details on overhang loads are available in Sec. 3 (*Loads and Load Factors*) of the CDOT Bridge Design Manual (CDOT 2020). The length of an overhang should be between 4 ft and 6 ft (Huang and Shahway 2005; CDOT 2020). In Colorado, contingent upon girder spacing, transverse and longitudinal reinforcing bars in overhangs are placed at a maximum spacing of 4.5 in. to 12 in. (CDOT 2020). A minimum gap between the ends of the top flange and overhang should be 6 in. to avoid water dripping (CDOT 2020). The overhangs of a composite tub girder influence distortional warping stress, as depicted in Fig. 20. If a single traffic lane is loaded, the warping stress noticeably increases (Yoo et al. 2015).

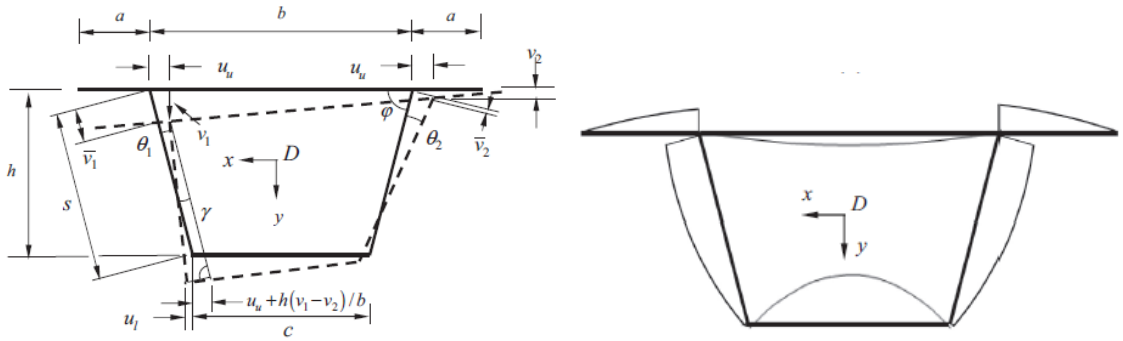

(a) (b)

Fig. 20. Overhangs of decked tub girders (Yoo et al. 2015): (a) distortional deformation; (b) static moment

Torsional moments created by overhang loadings need to be considered in superstructure design. Excessive overhangs should be avoided to control the torsional and bending stresses of the cantilever region. In a curved tub girder system, overhangs significantly raise the torsional stiffness of the superstructure (Monzon et al. 2014). Barriers in overhangs stiffen the superstructure behavior owing to the increased moment of inertia; however, this effect is generally ignored for design convenience. While a single cell girder with wide overhangs is beneficial for ramp structures, the overhangs' intolerable deflections and rotations are of concern.

The range of shoulders is typically between 6 ft and 10 ft for superstructures carrying one- to four-lanes of traffic. Considering the safety and mobility of traffic, the width of shoulders

should be sufficiently large and previous accident records are a good source for the determination of shoulder size. Frequent intervals of deck drains are necessary if full shoulders are not provided (NJDOT 2016). Some DOTs regulate the inclusion of shoulders based on the volume of design traffic (e.g., Michigan DOT requires the minimum clear width of a bridge to be a traveled way plus shoulders when average daily traffic is over 2,000, MDOT 2013).

A bridge drainage system, consisting of grates, inlets, pipes, and gutters, is an important component to properly manage runoff and remove waters from bridge decks. In many cases, the Hydraulic Engineering Circular No. 21 (HEC-21) of the Federal Highway Administration is referenced when designing the drainage of highway bridges. Deck drainage systems should be away from expansion joints and bearings (CDOT 2020) in order to enhance the safety and longevity of bridges.

1.9. Live Load Distribution

The partial occupancy of vehicle loadings causes uneven live load distributions. Girders adjacent to live loads are subjected to higher stress than those away from the loading. When a superstructure is loaded with more trucks, discrepancies between the supporting girders tend to diminish (Samaan et al. 2005). The geometric configuration of slab-on-girder bridges is salient for the distribution of live load, which is associated with mechanical interactions among the deck, girders, and other load-carrying elements (Kim et al. 2009).

Simple distribution factors were conventionally used for the design of superstructure (e.g., *S*/*D* format in the AASHTO Standard Specifications, where *S* is the girder spacing and *D* is an empirical constant). Since the first edition published in 1994, AASHTO LRFD BDS (AASHTO 2020) has included case-specific equations for live load distributions. The equations were calibrated with several variables (e.g., superstructure type, girder spacing, slab thickness, span length, number of loaded lanes, and stiffness) and empirical expressions were developed (Zokaie et al. 1991). The distribution equations are multiplied by bending moments and shear forces are determined from beam-line analysis in order to attain the magnitudes of live load on individual girders.

Truck loadings are positioned to generate the maximum moment and shear in tub girders (Fig. 21(a)). Usually, the placement of vehicle loadings near exterior girders is more sensitive than interior girders (Zokaie 2000). As shown in Figs. 21(b) and (c), the distribution factors for bending moment in exterior girders noticeably changed with the number of loaded lanes and the factors for shear remained almost constant; on interior girders, the shear distribution factors were higher than their moment counterparts. These observations justify the load categories specified in AASHTO LRFD BDS (AASHTO 2020): one-lane- and multiple-lane-loaded cases.

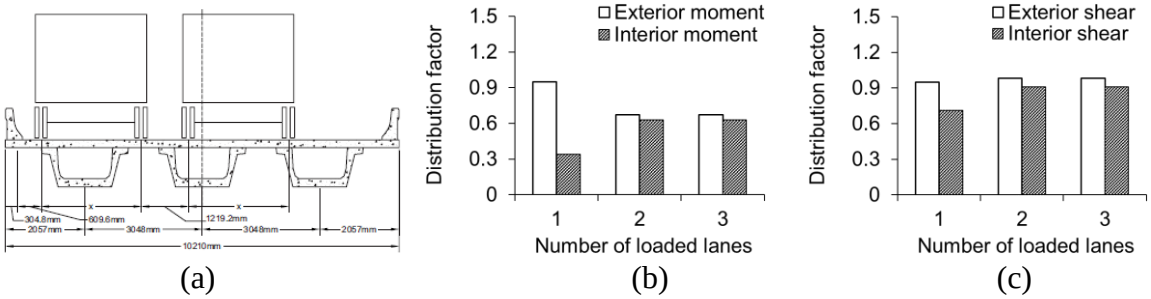

(a) (b) (c)

Fig. 21. Live load distribution factors in tub girder bridge (Mott and Diaz 2010): (a) positioning of truck loads; (b) moment factors with a span length between 65 ft and 120 ft; (c) shear factors with a span length between 65 ft and 120 ft

The number of diaphragms and lateral bracings is not influential in distributing live load (Eamon and Nowak 2002), whereas these elements are still necessary for the stability of a superstructure system (Samaan et al. 2005). As long as reasonable stiffness is given to deck slabs, their thickness may not alter live load distribution factors (Tarhini and Frederick 1992). The continuity of girders marginally affects live load distributions. Nutt et al. (1988) reported a difference of about 10% between simply-supported and continuous bridges. If a bridge is heavily loaded, distribution factors decrease (Bakht and Jaeger 1992) because of an altered load path.

While live load distribution factors can be estimated according to AASHTO LRFD BDS (AASHTO 2020), computer models (e.g., finite element analysis) are employed to determine refined distribution factors. Figure 22 displays several modeling options for slab-on-girder bridges:

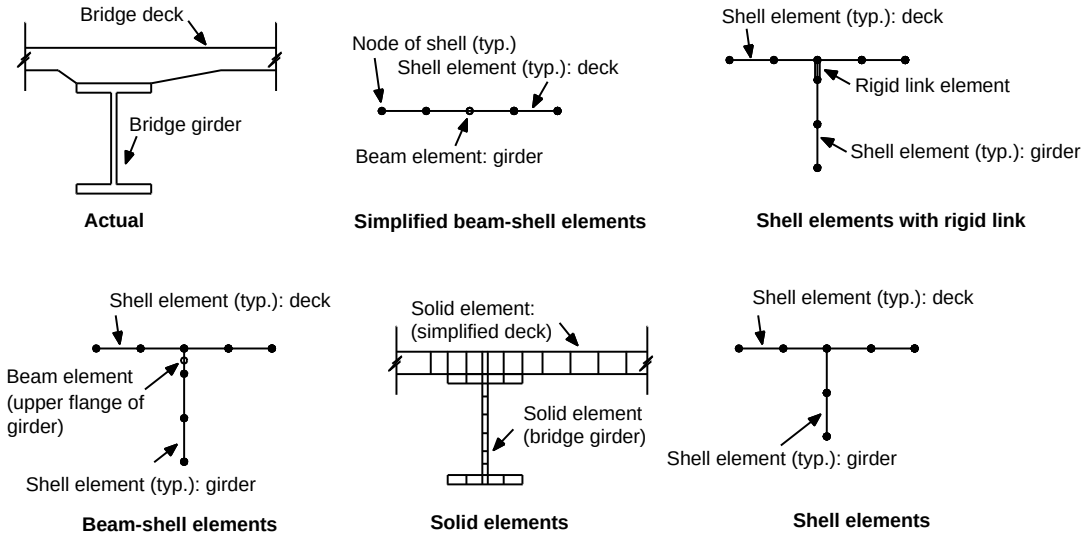

Fig. 22. Modeling methods for prediction of superstructure behavior (Kim et al. 2009)

The empirically calibrated equations of AASHTO LRFD BDS (AASHTO 2020) may not provide accurate information on live load distribution factors, as claimed by Petty (2019): the AASHTO equations overestimated load effects on interior girders. Hughs and Idriss (2006) evaluated the applicability of live load distribution factors calculated per AASHTO LRFD BDS (AASHTO 2020). Finite element modeling was conducted with a benchmark bridge superstructure supported by six prestressed concrete tub girders (4.5 ft deep). The applied truck load consisted of three axles: 15 kips (front), 21 kips (middle), and 21 kips (rear). As

summarized in Table 2, for interior girders, the distribution factors of AASHTO LRFD BDS (AASHTO 2020) agreed better than those of the AASHTO Standard Specifications; however, for exterior girders, both of the AASHTO specifications revealed conservative factors. It was recommended that field data be acquired to recalibrate the equations of tub girders for shear distribution factors.

Table 2. Distribution factors of a tub girder bridge (reproduced from Hughs and Idriss 2006)

Method	AASHTO Standard	AASHTO LRFD BDS	Finite element modeling
Interior girders			
Moment	0.716	0.555	0.565
Shear	0.564	0.890	0.791
Exterior girders			
Moment	0.808	0.966	0.550
Shear	0.808	1.065	0.714

1.10. Behavior of End Zones and Design Approaches

When a prestressed girder is tensioned and the force is transferred, multiple cracks can develop due to stress concentrations in the end region (Fig. 23). Splitting cracks occur in pretensioned members that are reliant upon the bond between the strands and concrete, while bursting cracks related to stress distributions degrade the performance of both pre- and post-tensioned members. The formation of these bursting and spalling cracks is either instantaneous, right after prestress transfer, or time-dependent within a few weeks from the transfer (Barrios 1994). The fact that many existing tub girders in the United States were empirically developed without physical testing leads to premature cracking in the end regions (Dunkman 2009).

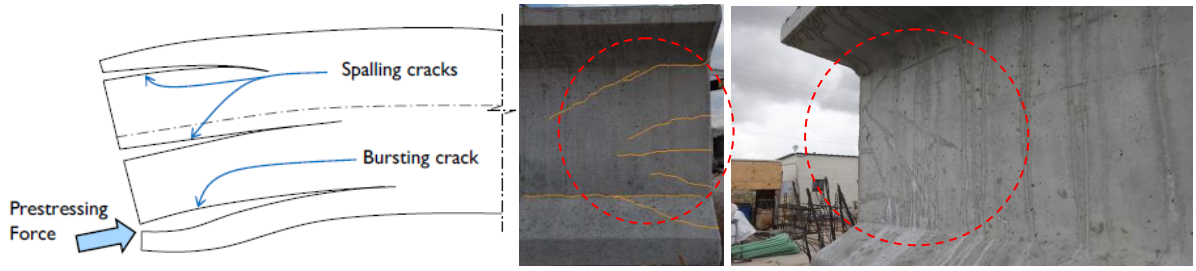

Fig. 23. Bursting and spalling at end-region of prestressed concrete girder (O'Callaghan and Bayrak 2008; Dunkman 2009; Kim 2017)

Since the 2008 Interim of AASHTO LRFD BDS, the term 'splitting reinforcement' has been used to describe end region reinforcement (Fig. 24).

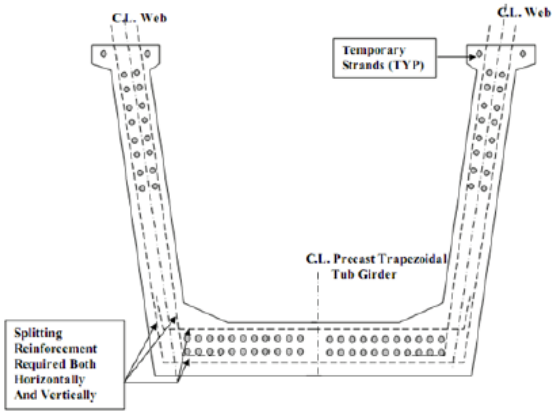

Fig. 24. Splitting reinforcement in end-region (AASHTO LRFD BDS)

Figure 25 depicts typical shear stress distributions in the end region of a tub girder (Huang and Shahway 2005). The high stresses at the strand level (e.g., cell numbers of 2, 6, 10, 14, and 18) cause bursting cracks, especially within the transfer length. The spalling stress of a girder dwindles with the increased distance from the end (Marshall and Mattock 1962).

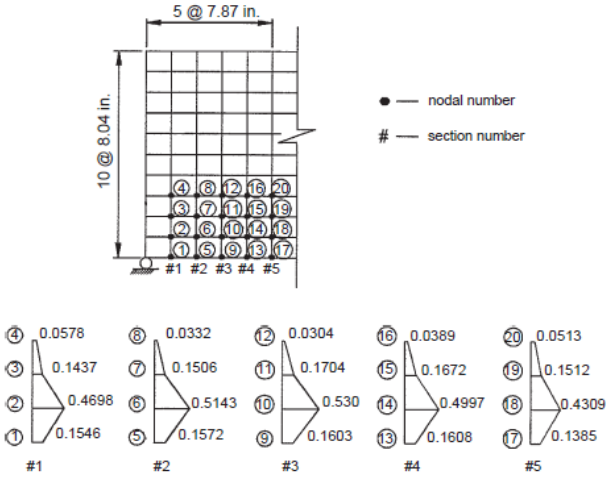

Fig. 25. Stress distribution in end-region of a tub-girder (Huang and Shahway 2005)

In accordance with the PCI Committee on Quality Control Performance Criteria (PCI 1985), several factors induce end region cracking: improper design and fabrication, concrete settlement, differential stresses between the web and flange, and insufficient cover depth. Specifically, at the girder level, the following parameters are responsible for end zone cracks: geometric details, strand arrangement and amount, prestressing force, concrete strength, thermal and shrinkage stresses, and curing (Tadros et al. 2010). Environmental factors can accelerate the cracking of end zones (e.g., temperature and drying shrinkage, Dunkman 2009).

When end region details are inadequate, bursting cracks are observed with complex stress states (Huang and Shahawy 2005). The width of these cracks is around 0.005 to 0.012 in. (Itani and Galbraith 1986; O'Callaghan and Bayrak 2008) and, if wider than 0.007 in., epoxy injections may be necessary (Tadros et al. 2010). Huang and Shahway (2005) argued that the articles in AASHTO LRFD BDS concerning end regions are only for addressing horizontal cracks. In a pretensioned girder, the maximum moment of the end zone takes place near the centroid of the section where spalling cracks form (Dunkman 2009), which redistribute the prestressing forces to the nearby concrete (Gergely et al. 1963).

Web-cracking may develop during the construction of tub girders, albeit uncommon, and sometimes cracks initiate at the junctions between the web and flanges owing to stress concentrations, rather than prestressing forces (Fig. 26)

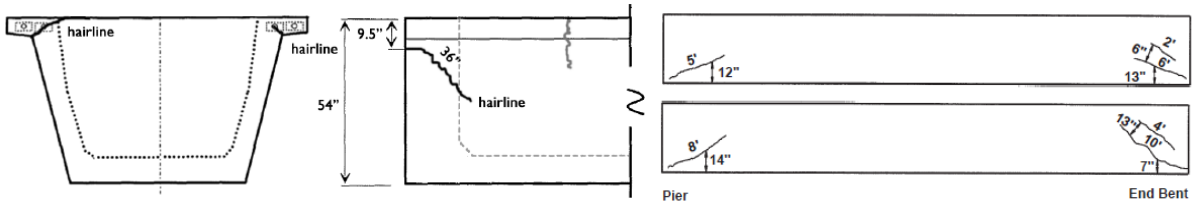

(a) (b)

Fig. 26. Cracking in tub girders: (a) short-term cracking (Barrios 1994); (b) web cracking during construction (Huang and Shahway 2005)

For the purpose of crack control, in addition to shear stirrups near the end of girders, transverse reinforcement is provided: vertical and lateral steel bars are necessary to alleviate the occurrence of spalling and bursting cracks. Although the behavior of an end zone becomes unstable due to cracking, the stress level of the transverse reinforcement is generally lower than its yield stress (Dunkman 2009). The variation of stress in the end zone reinforcement of a prestressed girder is plotted in Fig. 27.

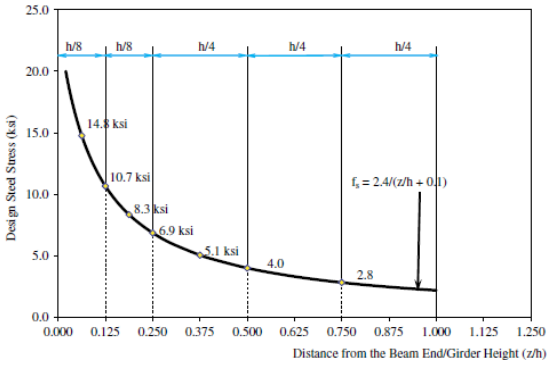

Fig. 27. End-zone stress in reinforcement (Tuan et al. 2004)

Typical parameters affecting stress development in the transverse reinforcement involve strand patterns, prestressing levels, concrete thickness, and bar size (Marshall and Mattock 1962). For the design of end region reinforcement, a couple of approaches are used, namely, finite element analysis (Huang and Shahawy 2005; Kim et al. 2019), analytical expressions (Yuan 2019), strut-

and-tie modeling (Zhang et al. 2020), and empirical equations (AASHTO 2020). Each approach has positive and negative facets. Finite element analysis generates detailed data in regard to stress and concrete cracking, whereas it requires significant endeavors for constructing a girder model. Strut-and-tie modeling is semi-theoretical and determines reinforcement with simplified force-transfer trajectories. The use of analytical and empirical equations is convenient; however, the level of accuracy is ambiguous and may cause a problem after erecting girders.

To address bursting and spalling cracks in the end zone of a tub girder, alternative reinforcing schemes were proposed (Fig. 28). With the increased diameter of steel strands from 0.5 in. to 0.6 in. or 0.7 in., end zone cracking became more prominent (Tadros et al. 2010). As such, conventional approaches for designing the end zone of a tub girder should be revised if 0.6-in. and 0.7-in. strands are used.

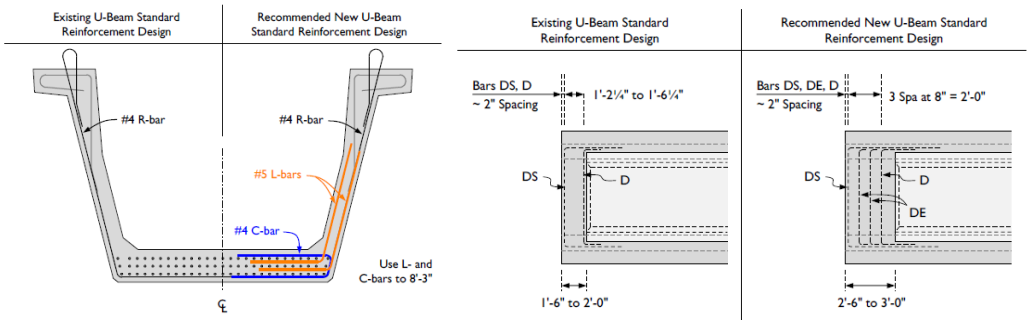

Fig. 28. Proposed reinforcing details for tub girders (Hovell et al. 2013)

Under the allowable prestressing force stipulated in AASHTO LRFD BDS (AASHTO 2020), the amount of transverse steel bars is determined to inhibit bursting and spalling cracks, including a due consideration on constructability. The article of AASHTO LRFD BDS (AASHTO 2020) requires that the stress level of reinforcing bars be less than 20 ksi, within $h/4$ of the girder end (h = girder depth), when subjected to at least 4% of the prestressing force. The $h/4$ requirement is intended to preclude spalling cracks near the centroid of a girder section, and the 4% resistance is based on an assumption that the ratio between the girder height and transfer length is 2.0 (Marshall and Mattock 1962). The AASHTO stress limit of 20 ksi was frequently exceeded (Tuan et al. 2004; O'Callaghan and Bayrak 2008; Dunkman 2009), which illustrates that the uniform stress distribution assumed in AASHTO LRFD BDS (AASHTO 2020) may not be accurate and should be reassessed with realistic stress profiles. In some cases, the

implementation of stress control is not consistent. For example, the stress of transverse reinforcement is limited to 18 ksi in Florida (Nickas 2004) and a design stress of 30 ksi is stated in the PCI design manual (PCI 2017).

2. Evaluation of Existing Tub Girders

2.1. Geometric Properties

Figures 29(a) to (c) show typical tub girders used by the Departments of Transportation in the nation. While all girders are composed of upper and lower flanges and inclined webs, specific configurations vary by state. For example, the inner side of the upper flanges in the Texas and Colorado girders is flat; on the other hand, the Washington girder has protruded upper flanges. For comparison, multiple variables were assigned to each segment of the girders (Fig. 29(d)) and summarized in Table 3, where 35 types are detailed (note that V_3 in the Colorado girders indicates the maximum value that can cover all possible scenarios in a conservative manner and its minimum would be 15 in. for the placement of stay-in-place panels). The depth of these existing girders ranged from 40 in. to 96 in. with a web thickness of 5 in. to 10 in. As enumerated in Table 1, the radius of gyration (r) and section moduli (S) of the girders rose with the increased girder depth. The cross-sectional area (A) and the moment of inertia (I) of the Washington girders are in general smaller than those of others because of the compact shape (Fig. 1(b)). The B618-U girders employed in Colorado have assorted depths (48, 60, 72, 84, and 96 in.) with the web thickness of 5, 7.5, and 10 in. and the bottom flange thickness of 6.35 and 8.1 in. (web thickness = 7.5 in. and flange thickness = 8.1 in. were used in Table 1 and the present study). In practice, a bridge system with twin tub girders is often constructed at a deck width varying from 33 ft to 47 ft with a girder spacing between 12 ft and 26 ft on center (Saindon and McMullen 2010).

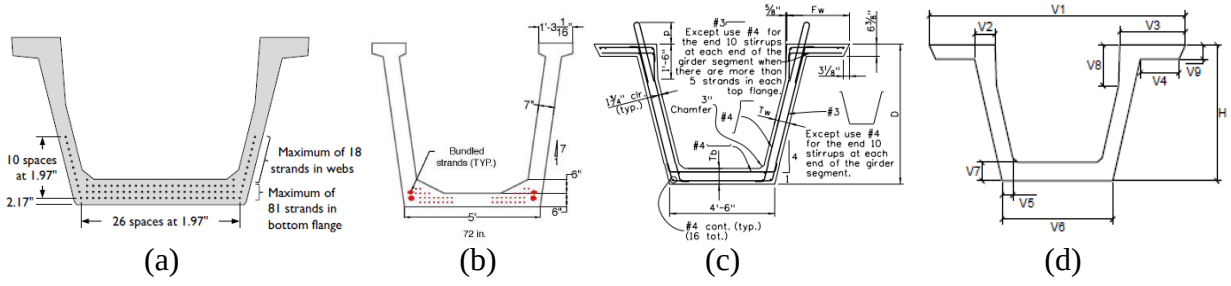

Fig. 29. Geometric configuration of tub girders: (a) Texas; (b) Washington; (c) Colorado; (d) variables of a trial section

Table 3. Geometric variable of existing tub girders

State/ agency	Girder type	Depth (in.)	V_1 (in.)	V_2 (in.)	V_3 (in.)	V_4 (in.)	V_5 (in.)	V_6 (in.)	V_7 (in.)	V_8 (in.)	V_9 (in.)	n	t_{web} (in.)
CA	UB1400	55	86.6	7.9	13.8	8.9	7.9	59.1	6.9	11.8	11.8	3.1	7.9
	UB 550	61	89.6	7.9	15.3	8.9	7.9	59.1	6.9	11.8	11.8	3.2	7.9
	UB1700	67	92.5	7.9	16.7	8.9	7.9	59.1	6.9	11.8	11.8	3.3	7.9
	UB1850	73	95.5	7.9	18.2	8.9	7.9	59.1	6.9	11.8	11.8	3.4	7.9
	UB2000	79	98.4	7.9	19.7	8.9	7.9	59.1	6.9	11.8	11.8	3.4	7.9
	UB2150	85	101.4	7.9	21.2	8.9	7.9	59.1	6.9	11.8	11.8	3.4	7.9
CO	U48	48	115	10	30	16.8	5.2	54	8.1	18	6.4	4	7.5
	U60	60	121	10	30	16.8	5.2	54	8.1	18	6.4	4	7.5
	U72	72	127	10	30	16.8	5.2	54	8.1	18	6.4	4	7.5
	U84	84	133	10	30	16.8	5.2	54	8.1	18	6.4	4	7.5
	U96	96	139	10	30	16.8	5.2	54	8.1	18	6.4	4	7.5
FL	FU48	48	94	6.6	16	8.5	-	56	10	21	7	4	5.5
	FU54	54	97	6.6	16	8.5	-	56	10	21	7	4	5.5
	FU63	63	102	6.6	16	8.5	-	56	10	21	7	4	5.5
	FU72	72	106	6.6	16	8.5	-	56	10	21	7	4	5.5
PCI	PCI72_9	72	121	10.3	20	7.5	-	70	9	21	9.3	4	9
	PCI84_9	84	127	10.3	20	7.5	-	70	9	21	9.3	4	9
	PCI96_9	96	133	10.3	20	7.5	-	70	9	21	9.3	4	9
	PCI72_10	72	123	11.3	21	7.5	-	72	9	21	9.3	4	10
	PCI84_10	84	129	11.3	21	7.5	-	72	9	21	9.3	4	10
	PCI96_10	96	135	11.3	21	7.5	-	72	9	21	9.3	4	10
TX	U 40	40	89	7.5	15.8	8.3	-	55	8.3	21.6	5.9	4	5
	U 54	54	96	7.5	15.8	8.3	-	55	8.3	21.6	5.9	4	5
	U72_9	72	121	10.3	20	7.5	-	70	9	21	9.3	4	9
	U84_9	84	127	10.3	20	7.5	-	70	9	21	9.3	4	9
	U96_9	96	133	10.3	20	7.5	-	70	9	21	9.3	4	9
	U72_10	72	123	11.3	21	7.5	-	72	9	21	9.3	4	10
	U84_10	84	129	11.3	21	7.5	-	72	9	21	9.3	4	10
	U96_10	96	135	11.3	21	7.5	-	72	9	21	9.3	4	10
WA	U54_4	54	71.7	7.1	15.1	5.0	-	48	6	-	4.5	7	7
	U66_4	66	75.1	7.1	15.1	5.0	-	48	6	-	4.5	7	7
	U78_4	78	78.6	7.1	15.1	5.0	-	48	6	-	4.5	7	7
	U54_5	54	83.7	7.1	15.1	5.0	-	60	6	-	4.5	7	7
	U66_5	66	87.1	7.1	15.1	5.0	-	60	6	-	4.5	7	7
	U78_5	78	90.6	7.1	15.1	5.0	-	60	6	-	4.5	7	7

n = slope of web; t_{web} = thickness of web

2.2. Structural Efficiency

2.2.1. Analytical Approach

The prestressed concrete community adopts the following structural efficiency factor (Eq. 3) and efficiency ratio (Eq. 4) to evaluate the geometry of a girder section (Rabbat and Russell 1982):

$$\rho = \frac{r^2}{y_t y_b} \tag{3}$$

$$\alpha = \frac{3.46 S_b}{Ah} \tag{4}$$

where ρ and α are the structural efficiency factor and ratio, respectively; r is the radius of gyration of the girder; y_t and y_b are the distances from the centroid of the girder section to the top and bottom fibers, respectively; S_b is the section modulus for the bottom fiber; and h is the depth of the girder. Listed in Table 4 are the calculated efficiency factors and ratios of the girders alongside unit weight in kips/ft. Although all ρ factors were within a similar boundary (Fig. 30(a)), the factors of the Washington and Texas girders exhibited the lowest and highest values of 0.41 and 0.51, respectively. As far as the α ratios are concerned (Fig. 30(b)), the Florida girders at an average of 1.0 were superior to others demonstrating analogous mean α values (Fig. 30(c)). The unit weight of the Colorado girders was heavier up to a depth of 60 in., beyond which the weight of the PCI and Texas girders was noticeable (Fig. 30(d)). Given that tub girders span 120 ft to 160 ft (FDOT 2020), a marginal difference in the unit weight can cause a substantial increase in the dead load of a bridge system. It is, thus, recommended that the weight of the Colorado girders be reduced to the level of the Florida and Washington girders with improved structural efficiency.

Table 4. Structural efficiency of existing tub girders

State/agency	Girder type	Depth (in.)	Efficiency factor (ρ)	Efficiency ratio (α)	Weight (kips/ft)
CA	UB1400	55	0.46	0.90	1.39
	UB1550	61	0.46	0.89	1.49
	UB1700	67	0.46	0.88	1.59
	UB1850	73	0.45	0.87	1.69
	UB2000	79	0.45	0.86	1.79
	UB2150	85	0.45	0.85	1.89
CO	U48	48	0.50	0.89	1.43
	U60	60	0.50	0.89	1.62
	U72	72	0.50	0.88	1.81
	U84	84	0.49	0.86	2.01
	U96	96	0.48	0.85	2.20
FL	FU48	48	0.48	0.99	1.26
	FU54	54	0.49	1.00	1.33
	FU63	63	0.50	1.01	1.43
	FU72	72	0.50	1.01	1.54
PCI	PCI72_9	72	0.48	0.92	2.12
	PCI84_9	84	0.47	0.90	2.35
	PCI96_9	96	0.47	0.88	2.59
	PCI72_10	72	0.47	0.89	2.28
	PCI84_10	84	0.46	0.87	2.53
	PCI96_10	96	0.46	0.86	2.79
TX	U 40	40	0.48	0.99	1.02
	U 54	54	0.51	1.03	1.17
	U72_9	72	0.48	0.91	2.12
	U84_9	84	0.47	0.90	2.35
	U96_9	96	0.47	0.88	2.59
	U72_10	72	0.47	0.89	2.28
	U84_10	84	0.46	0.87	2.53
	U96_10	96	0.46	0.86	2.79
WA	U54_4	54	0.41	0.86	1.08
	U66_4	66	0.41	0.85	1.26
	U78_4	78	0.41	0.83	1.44
	U54_5	54	0.42	0.93	1.16
	U66_5	66	0.42	0.90	1.33
	U78_5	78	0.42	0.88	1.51

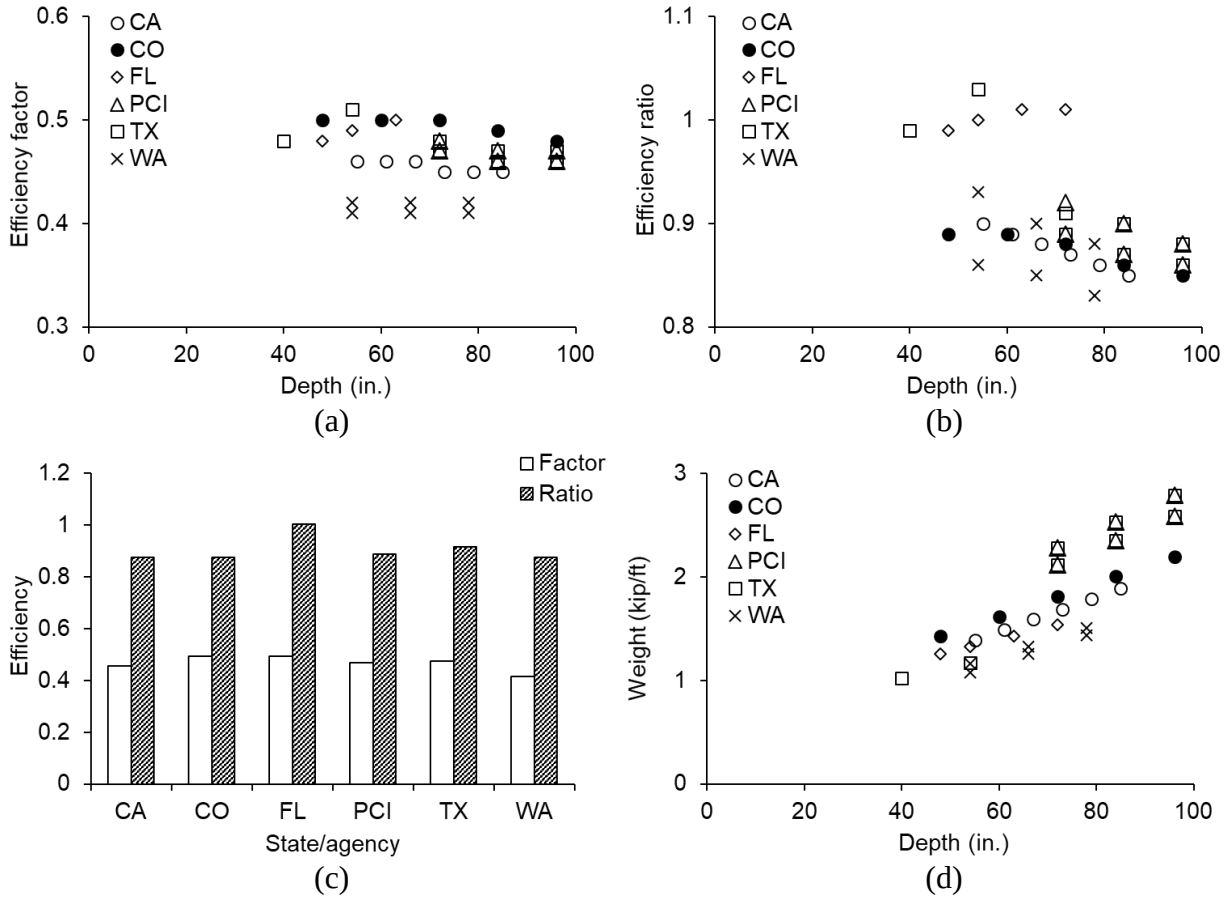

Fig. 30. Comparison of efficiency in existing girders: (a) efficiency factor; (b) efficiency ratio; (c) average; (d) weight

2.2.2. Computational Approach

Computational modeling was carried out to investigate the implications of geometric components in the structural efficiency of the tub girders (since Eq. 4 contained an empirical constant, Eq. 3 was focused). The B618-U series of Colorado was selected and an open-source cross-platform, called NetLogo, was employed. This program utilizes discrete entities in a grid space to simulate their mutual interactions with a preset rule. The principles and implementation procedure of the software are explained in Wilensky and Rand (2015). The size of each entity was 0.125 in. by 0.125 in. and the number of the entities varied from 43,762 to 67,474, contingent upon girder depth (U48 to U96). The model represented one half of the symmetric girder section. Aligning with the definition of the efficiency factor (ρ), Eqs. 5 to 7 were formulated

$$\rho = \frac{r^2}{y_t y_b} = \frac{I / A}{(h - y_b) y_b} \tag{5}$$

$$A = \sum_{i=1}^{n} s^2 \tag{6}$$

$$I = \sum_{i=1}^{n} \left(\frac{s^4}{12} + s^2 (y_i - y_b)^2 \right) \tag{7}$$

where s is the width and depth of the entity; n is the number of the entities covering the girder section; and y_i is the distance from the bottom of the girder to the centroid of the i^{th} entity. The distance from the neutral axis of the girder to the bottom fiber (y_b) is expressed as

$$y_b = \frac{\sum_{i=1}^{n} s^2 y_i}{\sum_{i=1}^{n} s^2} \tag{8}$$

Substituting Eqs. 6 and 7 into Eq. 5,

$$\rho = \frac{\frac{s^2}{12} + \frac{1}{n} \sum_{i=1}^{n} (y_i - y_b)^2}{(h - y_b) y_b} \tag{9}$$

The portion of the respective entity is calculated by

$$\rho_i = \frac{\frac{s^2}{12} + (y_i - y_b)^2}{n (h - y_b) y_b} \tag{10}$$

$$\rho = \sum_{i=1}^{n} \rho_i \tag{11}$$

where ρ_i is the efficiency fraction of the i^{th} entity. After solving the model, the distribution of the efficiency factors was contoured in color. Figure 31 describes the contribution of the girder components to the global efficiency factor (Eq. 11), and the discrepancy between the analytical and computational models was less than 0.41% (Table 5). The flanges controlled the ρ factors in all cases; by contrast, the web was uninfluential. This fact signifies that the dimensions of the flanges and nearby regions (transition from the flanges to the web) can be modified to raise the efficiency of the girders.

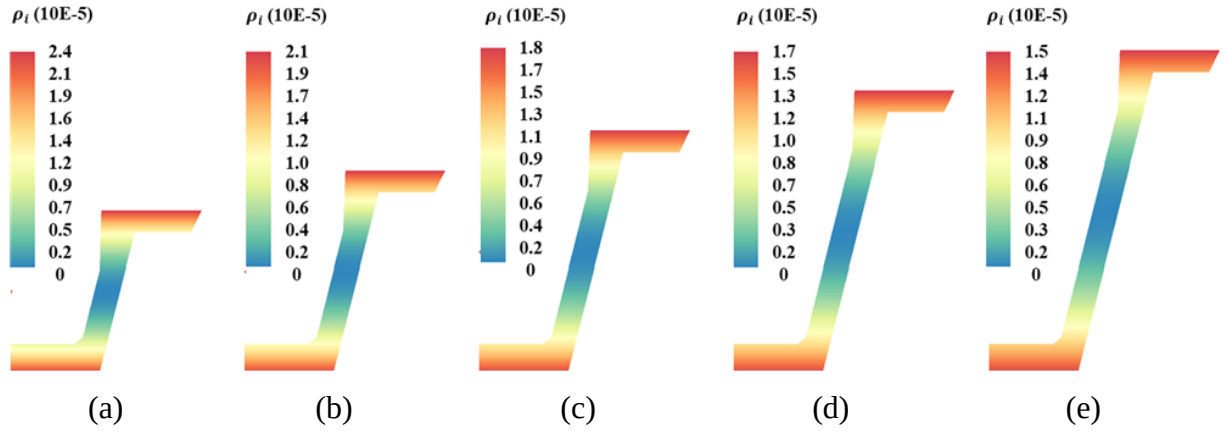

(a) (b) (c) (d) (e)

Fig. 31. Contribution of geometric components to efficiency factor: (a) U48; (b) U60; (c) U72; (d) U84; (d) U96

Table 5. Effect of girder geometry on structural efficiency

State/agency	Girder type	Efficiency factor (ρ)		
		Analytical	Computational	Difference (%)
CO	U48	0.503	0.504	0.19
	U60	0.504	0.505	0.19
	U72	0.499	0.500	0.20
	U84	0.491	0.493	0.41
	U96	0.484	0.485	0.21

3. Development of Prototype Tub Girders

3.1. Optimized Section

To enhance the structural efficiency of tub girders in Colorado, the conceptual outline depicted in Fig. 32(a) were optimized. The simple sketch drawn in Fig. 29(d) was refined with minor modifications such as haunches and flange cornering to mitigate stress concentrations. A mathematical algorithm called the Generalized Reduced Gradient (GRG) method was employed to determine the most suitable variables under a given condition. An objective function was defined with the efficiency factor (Eq. 1) alongside the geometric variables, and the goal was to maximize the factor. The objective comprising vectorial components was constrained by upper and lower bounds, established as per a possible range taken from the existing state girders (Table 3). Afterward, the objective function was differentiated with respect to the individual variable to find a solution. The Newton-Rapson method (also known as the Newton method) iterated the established procedure until converged values were attained at an estimated difference of 0.0001 between successive gradients. It is worth noting that the gradients of only active constraints were considered to save computational effort. Further details on the GRG algorithm are available elsewhere (Lasdon et al. 1973). Shown in Fig. 32(b) is the optimized section at a depth of 48 in. Compared with the existing B618-U girder (Fig. 29(c)), the straight portion of the webs increased from 18 in. to 21.5 in. (V_8 in Fig. 32(a)) and the width of the bottom flange was enlarged from 54 in. to 58 in. (V_6 in Fig. 32(a)). The optimized section will not exceed shipping and handling limits in Colorado. Figures 33 and 34 display the sensitivity of the efficiency factor and ratio with the constituting variables, respectively, and the optimized dimensions were added for visual appraisal. It should be noted that primary variables were graphed without secondary ones (for instance, $V_4 = V_3 - V_2$). When one variable was changed to examine the efficiency of the girder, other variables were kept constant based on the average of the sampled girders (Table 3). For this reason, the optimized values occasionally deviated from the maximum factors and ratios provided in Figs. 33 and 34. The efficiency factors were more reliant upon the magnitudes of V_2 and V_3 than those of others (Fig. 33), which is ascribed to the fact that the upper flanges of the section dominated the moment of inertia, thereby affecting the radius of gyration in Eq. 1. The variation trend of the efficiency ratio was analogous in general (Fig. 34), whereas the effects of some variables differed owing to the distinct formulation between Eqs. 3 and 4.

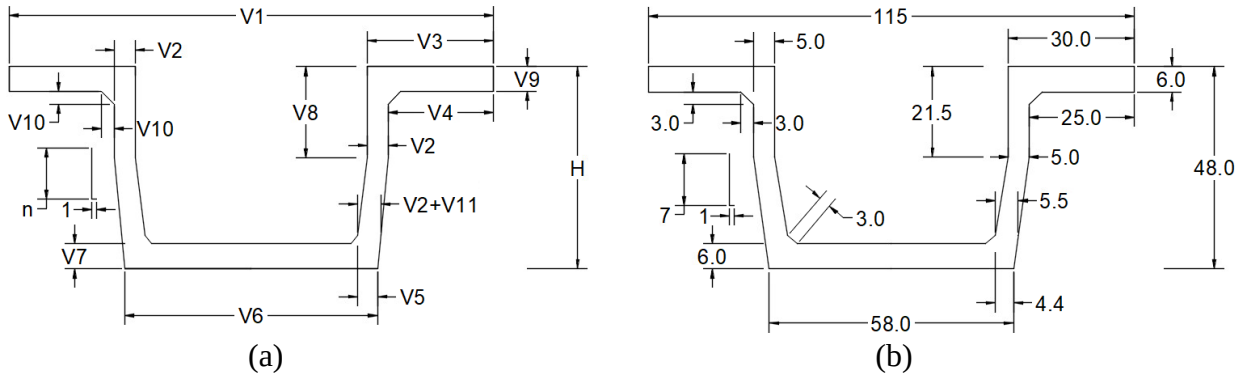

Fig. 32. Development of prototype girder (depth = 48 in.): (a) indication of variables; (b) optimized section

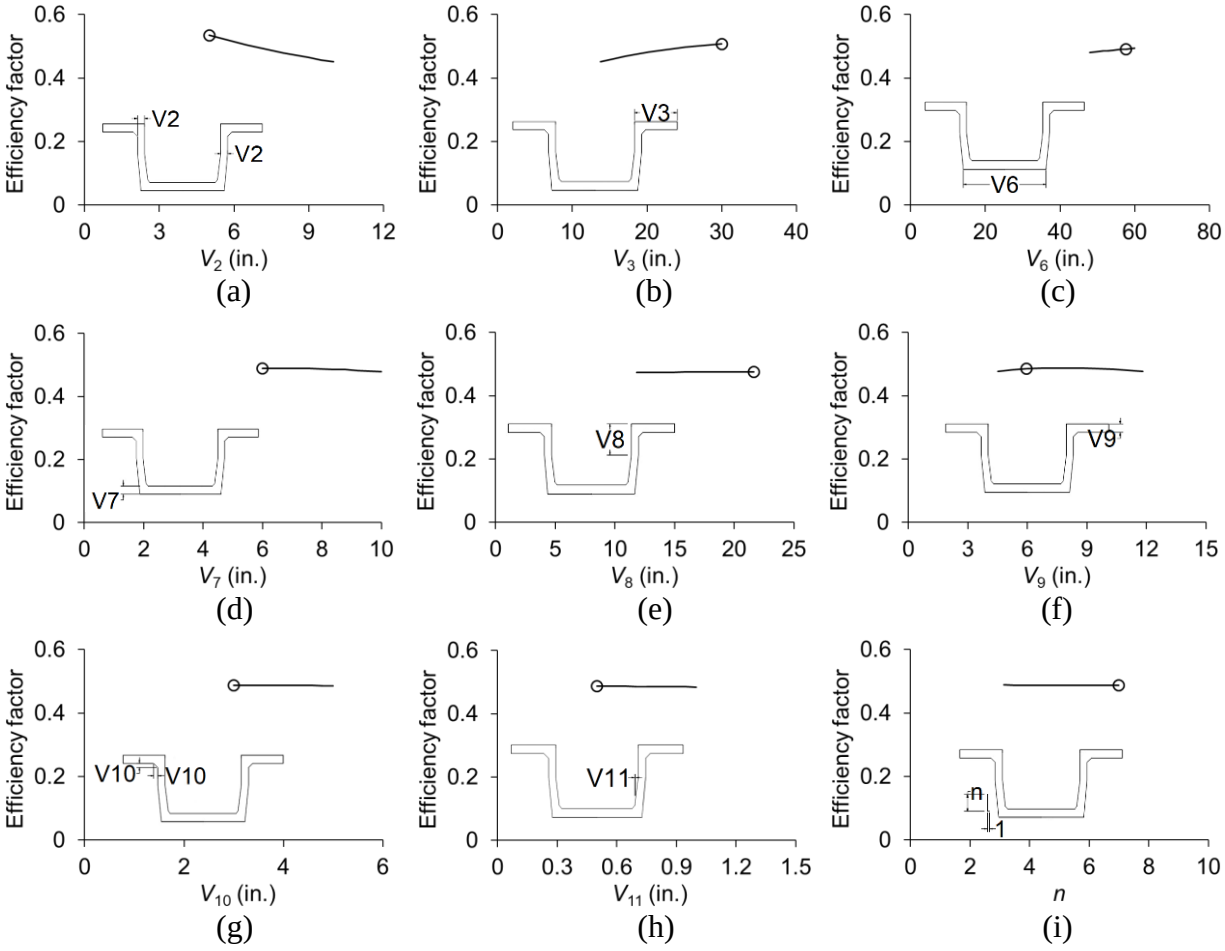

Fig. 33. Variation of efficiency factor with geometric properties (circle = optimized value): (a) V_2; (b) V_3; (c) V_6; (d) V_7; (e) V_8; (f) V_9; (g) V_{10}; (h) V_{11}; (i) n

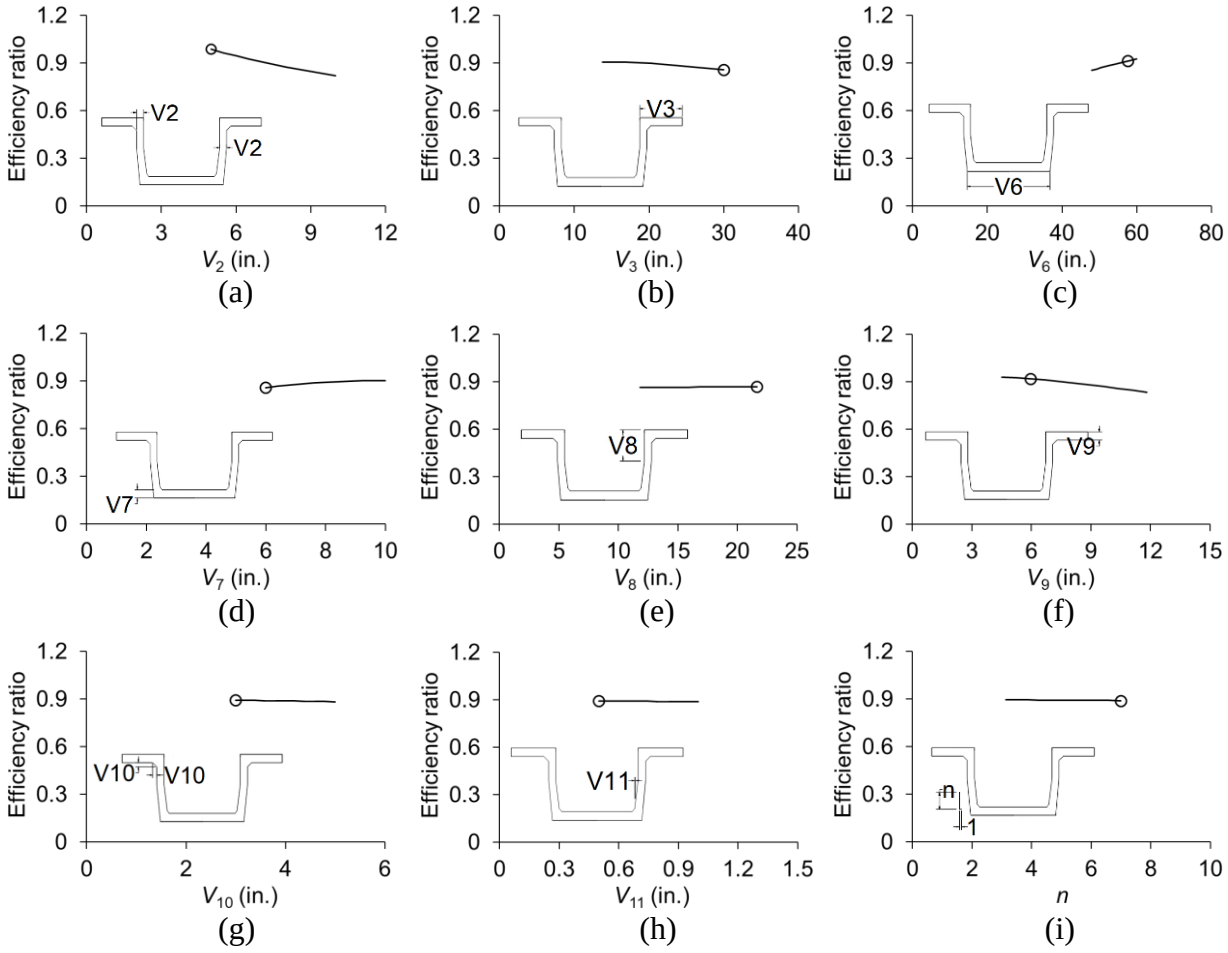

Fig. 34. Variation of efficiency ratio with geometric properties (circle = optimized value): (a) V_2; (b) V_3; (c) V_6; (d) V_7; (e) V_8; (f) V_9; (g) V_{10}; (h) V_{11}; (i) n

3.2. Web Thickness

Because the optimized girder section was solely dependent upon geometric property, the level of stress in the web where prestressing strands are placed was checked. In line with the web thickness of the existing girders (Table 3), a range of t_{web} = 5 in. to 10 in. was taken into account with a strand diameter of ϕ = 0.5 in., 0.6 in., and 0.7 in. (A_p = 0.153 in.^{2}, 0.217 in.^{2}, and 0.294 in.^{2}, respectively, in which A_p is the cross-sectional area of each strand). In accordance with AASHTO LRFD BDS (AASHTO 2020), the specified compressive strength of concrete was f'_c = 9 ksi, 10 ksi, and 11 ksi, and the strength at transfer was $f'_{ci} = 0.8f'_c$. Likewise, pursuant to AASHTO LRFD BDS (AASHTO 2020), the transfer stress of the strands (f_i) was conservatively taken as 90% of the allowable jacking stress of $0.75f_{pu}$ (that is, $f_i = 0.675f_{pu}$), where f_{pu} is the ultimate strength of the prestressing steel, 270 ksi. A tributary area of the web concrete per strand was assumed with a spacing of 2 in. and corresponding stresses were obtained, as plotted in Figs. 35(a) to (c). The stress profiles gradually decreased with an increase in the web thickness. The optimized thickness of t_{web} = 5 in. was acceptable to all ϕ = 0.5 in. and 0.6 in. cases, regardless of the concrete strength; in other words, the stress magnitudes induced by the maximum tensioning of the strands were lower than the AASHTO limits of $0.6f'_{ci}$ and $0.45f'_c$ for the compressive stresses before and after losses, respectively. In contrast, the stresses belonging to ϕ = 0.7 in. were as high as 92.2% relative to their 0.5 in. counterpart. Figure 35(d) illustrates the critical thickness of the girder web, representing the intersection between the stress profiles and the AASHTO limits in Figs. 35(a) to (c). When the strand size of ϕ = 0.5 in. and 0.6 in. was used, a thickness of 4.9 in. was predicted to be sufficient; however, as the strand diameter was increased to ϕ = 0.7 in., a thickness of 6.6 in. was necessary.

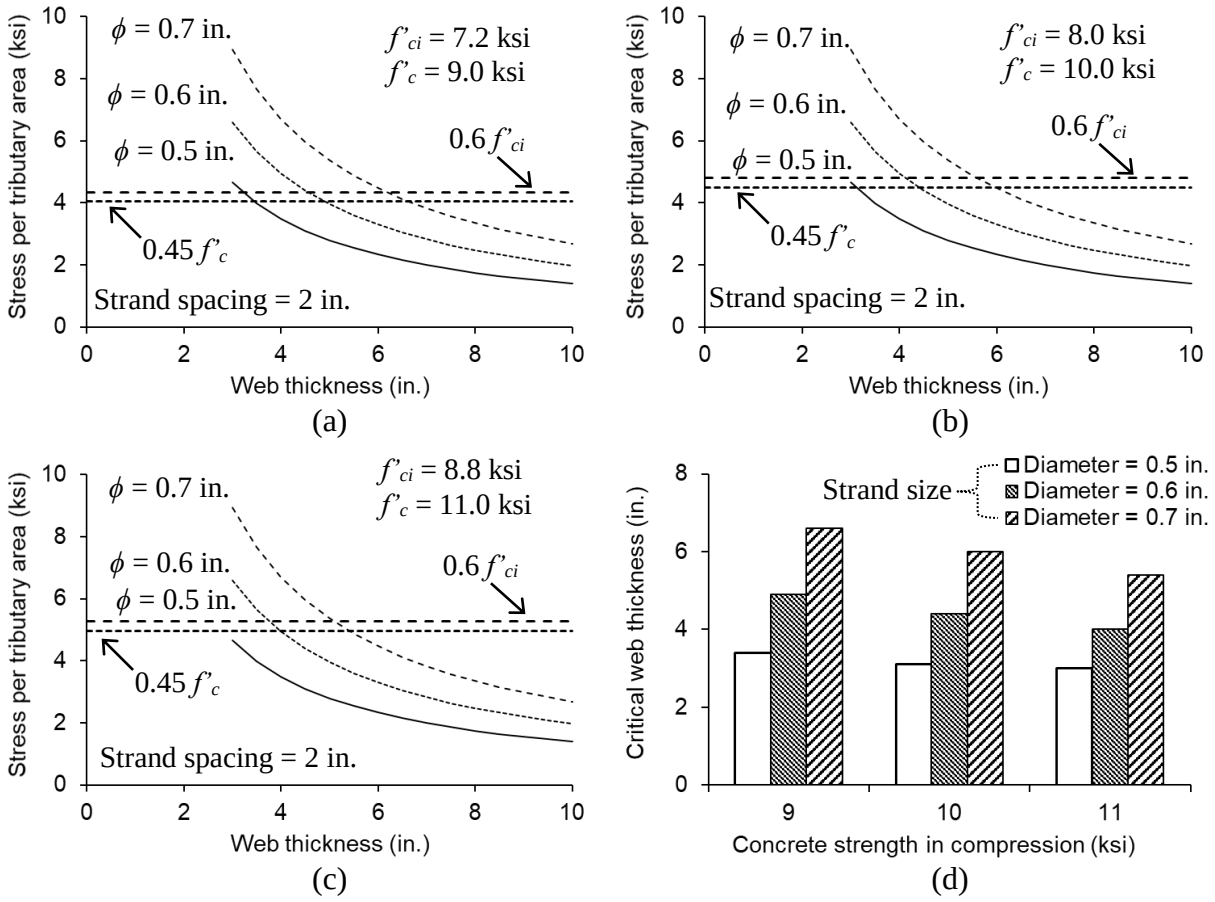

Fig. 35. Stress check in the web at transfer against the limit of AASHTO LRFD BDS (f_{pi} = $0.9f_{pj}$): (a) f'_c = 9 ksi; (b) f'_c = 10 ksi; (c) f'_c = 11 ksi; (d) critical web width

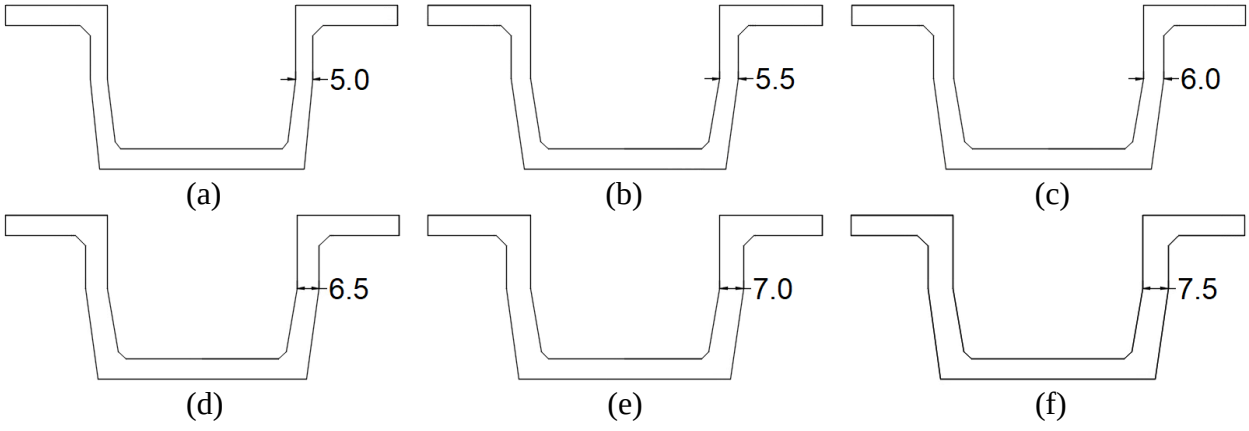

Fig. 36. Prototype sections (units in inches): (a) Prototype-O; (b) Prototype-5.5; (c) Prototype-6.0; (d) Prototype-6.5; (e) Prototype-7.0; (f) Prototype-7.5

3.3. Adjusted Section

On the basis of the practical significance examined above, the optimized section was adjusted to provide multiple options with regard to a web thickness of 5 in. to 7.5 in. (Fig. 36). The effects of the web thickness are visible in Fig. 37, where invariant properties are indicated. The incremental thickness broadened V_2 (Fig. 37(a)), while it reduced V_4 (Fig. 37(b)) due to the fixed girder width of V_1 = 115 in. The response slope of V_5 (Fig. 37(c)) was akin to that of V_2, which was more susceptible than V_6 (Fig. 37(d)). The proposed dimensions of the adjusted sections were normalized by those of the B618-U girder (48 in. deep), as charted in Fig. 38. Except for the vertical portion of the upper web (V_8), all variable ratios associated with the invariant properties were less than unity (Fig. 38(a)), meaning that the elements of the proposed section were relatively small and thus a reduction in the self-weight of a new girder series would be expected. Figure 38(b) reveals the implications of other variables related to the web thickness. The intersection between the upper flange and the web (V_2) was consistently below a variable ratio of 1.0 at which the proposed and existing dimensions were equal; on the contrary, the lower flange components (V_5 and V_6) gradually went up and exceeded the threshold ratio of 1.0 at a web thickness of 6.5 in. The cross-sectional area and the moment of inertia of the tub girders, consisting of the aforementioned segmental variables, are shown in Figs. 39(a) and (b), respectively, as well as in Table 6. There was a remarkable gap between the cross-sectional areas of the B618-U and the optimized (Prototype-O) girders at a depth of 48 in. to 96 in. (Fig. 39(a)), and their difference became reduced with the increased web thickness (Prototype-5.5 to Prototype-7.5 representing a thickness of 5.5 in. to 7.5 in.). As the girder was deepened, the moment of inertia of B618-U diverged from that of the prototype sections (Fig. 39(b)). The patterns of the section moduli were comparable for the top and bottom fibers (S_t and S_b in Figs. 39(c) and (d), respectively). Since the B618-U sections maintained the moduli higher than the prototype sections, serviceability requirements need to be checked for the latter (to be explained in the parametric study section).

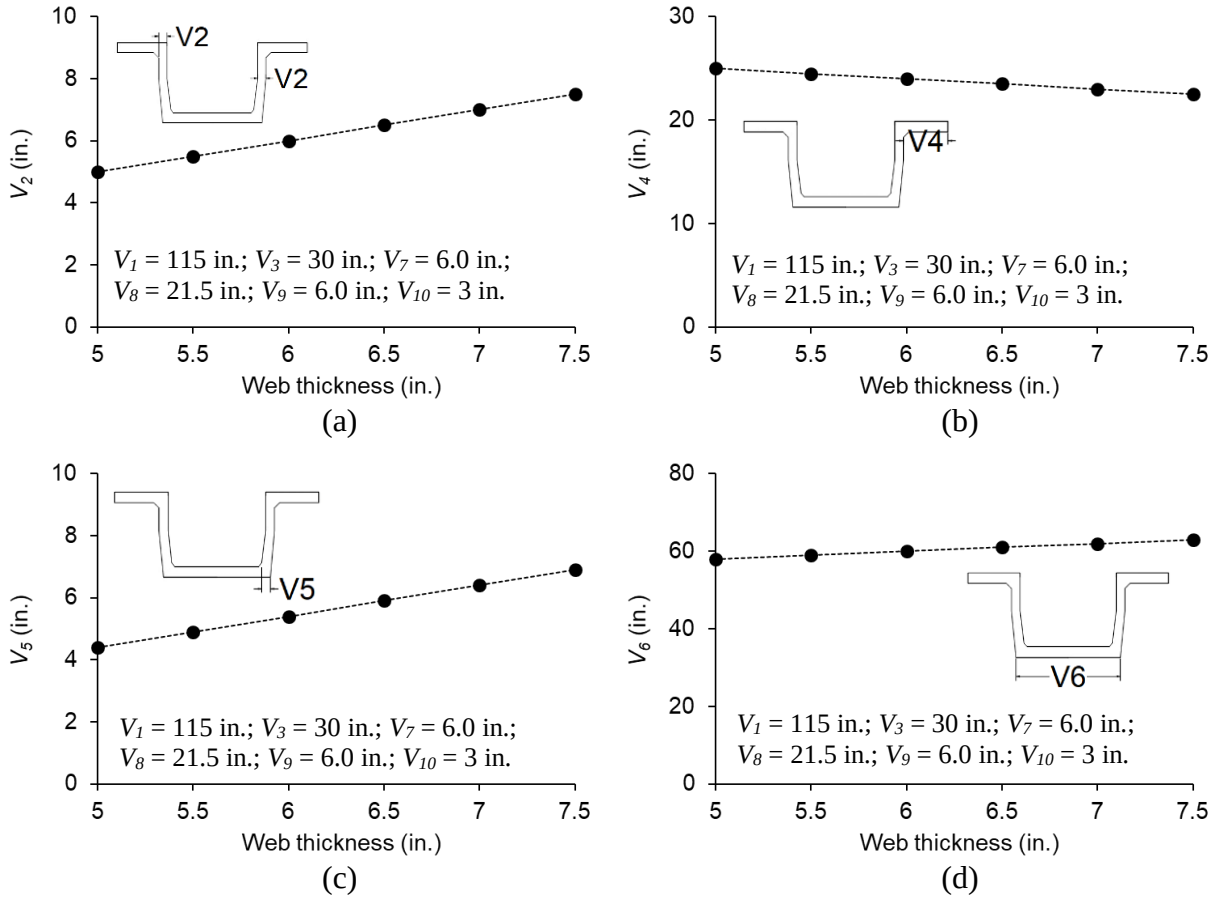

Fig. 37. Effects of web thickness on girder geometry (48 in. deep): (a) V_2; (b) V_4; (c) V_5; (d) V_6

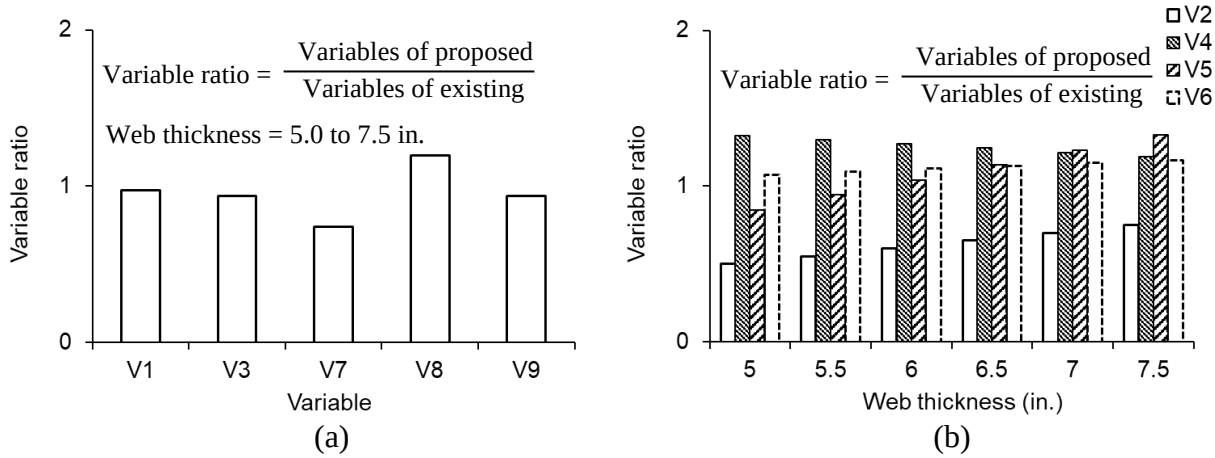

Fig. 38. Dimensional analysis (48 in. deep girder): (a) variables independent of web thickness; (b) variables dependent upon web thickness

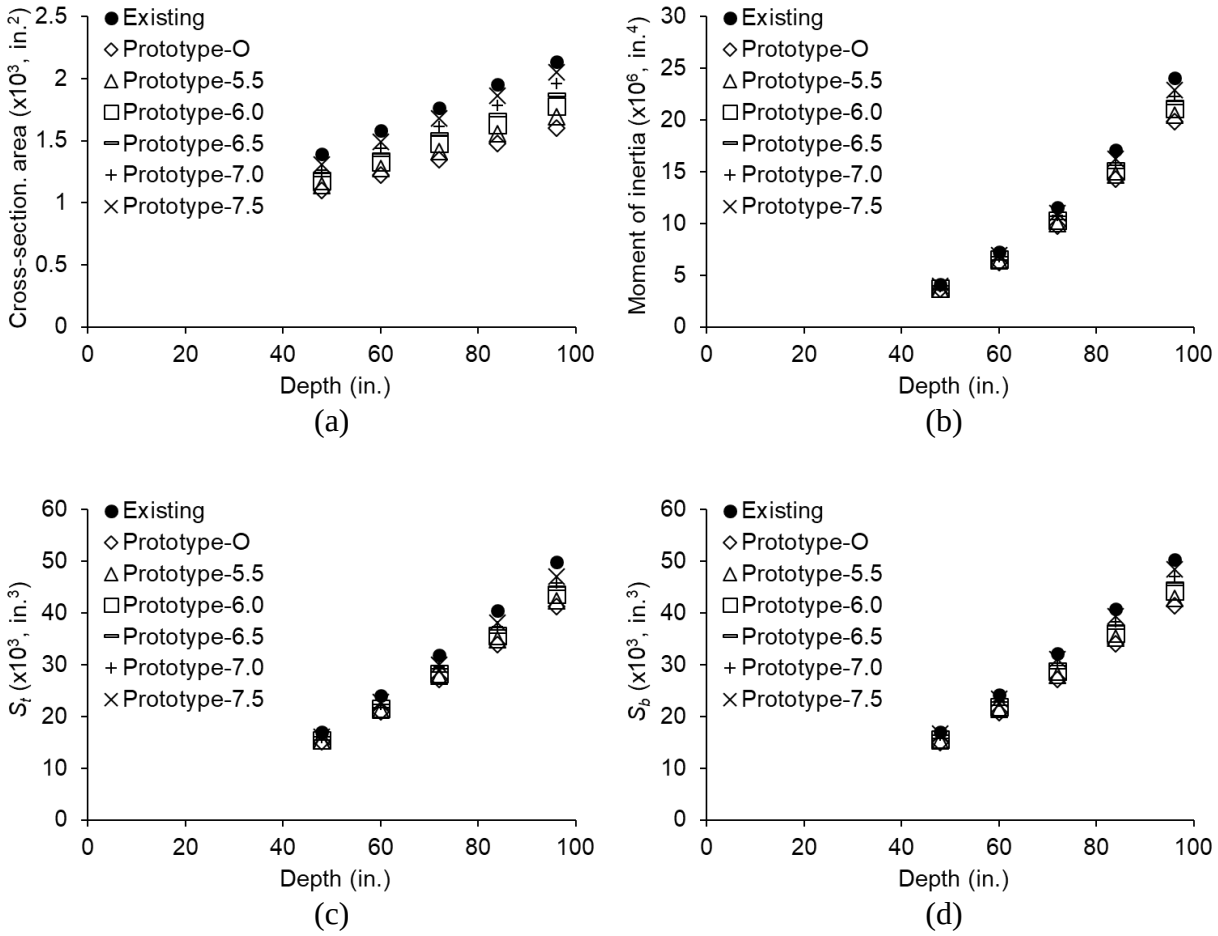

Fig. 39. Geometric properties of prototype girders: (a) cross-sectional area; (b) moment of inertia; (c) section modulus-top; (d) section modulus-bottom

Table 6. Properties of tub girders

Class	Girder type	Depth (in.)	Area ($in.^2$)	Inertia ($in.^4$)	y_t (in.)	y_b (in.)	S_t ($in.^3$)	S_b ($in.^3$)	r
Existing	U48	48	1,370.1	396,933.1	24.467	23.533	16,223.2	16,867.1	17.02
	U60	60	1,555.5	704,930.0	30.556	29.444	23,070.1	23,941.4	21.29
	U72	72	1,740.9	1,124,596.4	36.626	35.374	30,704.9	31,791.6	25.42
	U84	84	1,926.3	1,669,285.2	42.683	41.317	39,108.9	40,401.9	29.44
	U96	96	2,111.7	2,352,348.1	48.730	47.270	48,273.1	49,764.1	33.38
Prototype (P-O)	P(O)48	48	1,097.2	360,715.9	23.901	24.099	15,092.1	14,968.1	18.13
	P(O)60	60	1,223.2	624,769.8	29.935	30.065	20,870.9	20,780.6	22.60
	P(O)72	72	1,349.2	977,223.6	35.981	36.019	27,159.4	27,130.8	26.91
	P(O)84	84	1,475.2	1,427,144.2	42.035	41.965	33,951.3	34,008.0	31.10
	P(O)96	96	1,601.2	1,983,598.2	48.096	47.904	41,242.5	41,407.8	35.20
Prototype (P-5.5)	P(5.5)48	48	1,139.2	367,278.6	24.015	23.985	15,293.7	15,312.8	17.96
	P(5.5)60	60	1,277.2	638,377.7	30.065	29.935	21,233.3	21,325.5	22.36
	P(5.5)72	72	1,415.2	1,001,755.2	36.122	35.878	27,732.6	27,921.2	26.61
	P(5.5)84	84	1,553.2	1,467,341.6	42.184	41.816	34,784.3	35,090.4	30.74
	P(5.5)96	96	1,691.2	2,045,066.9	48.251	47.749	42,383.9	42,829.5	34.77
Prototype (P-6.0)	P(6.0)48	48	1,181.2	373,813.7	24.121	23.879	15,497.4	15,654.5	17.79
	P(6.0)60	60	1,331.2	651,946.3	30.184	29.816	21,599.1	21,865.7	22.13
	P(6.0)72	72	1,481.2	1,026,235.8	36.250	35.750	28,310.0	28,705.9	26.32
	P(6.0)84	84	1,631.2	1,507,476.6	42.319	41.681	35,621.7	36,167.0	30.40
	P(6.0)96	96	1,781.2	2,106,463.0	48.390	47.610	43,531.0	44,244.1	34.39
Prototype (P-6.5)	P(6.5)48	48	1,223.2	380,324.0	24.220	23.780	15,702.9	15,993.4	17.63
	P(6.5)60	60	1,385.2	665,480.0	30.294	29.706	21,967.4	22,402.2	21.92
	P(6.5)72	72	1,547.2	1,050,671.7	36.367	35.633	28,890.8	29,485.9	26.06
	P(6.5)84	84	1,709.2	1,547,557.8	42.441	41.559	36,463.7	37,237.6	30.09
	P(6.5)96	96	1,871.2	2,167,797.0	48.515	47.485	44,683.0	45,652.2	34.04
Prototype (P-7.0)	P(7.0)48	48	1,265.2	386,811.9	24.312	23.688	15,910.3	16,329.4	17.49
	P(7.0)60	60	1,439.2	678,982.8	30.395	29.605	22,338.6	22,934.7	21.72
	P(7.0)72	72	1,613.2	1,075,068.6	36.475	35.525	29,474.1	30,262.3	25.82
	P(7.0)84	84	1,787.2	1,587,592.4	42.553	41.447	37,308.6	38,304.2	29.80
	P(7.0)96	96	1,961.2	2,229,077.3	48.629	47.371	45,838.4	47,055.7	33.71
Prototype (P-7.5)	P(7.5)48	48	1,307.2	393,279.7	24.399	23.601	16,118.7	16,663.7	17.35
	P(7.5)60	60	1,493.2	692,458.1	30.489	29.511	22,711.7	23,464.4	21.53
	P(7.5)72	72	1,679.2	1,099,430.9	36.574	35.426	30,060.5	31,034.6	25.59
	P(7.5)84	84	1,865.2	1,627,586.1	42.655	41.345	38,157.0	39,366.0	29.54
	P(7.5)96	96	2,051.2	2,290,311.2	48.733	47.267	46,997.1	48,454.8	33.42

y_t and y_b = distances from neutral axis of girder to top and bottom, respectively; S_t and S_b = section moduli for top and bottom components, respectively; r = radius of gyration
P-O: prototype (optimized); P-number: prototype (web thickness in inches)

3.4. Assessment of Efficiency

Table 7 specifies the efficiency of the prototype girders. Irrespective of girder depth, the optimized Prototype-O sections outperformed B618-U (Figs. 40(a) and (b)). Regarding the prototype girders with the adjusted web size, the degree of betterment diminished as the web was widened. This observation is attributed to the fact that, despite the constant neutral axis depth, the increased moment of inertia tended to be offset by the enlarged cross-sectional area in Eqs. 1 and 2. The normalized efficiency factors shown in Fig. 40(c) clarify the structural advantage of the prototype girders; specifically, the efficiency factor and ratio of the tub girders were improved by 12.9% and 10.1%, respectively, on average (Fig. 40(d)). Furthermore, the unit weight of the prototype girders was lowered prominently in comparison with that of B618-U (Fig. 41(a)), which would save construction expense by lessening dead load. The extent of an average weight reduction was 22.3% for Prototype-O and 3.7% for Prototype-7.5 (Fig. 41(b)).

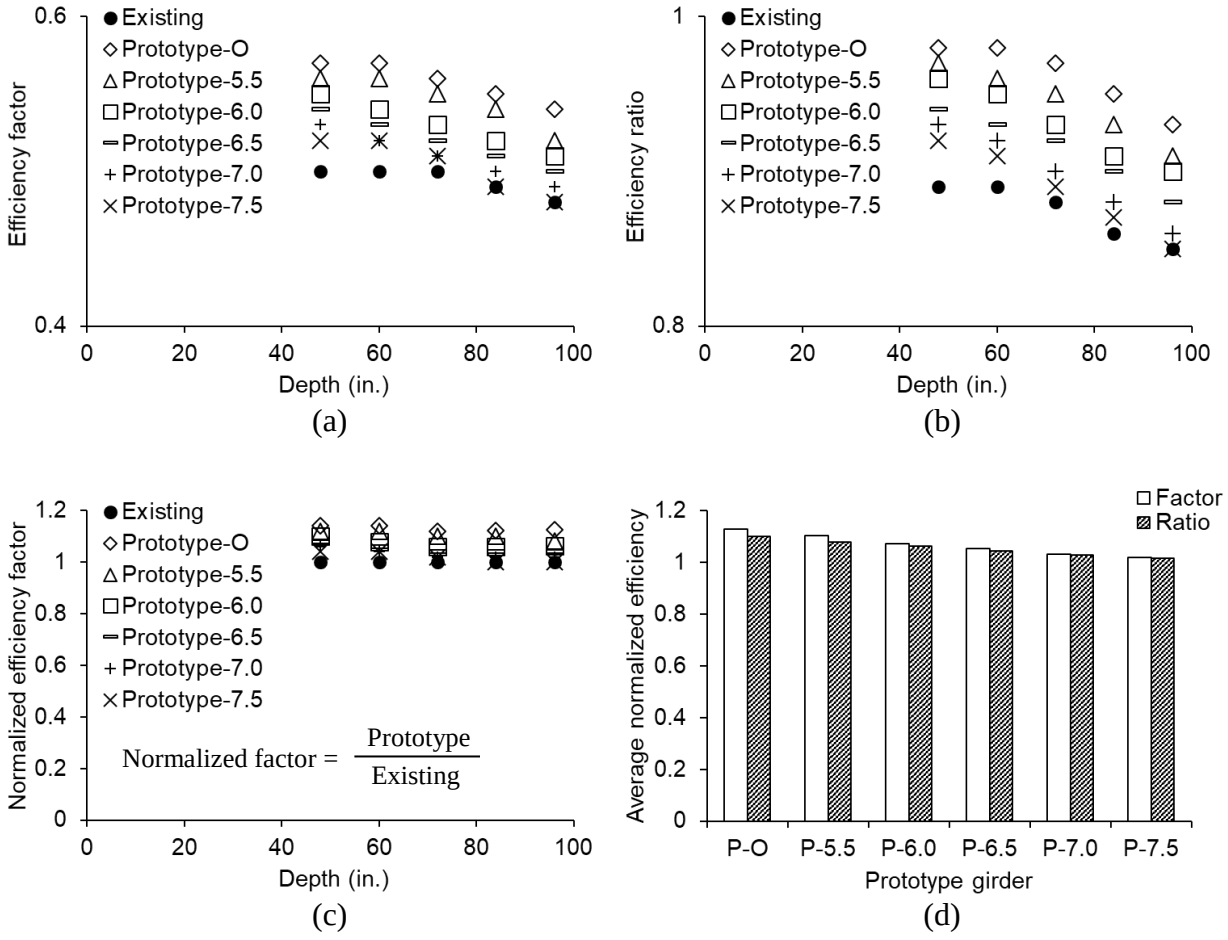

Fig. 40. Evaluation of efficiency: (a) factor; (b) ratio; (c) normalized factor; (d) average efficiency

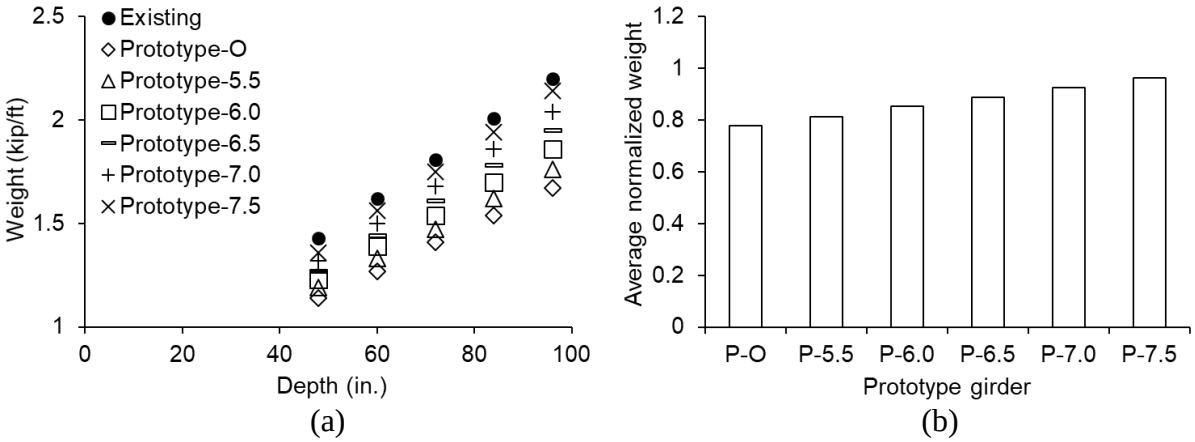

Fig. 41. Assessment of prototype girders: (a) unit weight; (b) average of normalized unit weight

Table 7. Comparison of structural efficiency between existing Colorado and prototype girders

Class	Girder type	Depth (in.)	Efficiency factor (ρ)	Efficiency ratio (α)	Weight (kips/ft)
Existing	U48	48	0.50	0.89	1.43
	U60	60	0.50	0.89	1.62
	U72	72	0.50	0.88	1.81
	U84	84	0.49	0.86	2.01
	U96	96	0.48	0.85	2.20
Prototype-O	P(O)48	48	0.57	0.98	1.14
	P(O)60	60	0.57	0.98	1.27
	P(O)72	72	0.56	0.97	1.41
	P(O)84	84	0.55	0.95	1.54
	P(O)96	96	0.54	0.93	1.67
Prototype-5.5	P(5.5)48	48	0.56	0.97	1.19
	P(5.5)60	60	0.56	0.96	1.33
	P(5.5)72	72	0.55	0.95	1.47
	P(5.5)84	84	0.54	0.93	1.62
	P(5.5)96	96	0.52	0.91	1.76
Prototype-6.0	P(6.0)48	48	0.55	0.96	1.23
	P(6.0)60	60	0.54	0.95	1.39
	P(6.0)72	72	0.53	0.93	1.54
	P(6.0)84	84	0.52	0.91	1.70
	P(6.0)96	96	0.51	0.90	1.86
Prototype-6.5	P(6.5)48	48	0.54	0.94	1.27
	P(6.5)60	60	0.53	0.93	1.44
	P(6.5)72	72	0.52	0.92	1.61
	P(6.5)84	84	0.51	0.90	1.78
	P(6.5)96	96	0.50	0.88	1.95
Prototype-7.0	P(7.0)48	48	0.53	0.93	1.32
	P(7.0)60	60	0.52	0.92	1.50
	P(7.0)72	72	0.51	0.90	1.68
	P(7.0)84	84	0.50	0.88	1.86
	P(7.0)96	96	0.49	0.86	2.04
Prototype-7.5	P(7.5)48	48	0.52	0.92	1.36
	P(7.5)60	60	0.52	0.91	1.56
	P(7.5)72	72	0.51	0.89	1.75
	P(7.5)84	84	0.49	0.87	1.94
	P(7.5)96	96	0.48	0.85	2.14

4. Parametric Investigations

A parametric study is conducted to examine the compliance of the prototype girders developed in a previous task (Fig. 32) against the requirements of AASHTO LRFD BDS (AASHTO 2020), including the serviceability and ultimate limit states. A total of ten section types are evaluated with an overall depth varying from 48 in. to 96 in.: the U and P girder series indicate the existing B618-U and the prototype girders, respectively. On average, the structural efficiency of the P girders is 12.9% higher than that of the U girders. The configuration of bridge superstructures is composed of one to four traffic lanes supported by one to four tub girders (Fig. 42). For consistency, an overhang of six feet is used (CDOT Bridge Design Manual), while the width of shoulders is determined in accordance with the AASHTO and FHWA guidelines. Based on the geometric details of the girders enumerated in Tables 8 to 12, the maximum achievable span lengths and load effects are calculated (Tables 13 to 16). As illustrated in Fig. 43, the prototype girders offer longer spans with almost the same number of steel strands relative to their B618-U counterparts. The prototype girders satisfy the serviceability requirements of AASHTO LRFD BDS (Figs. 44 and 45 where average stresses and deflections are displayed). Figure 46 exhibits unfactored load effects (dead and live loads) and factored load effects vs. flexural capacities of the girder sections. Summarized in Fig. 47 are the average responses of the girders, considering span length, in order to display the superior performance of the prototype girders. The supplementary information of all girders is visible in Figs. 48 through 83, which are the source of the average plots provided in Figs. 43 to 47.

Table 8. Geometric details of superstructure with one lane and one girder

Class	Type	Total width (ft)	Number of girders	Each overhang (ft)	Each shoulder (ft)	V_1 (in.)	V_2 (in.)	V_3 (in.)
Existing	U48	17.33	1	6	1.2	115	10	30
	U60	17.83	1	6	1.4	121	10	30
	U72	18.33	1	6	1.7	127	10	30
	U84	18.83	1	6	1.9	133	10	30
	U96	19.33	1	6	2.2	139	10	30
Prototype	P48	17.42	1	6	1.2	115	30	10
	P60	17.75	1	6	1.4	119	30	10
	P72	18.00	1	6	1.5	122	30	10
	P84	18.33	1	6	1.7	126	30	10
	P96	18.58	1	6	1.8	129	30	10

Table 9. Geometric details of superstructure with two lanes and two girders

Class	Type	Total width (ft)	Number of girders	Each overhang (ft)	Girder spacing (ft)	V_1 (in.)	V_2 (in.)	V_3 (in.)
Existing	U48	43	2	6	25.7	115	10	30
	U60	43	2	6	25.2	121	10	30
	U72	43	2	6	24.7	127	10	30
	U84	43	2	6	24.2	133	10	30
	U96	43	2	6	23.7	139	10	30
Prototype	P48	43	2	6	25.6	115	30	10
	P60	43	2	6	25.3	119	30	10
	P72	43	2	6	25.0	122	30	10
	P84	43	2	6	24.7	126	30	10
	P96	43	2	6	24.4	129	30	10

Table 10. Geometric details of superstructure with two lanes and three girders

Class	Type	Total width (ft)	Number of girders	Each overhang (ft)	Girder spacing (ft)	V_1 (in.)	V_2 (in.)	V_3 (in.)
Existing	U48	43	3	6	12.8	115	10	30
	U60	43	3	6	12.6	121	10	30
	U72	43	3	6	12.3	127	10	30
	U84	43	3	6	12.1	133	10	30
	U96	43	3	6	12.0	139	10	30
Prototype	P48	43	3	6	12.8	115	30	10
	P60	43	3	6	12.6	119	30	10
	P72	43	3	6	12.5	122	30	10
	P84	43	3	6	12.3	126	30	10
	P96	43	3	6	12.2	129	30	10

Table 11. Geometric details of superstructure with three lanes and three girders

Class	Type	Total width (ft)	Number of girders	Each overhang (ft)	Girder spacing (ft)	V_1 (in.)	V_2 (in.)	V_3 (in.)
Existing	U48	55	3	6	18.8	115	10	30
	U60	55	3	6	18.6	121	10	30
	U72	55	3	6	18.3	127	10	30
	U84	55	3	6	18.1	133	10	30
	U96	55	3	6	17.8	139	10	30
Prototype	P48	55	3	6	18.8	115	30	10
	P60	55	3	6	18.6	119	30	10
	P72	55	3	6	18.5	122	30	10
	P84	55	3	6	18.3	126	30	10
	P96	55	3	6	18.2	129	30	10

Table 12. Geometric details of superstructure with four lanes and four girders

Class	Type	Total width (ft)	Number of girders	Each overhang (ft)	Girder spacing (ft)	V_1 (in.)	V_2 (in.)	V_3 (in.)
Existing	U48	67	4	6	16.6	115	10	30
	U60	67	4	6	16.4	121	10	30
	U72	67	4	6	16.2	127	10	30
	U84	67	4	6	16.1	133	10	30
	U96	67	4	6	15.9	139	10	30
Prototype	P48	67	4	6	16.5	115	30	10
	P60	67	4	6	16.4	119	30	10
	P72	67	4	6	16.3	122	30	10
	P84	67	4	6	16.2	126	30	10
	P96	67	4	6	16.1	129	30	10

Table 13. Structural configuration of girders

Number of lanes	Number of girders	Girder type	Max. span (ft)	Number of strands	Number of lanes	Number of girders	Girder type	Max. span (ft)	Number of strands
1	1	U48	95	52	2	3	P48	98	60
1	1	U60	110	58	2	3	P60	115	66
1	1	U72	125	68	2	3	P72	130	72
1	1	U84	138	74	2	3	P84	145	80
1	1	U96	152	90	2	3	P96	158	86
1	1	P48	100	60	3	3	U48	90	54
1	1	P60	115	64	3	3	U60	105	65
1	1	P72	130	70	3	3	U72	120	76
1	1	P84	145	80	3	3	U84	133	84
1	1	P96	158	86	3	3	U96	145	88
2	2	U48	85	54	3	3	P48	93	60
2	2	U60	100	64	3	3	P60	108	66
2	2	U72	115	76	3	3	P72	123	72
2	2	U84	128	84	3	3	P84	137	76
2	2	U96	140	90	3	3	P96	150	84
2	2	P48	85	50	4	4	U48	90	46
2	2	P60	100	56	4	4	U60	108	54
2	2	P72	115	66	4	4	U72	120	68
2	2	P84	130	76	4	4	U84	135	82
2	2	P96	145	86	4	4	U96	148	92
2	3	U48	95	58	4	4	P48	93	56
2	3	U60	110	60	4	4	P60	110	66
2	3	U72	125	72	4	4	P72	125	72
2	3	U84	138	74	4	4	P84	140	80
2	3	U96	150	86	4	4	P96	153	86

Max. span = maximum achievable span as per the requirements of the AASHTO LRFD Bridge Design Specifications

Table 14. Load effects and capacity of girders under flexure (one and two girders)

Number of lanes	Number of girders	Girder type	Unfactored load components		Factored load effects (k-ft)	Factored resistance (k-ft)
			Dead (k-ft)	Live (k-ft)		
1	1	U48	4,191	2,565	9,728	12,182
1	1	U60	6,003	3,167	13,046	16,415
1	1	U72	8,243	3,804	16,961	21,956
1	1	U84	10,522	4,386	20,828	27,317
1	1	U96	13,623	5,043	25,854	35,412
1	1	P48	4,288	2,762	10,194	13,232
1	1	P60	5,964	3,375	13,361	17,395
1	1	P72	7,964	4,025	16,999	22,303
1	1	P84	10,363	4,710	21,196	28,504
1	1	P96	12,801	5,334	25,336	34,561
2	2	U48	3,422	3,717	10,782	12,579
2	2	U60	4,998	4,738	14,539	17,523
2	2	U72	6,949	5,840	18,906	23,428
2	2	U84	9,019	6,869	23,295	29,372
2	2	U96	11,277	7,885	27,895	35,547
2	2	P48	3,153	3,722	10,455	11,957
2	2	P60	4,552	4,732	13,971	16,140
2	2	P72	6,252	5,806	17,976	21,683
2	2	P84	8,292	6,963	22,550	27,881
2	2	P96	10,675	8,182	27,662	34,732

Table 15. Load effects and capacity of exterior girders under flexure (more than three girders)

Number of lanes	Number of girders	Girder type	Unfactored load components		Factored load effects (k-ft)	Factored resistance (k-ft)
			Dead (k-ft)	Live (k-ft)		
2	3	U48	3,546	3,654	10,827	13,333
2	3	U60	4,978	4,531	14,152	16,654
2	3	U72	6,843	5,554	18,273	22,485
2	3	U84	8,841	6,535	22,488	27,141
2	3	U96	11,057	7,561	27,053	34,327
2	3	P48	3,341	3,776	10,784	13,132
2	3	P60	4,852	4,816	14,493	17,549
2	3	P72	6,500	5,796	18,268	22,478
2	3	P84	8,473	6,877	22,626	28,288
2	3	P96	10,495	7,863	26,879	34,299
3	3	U48	3,403	3,781	10,871	12,498
3	3	U60	4,931	4,783	14,534	17,700
3	3	U72	6,827	5,872	18,810	23,280
3	3	U84	8,243	7,104	22,736	27,734
3	3	U96	11,075	7,926	27,714	34,971
3	3	P48	3,317	3,972	11,097	13,257
3	3	P60	4,698	4,970	14,570	17,699
3	3	P72	6,364	6,028	18,504	22,656
3	3	P84	8,002	6,955	22,174	27,317
3	3	P96	10,277	8,150	27,109	34,118
4	4	U48	3,239	3,221	9,686	11,168
4	4	U60	4,989	4,248	13,670	15,633
4	4	U72	6,546	5,703	18,163	21,908
4	4	U84	8,779	6,869	22,995	28,800
4	4	U96	11,137	7,975	27,878	35,647
4	4	P48	3,142	3,835	10,639	12,736
4	4	P60	4,633	4,937	14,431	17,650
4	4	P72	6,265	5,978	18,293	22,599
4	4	P84	8,229	7,117	22,741	28,437
4	4	P96	10,243	8,157	27,079	34,472

Table 16. Load effects and capacity of interior girders under flexure (more than three girders)

Number of lanes	Number of girders	Girder type	Unfactored load components		Factored load effects (k-ft)	Factored resistance (k-ft)
			Dead (k-ft)	Live (k-ft)		
2	3	U48	3,294	2,107	7,805	8,997
2	3	U60	4,591	2,509	10,130	11,669
2	3	U72	6,270	4,523	15,753	18,076
2	3	U84	8,054	5,141	19,064	21,737
2	3	U96	10,045	5,771	22,656	26,321
2	3	P48	3,071	2,155	7,610	8,977
2	3	P60	4,439	2,652	10,190	11,670
2	3	P72	5,932	4,830	15,868	18,086
2	3	P84	7,700	5,601	19,427	22,946
2	3	P96	9,520	6,299	22,923	27,017
3	3	U48	3,476	3,486	10,446	12,518
3	3	U60	4,981	4,330	13,804	16,439
3	3	U72	6,826	5,218	17,664	21,573
3	3	U84	8,771	6,018	21,495	25,930
3	3	U96	10,880	6,779	25,463	31,073
3	3	P48	3,389	3,652	10,627	13,047
3	3	P60	4,759	4,514	13,848	16,791
3	3	P72	6,410	5,425	17,506	21,175
3	3	P84	8,242	6,313	21,350	26,420
3	3	P96	10,226	7,177	25,342	31,092
4	4	U48	3,200	2,348	8,109	9,069
4	4	U60	4,886	2,974	11,312	12,843
4	4	U72	6,360	4,964	16,637	19,272
4	4	U84	8,469	5,853	20,829	24,819
4	4	U96	10,674	6,650	24,980	30,392
4	4	P48	3,096	2,439	8,138	9,069
4	4	P60	4,535	3,044	10,996	12,844
4	4	P72	6,106	5,279	16,871	19,759
4	4	P84	7,975	6,195	20,810	24,827
4	4	P96	9,893	7,027	24,664	29,817

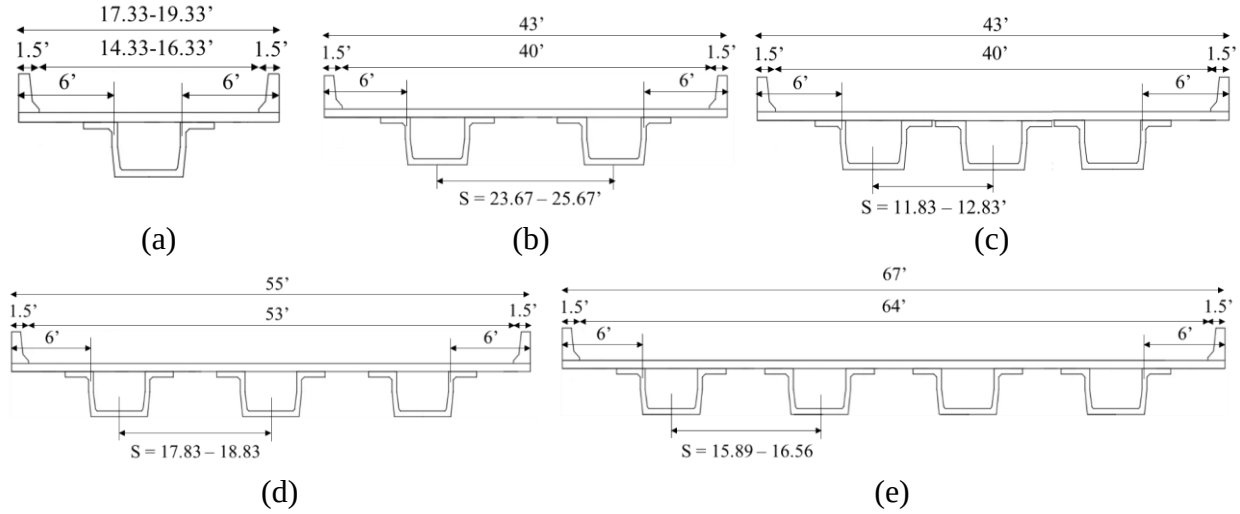

Fig. 42. Configuration of superstructure (units in ft): (a) one lane with one girder; (b) two lanes with two girders; (c) two lanes with three girders; (d) three lanes with three girders; (e) four lanes with four girders

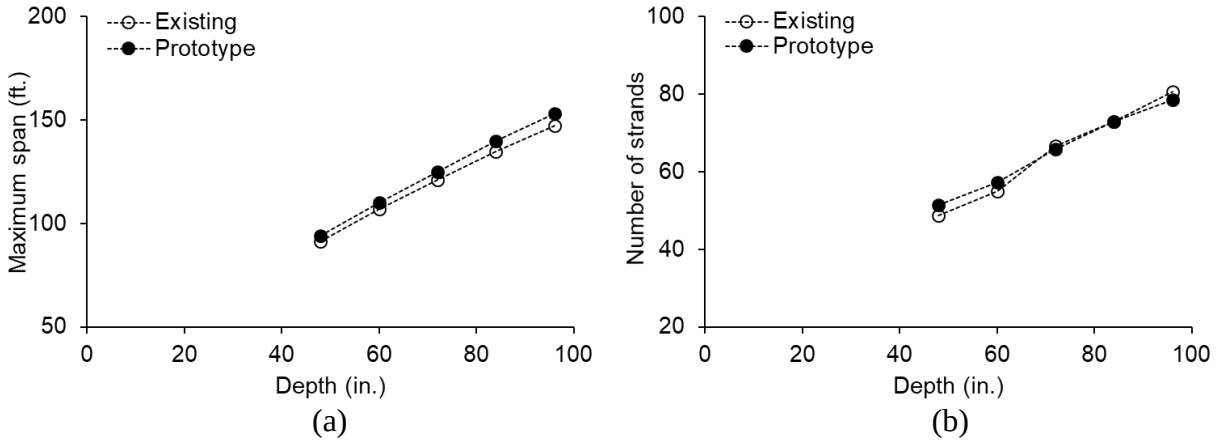

Fig. 43. Average configuration of girders: (a) maximum achievable span; (b) number of strands

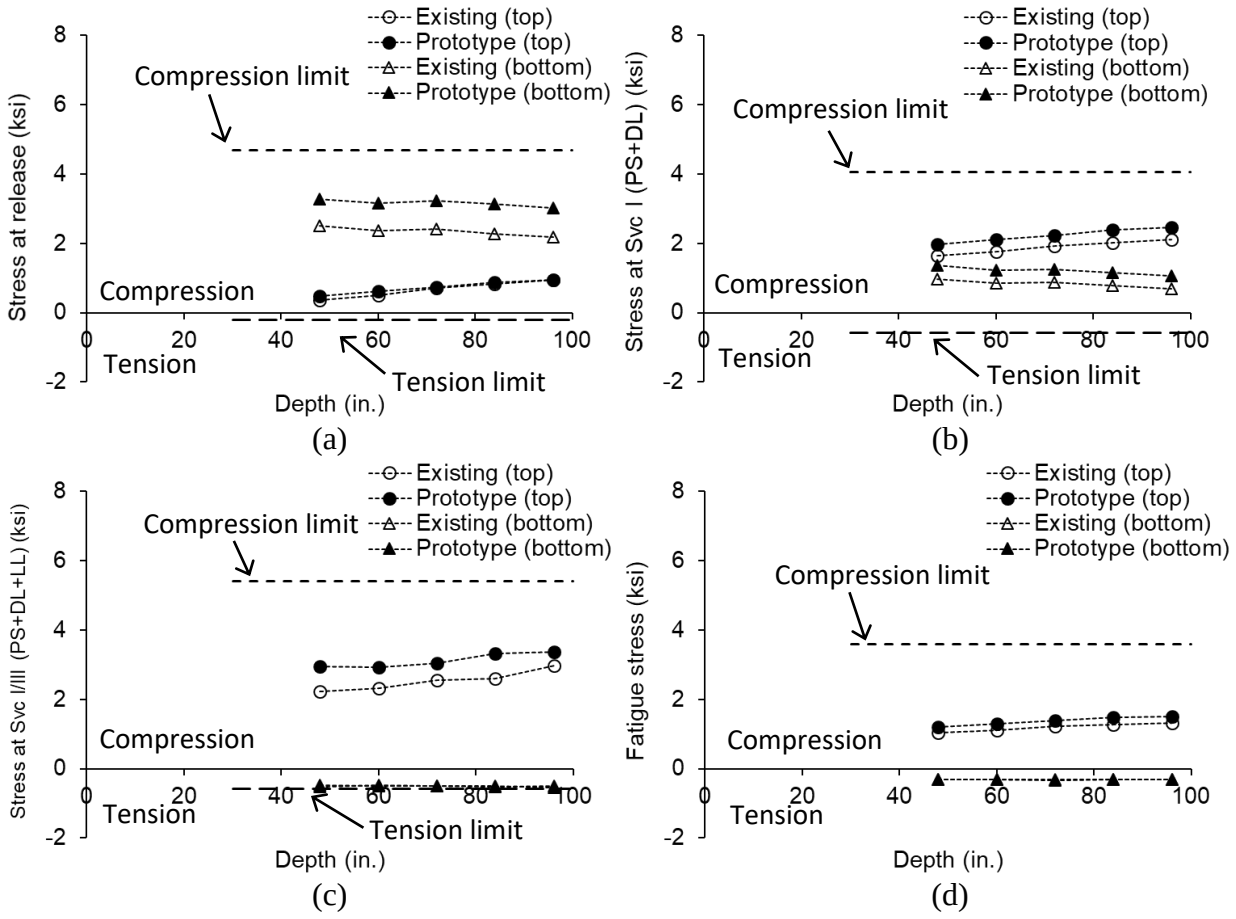

Fig. 44. Average stress variation: (a) release; (b) Service I (PS+DL); (c) Service I/III (PS+DL+LL); (d) fatigue

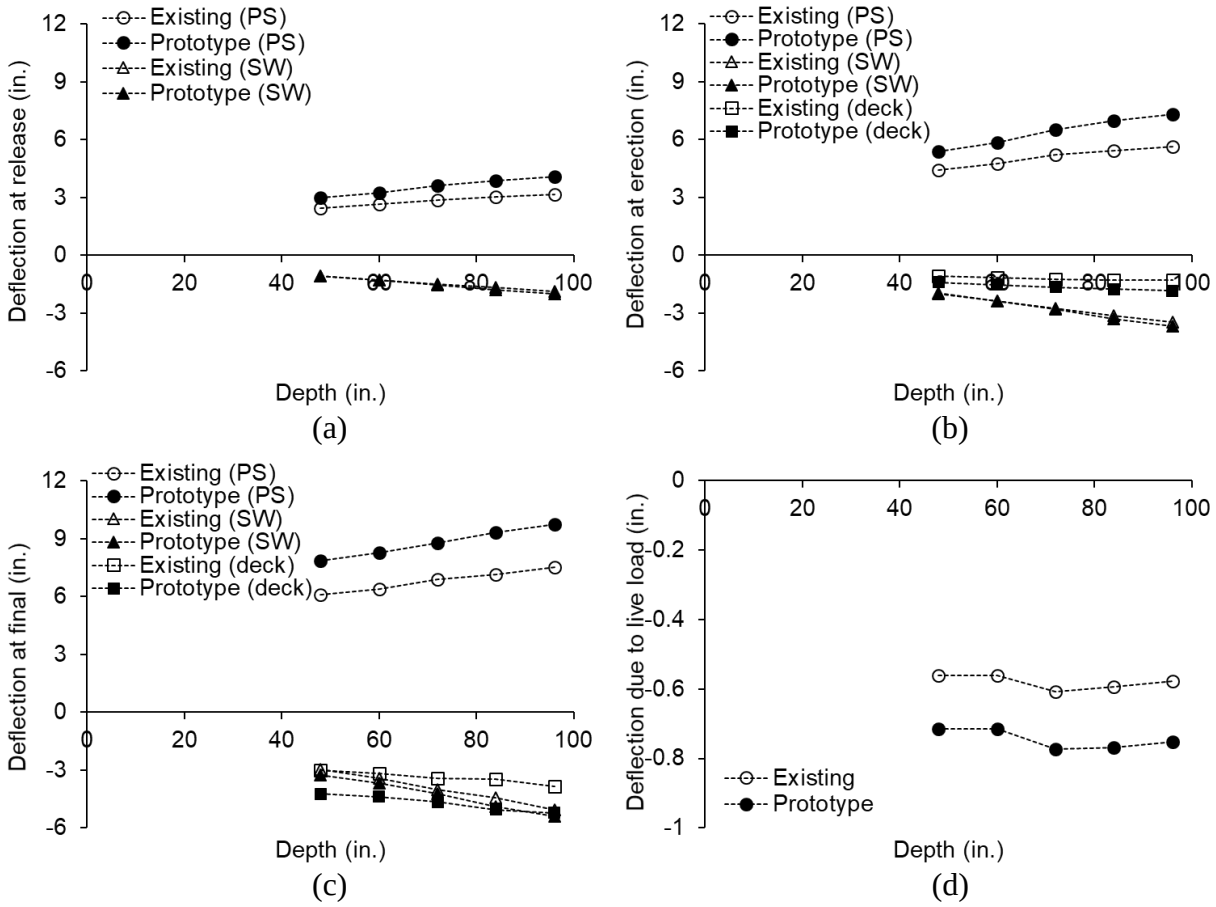

Fig. 45. Average deflection: (a) release; (b) erection; (c) final; (d) due to live load

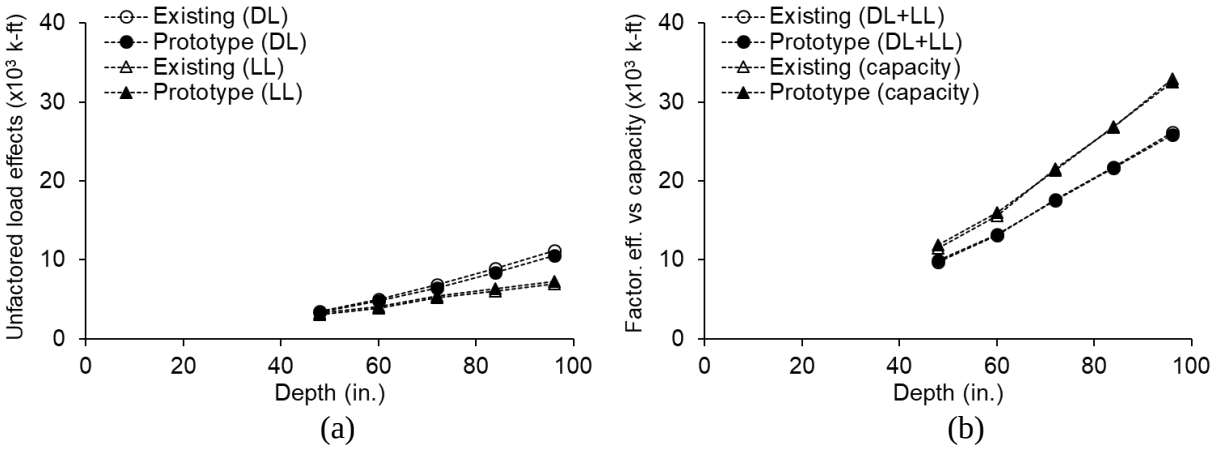

Fig. 46. Average ultimate limit state without considering span length: (a) unfactored load effects; (b) factored load effects versus capacity

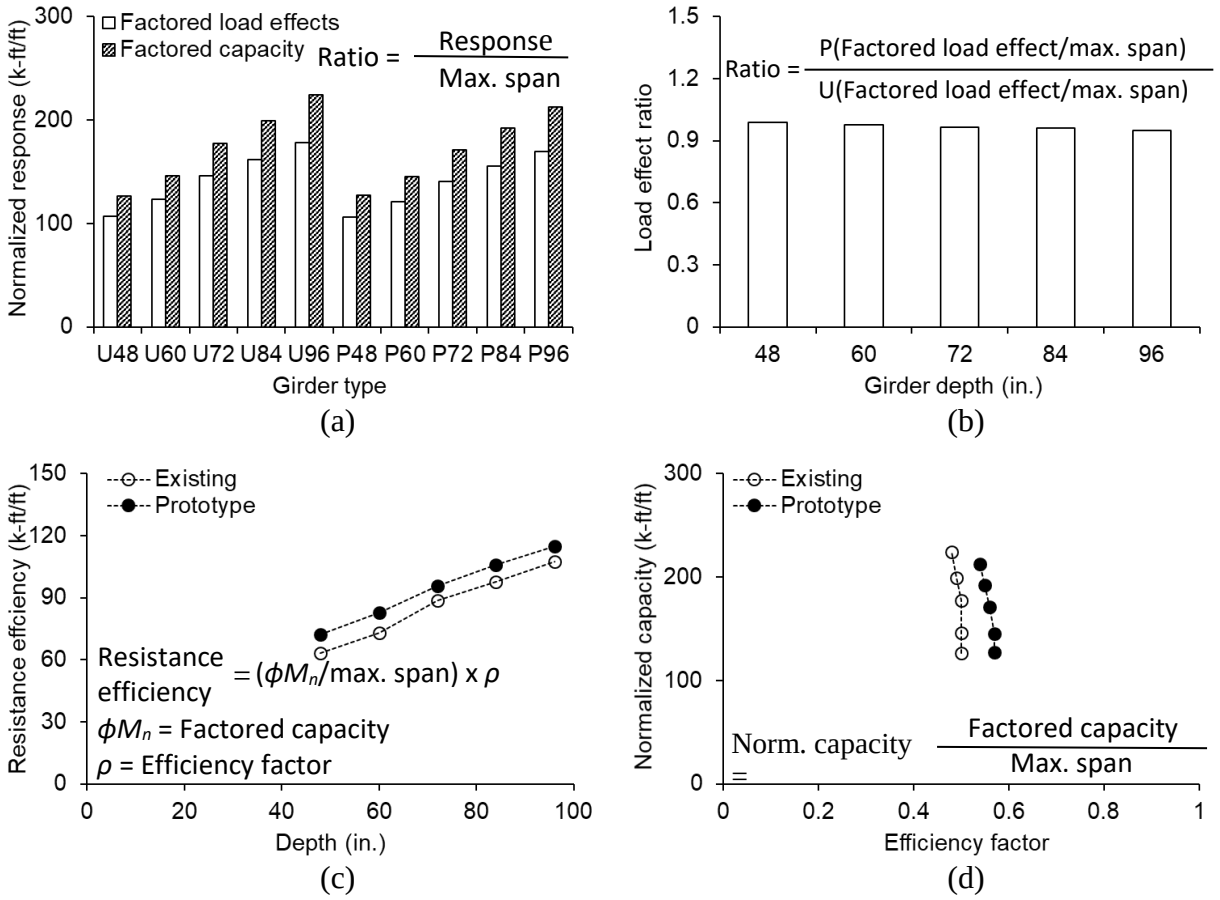

Fig. 47. Average response with considering span length: (a) normalized factored response; (b) load effect ratio; (c) resistance efficiency; (d) capacity vs. efficiency factor

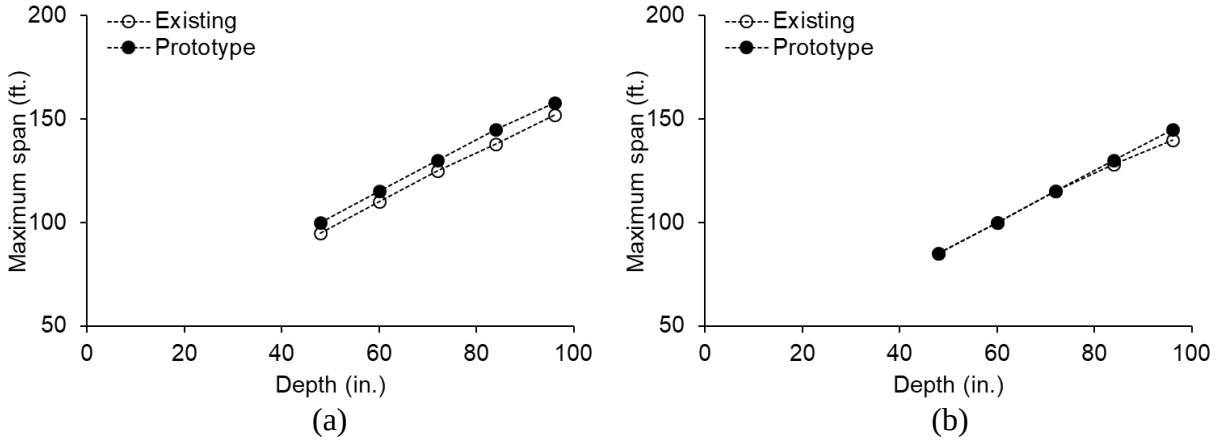

Fig. 48. Maximum achievable span length for one and two girders: (a) one lane with one girder; (b) two lanes with two girders

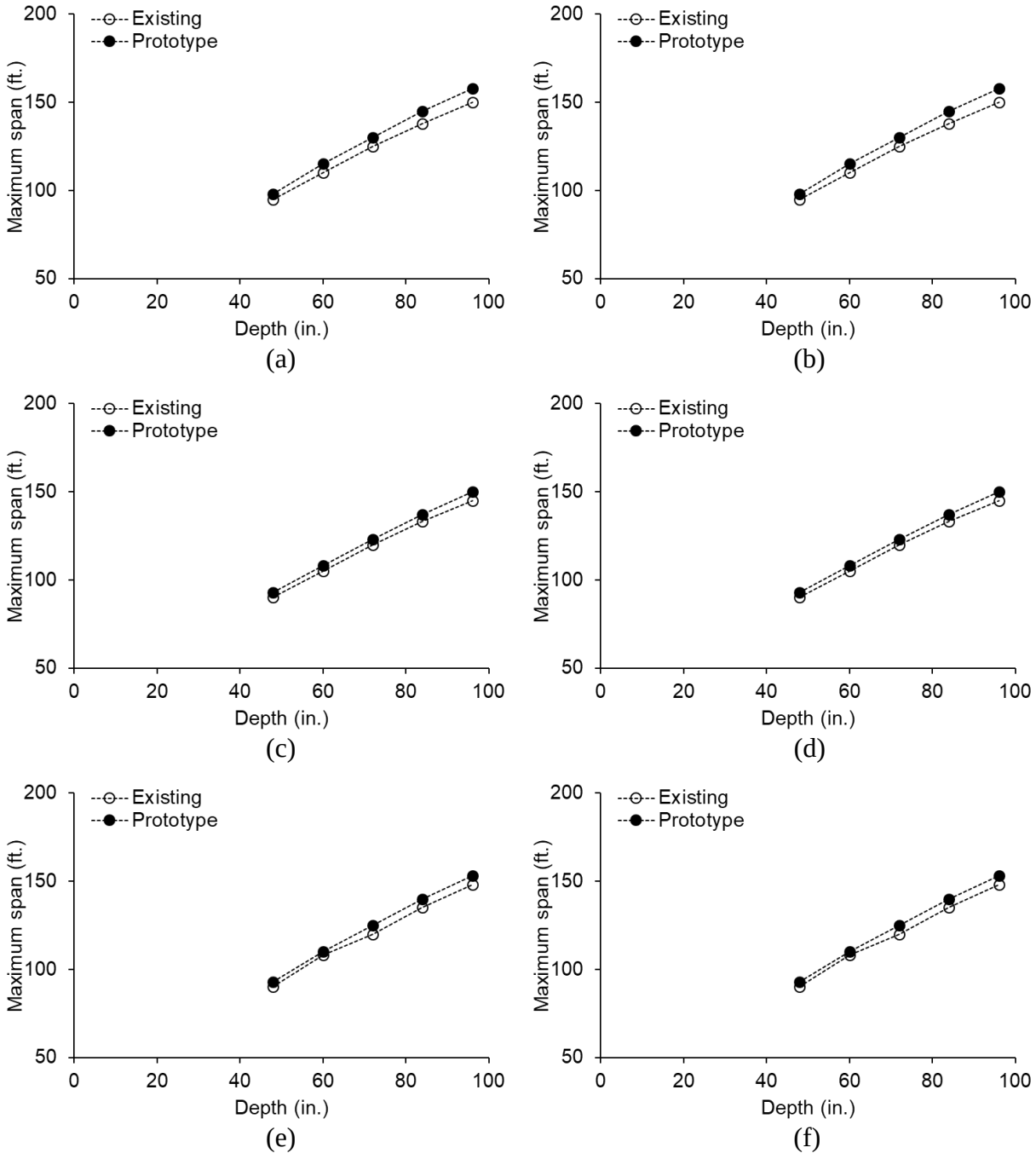

Fig. 49. Maximum achievable span length for three and four girders: (a) two lanes with three girders for exterior girder; (b) two lanes with three girders for interior girder; (c) three lanes with three girders for exterior girder; (d) three lanes with three girders for interior girder; (e) four lanes with four girders for exterior girder; (f) four lanes with four girders for interior girder

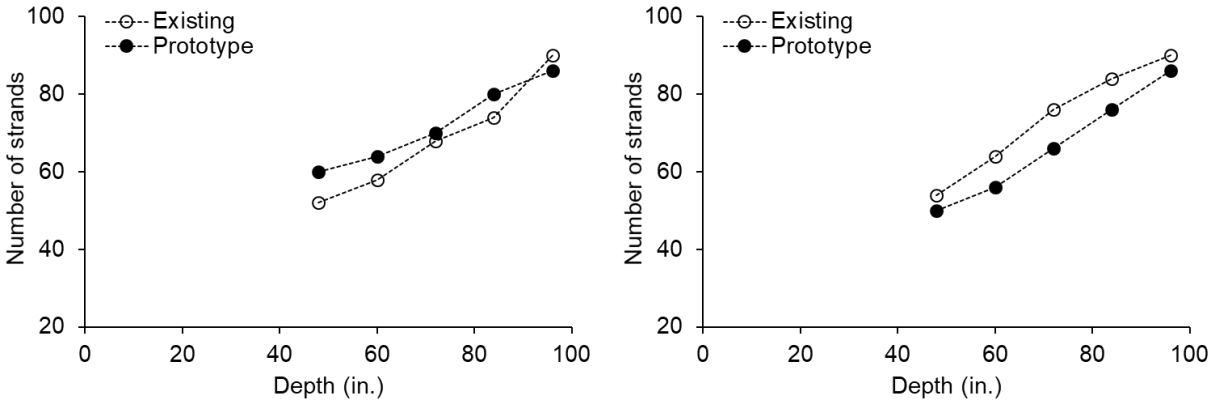

Fig. 50. Number of strands for one and two girders: (a) one lane with one girder; (b) two lanes with two girders

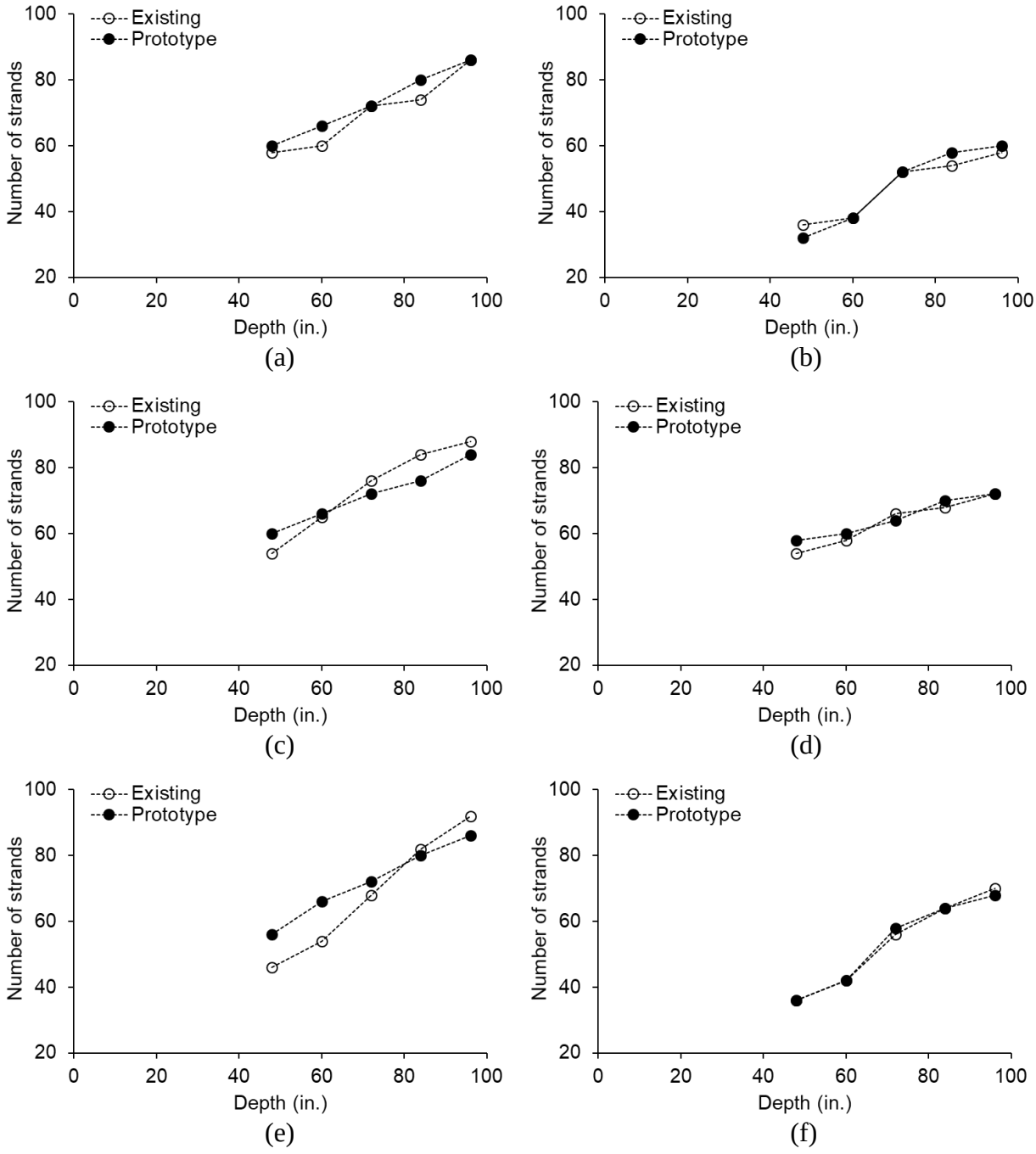

Fig. 51. Number of strands for three and four girders: (a) two lanes with three girders for exterior girder; (b) two lanes with three girders for interior girder; (c) three lanes with three girders for exterior girder; (d) three lanes with three girders for interior girder; (e) four lanes with four girders for exterior girder; (f) four lanes with four girders for interior girder

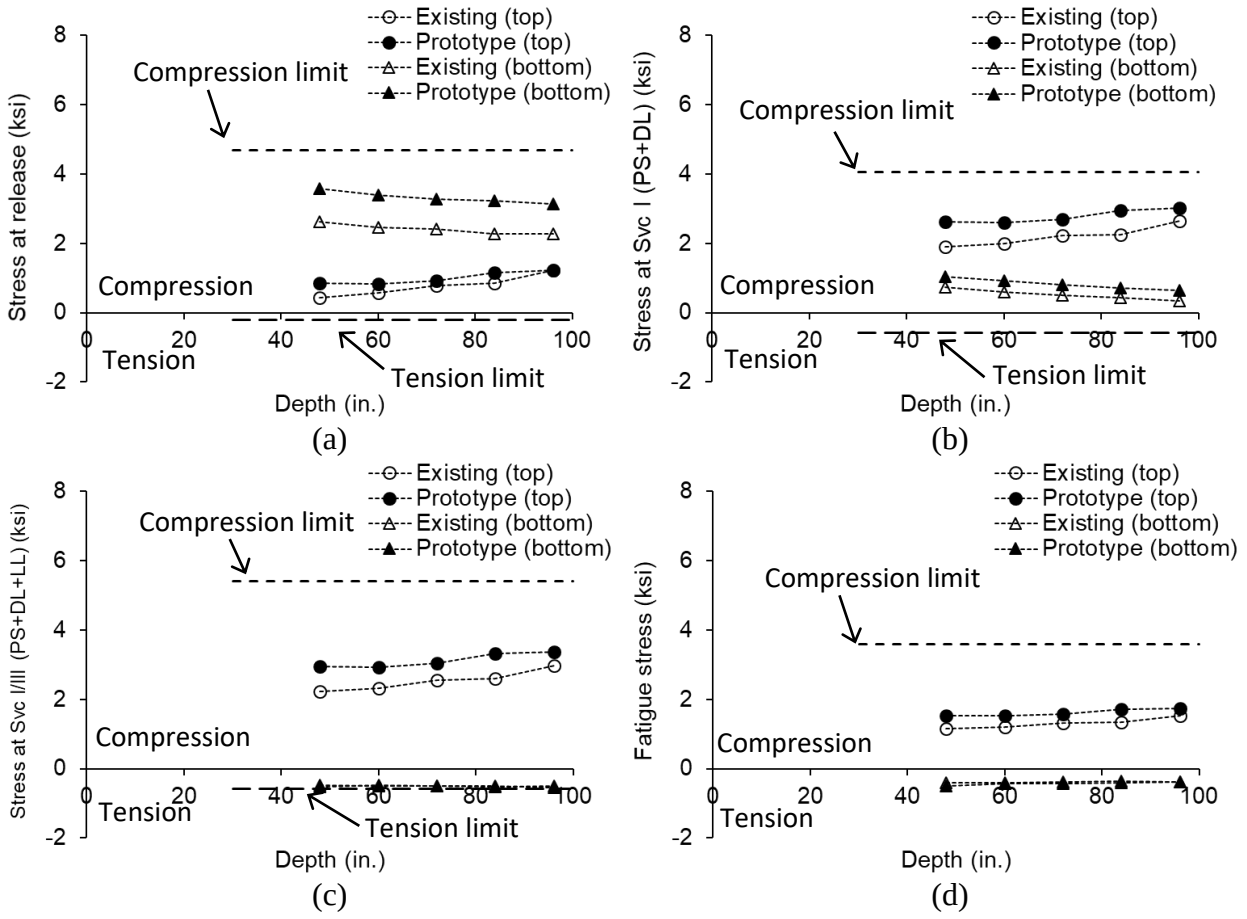

Fig. 52. Stress variation for one lane with one girder: (a) release; (b) Service I (PS+DL); (c) Service I/III (PS+DL+LL); (d) fatigue

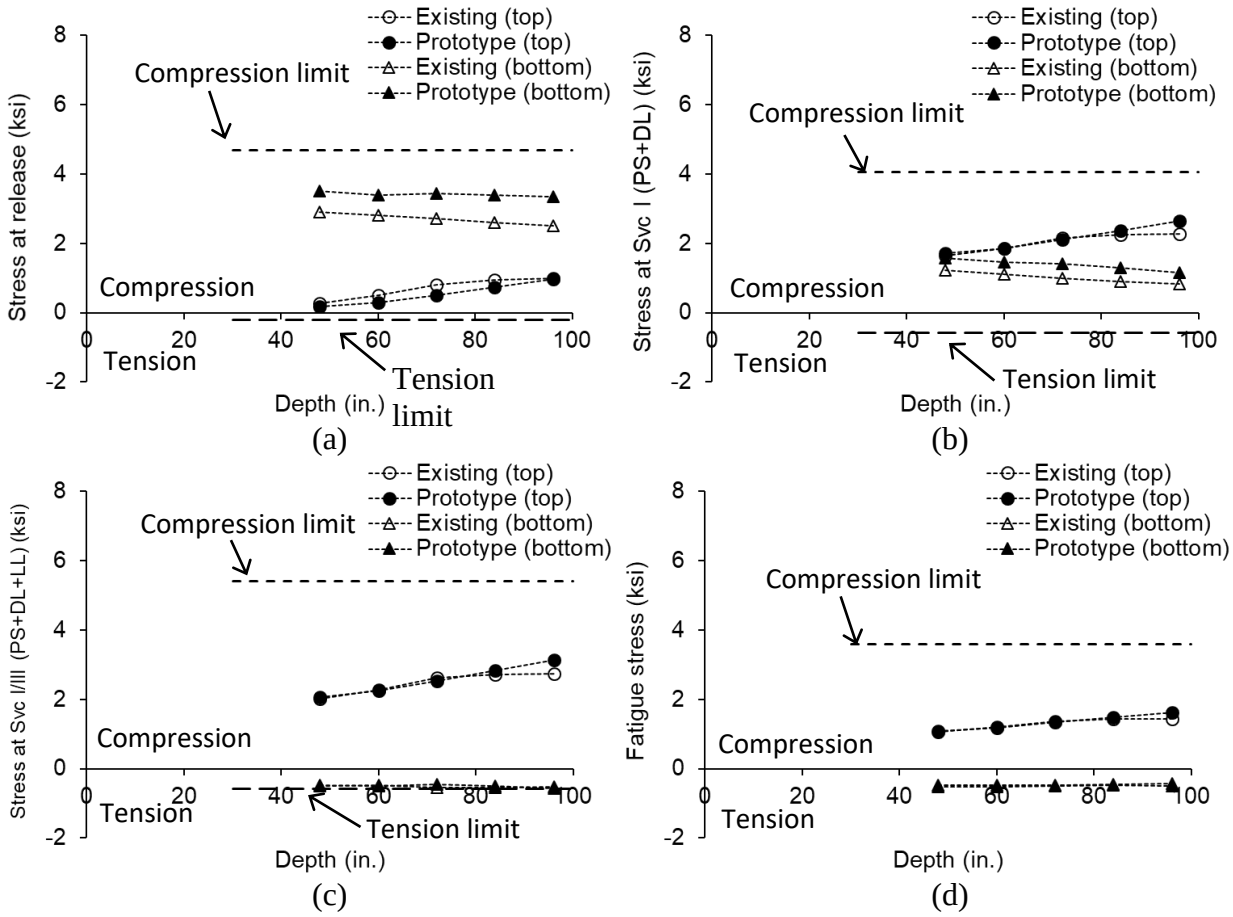

Fig. 53. Stress variation for two lanes with two girders: (a) release; (b) Service I (PS+DL); (c) Service I/III (PS+DL+LL); (d) fatigue

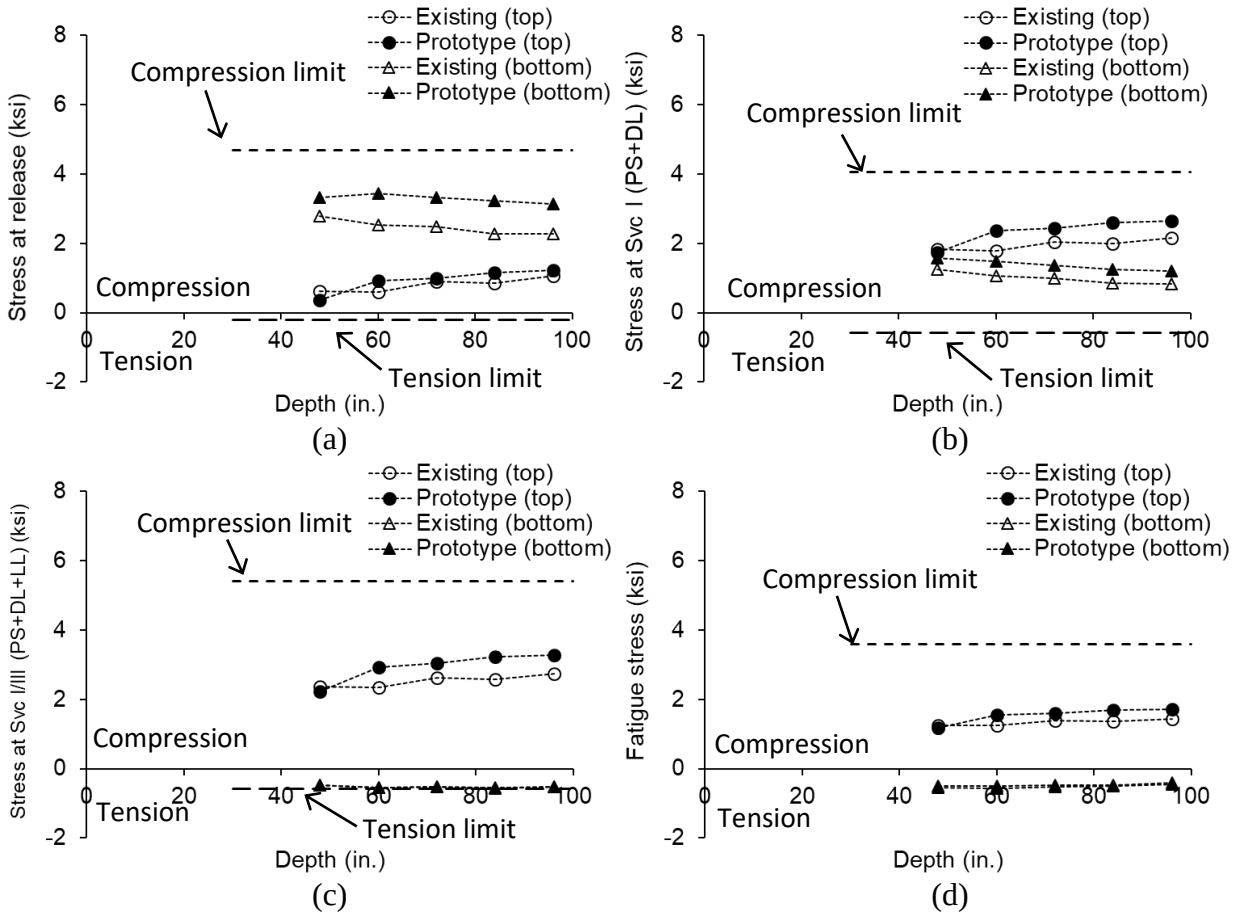

Fig. 54. Stress variation for two lanes with three girders- exterior girder: (a) release; (b) Service I (PS+DL); (c) Service I/III (PS+DL+LL); (d) fatigue

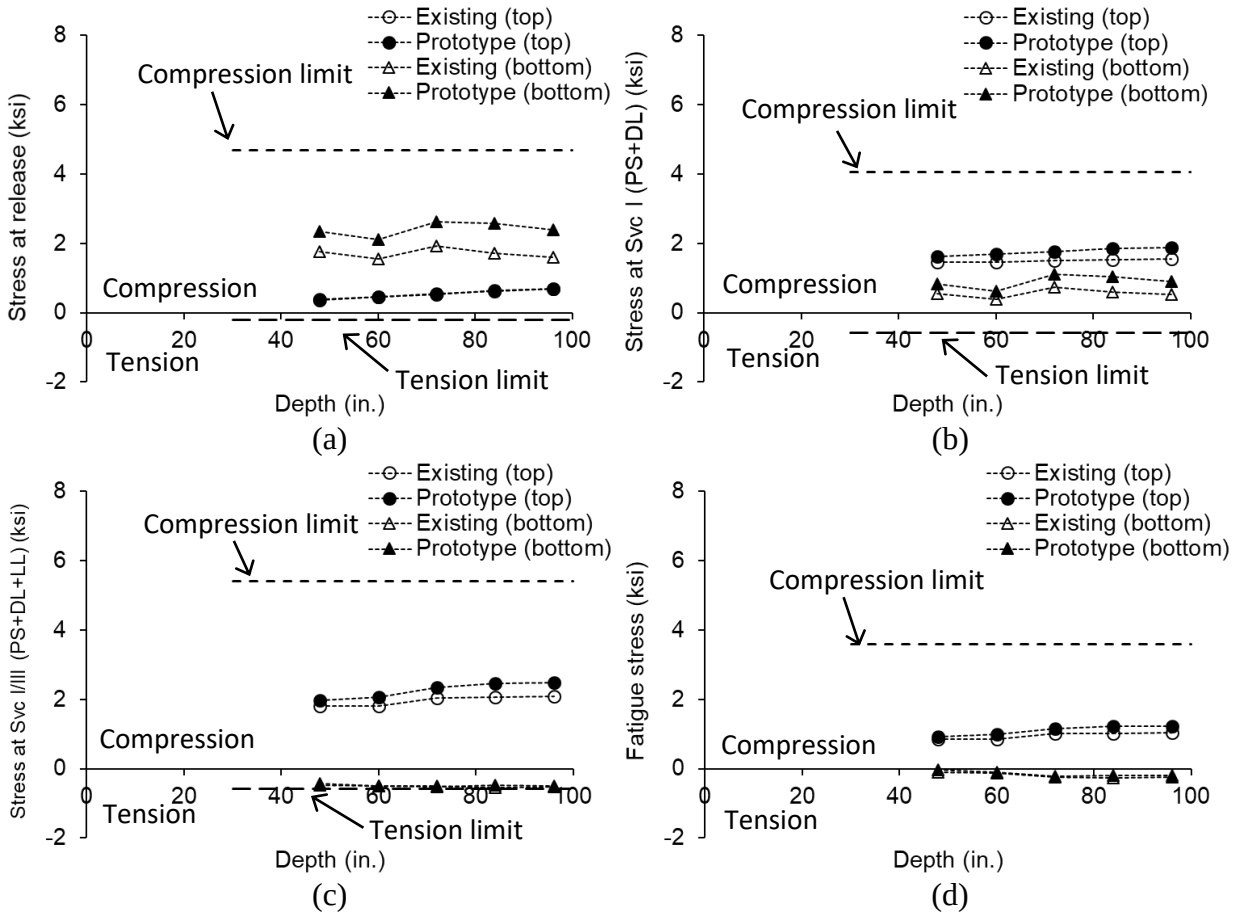

Fig. 55. Stress variation for two lanes with three girders- interior girder: (a) release; (b) Service I (PS+DL); (c) Service I/III (PS+DL+LL); (d) fatigue

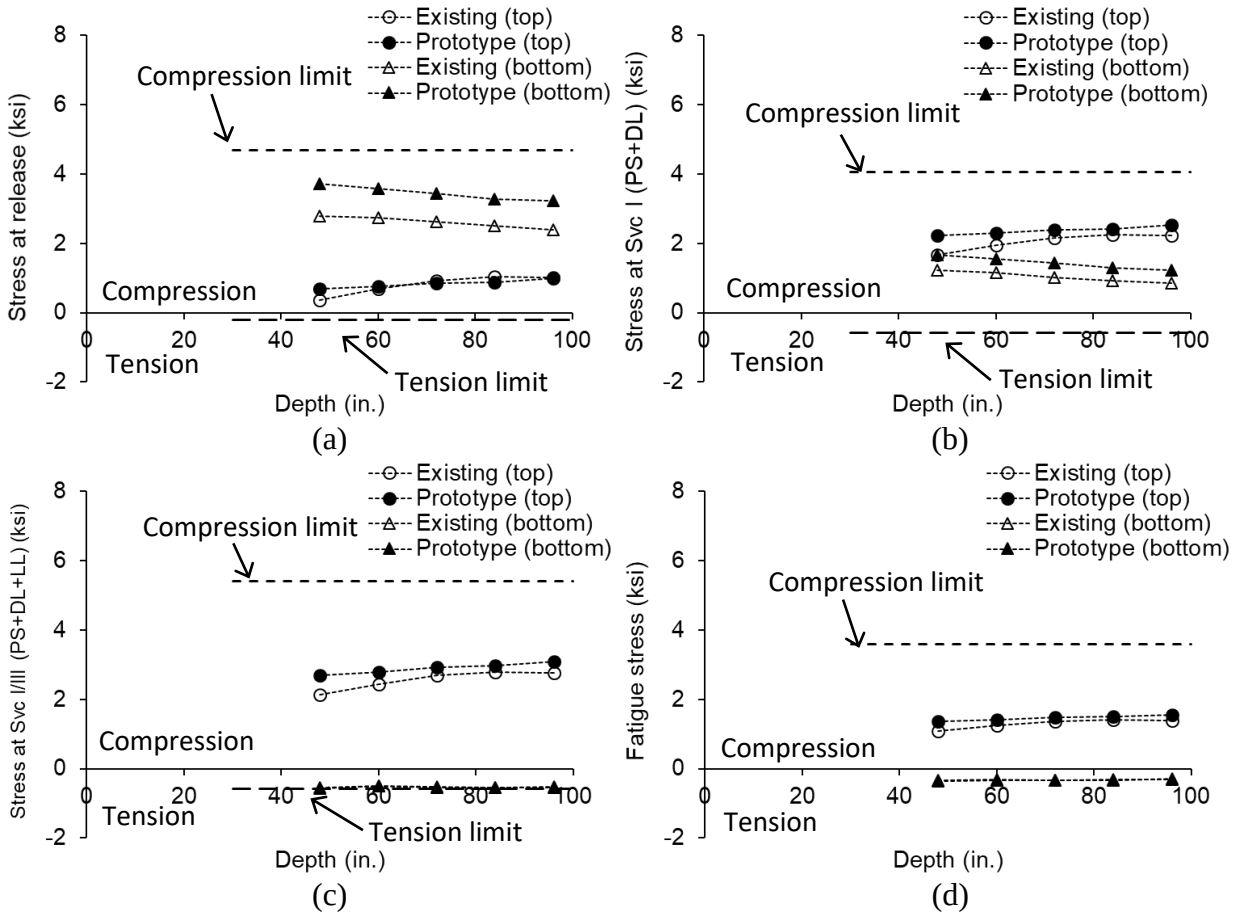

Fig. 56. Stress variation for three lanes with three girders- exterior girder: (a) release; (b) Service I (PS+DL); (c) Service I/III (PS+DL+LL); (d) fatigue

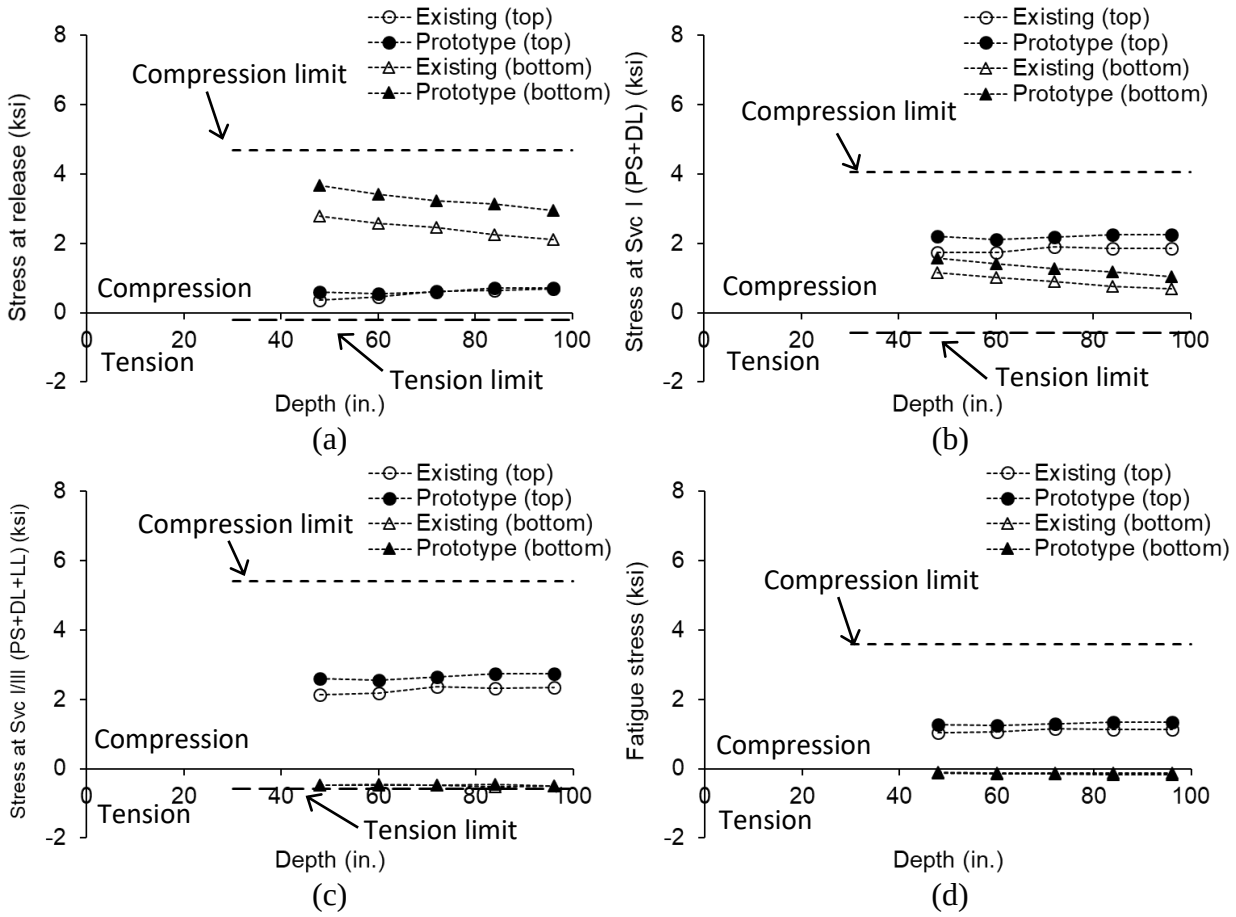

Fig. 57. Stress variation for three lanes with three girders- interior girder: (a) release; (b) Service I (PS+DL); (c) Service I/III (PS+DL+LL); (d) fatigue

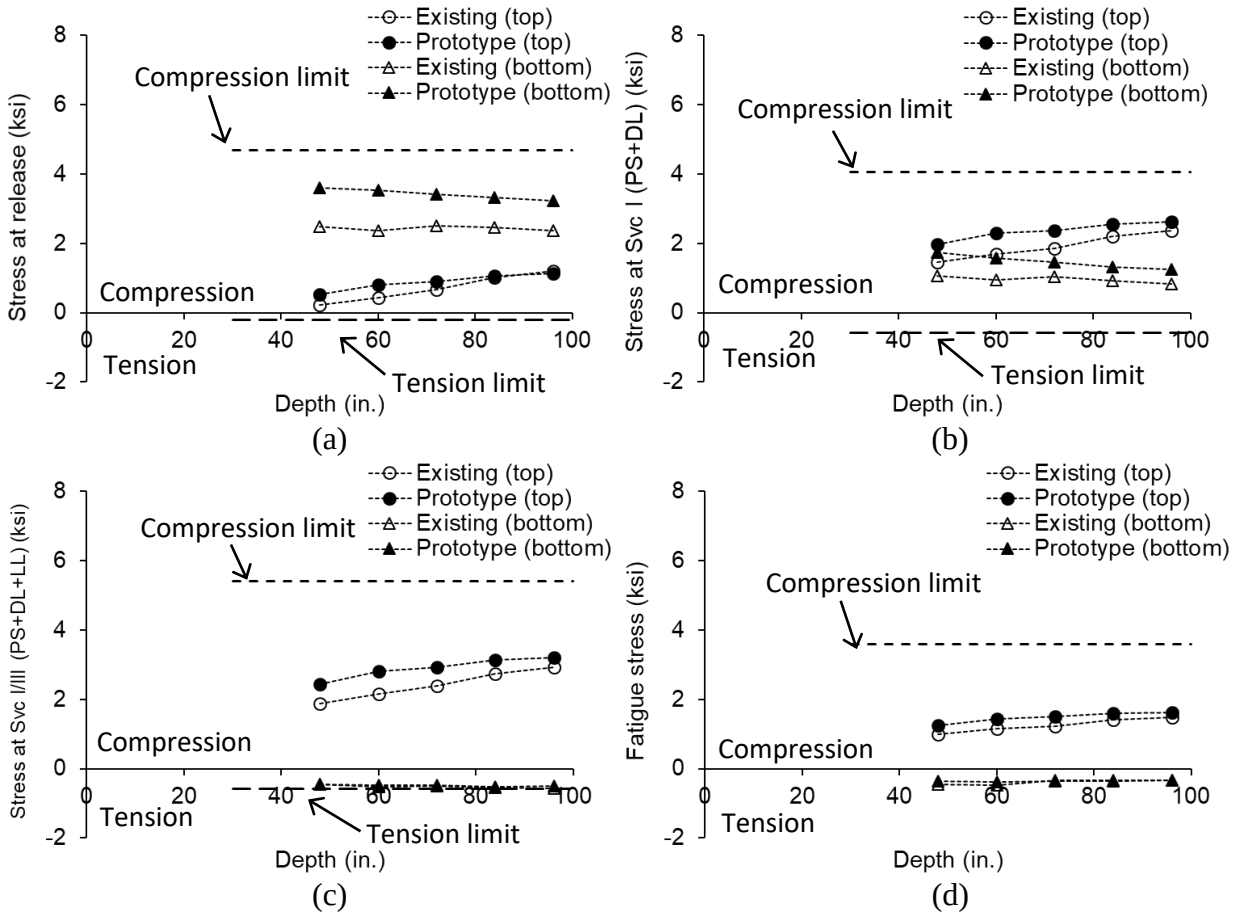

Fig. 58. Stress variation for four lanes with four girders- exterior girder: (a) release; (b) Service I (PS+DL); (c) Service I/III (PS+DL+LL); (d) fatigue

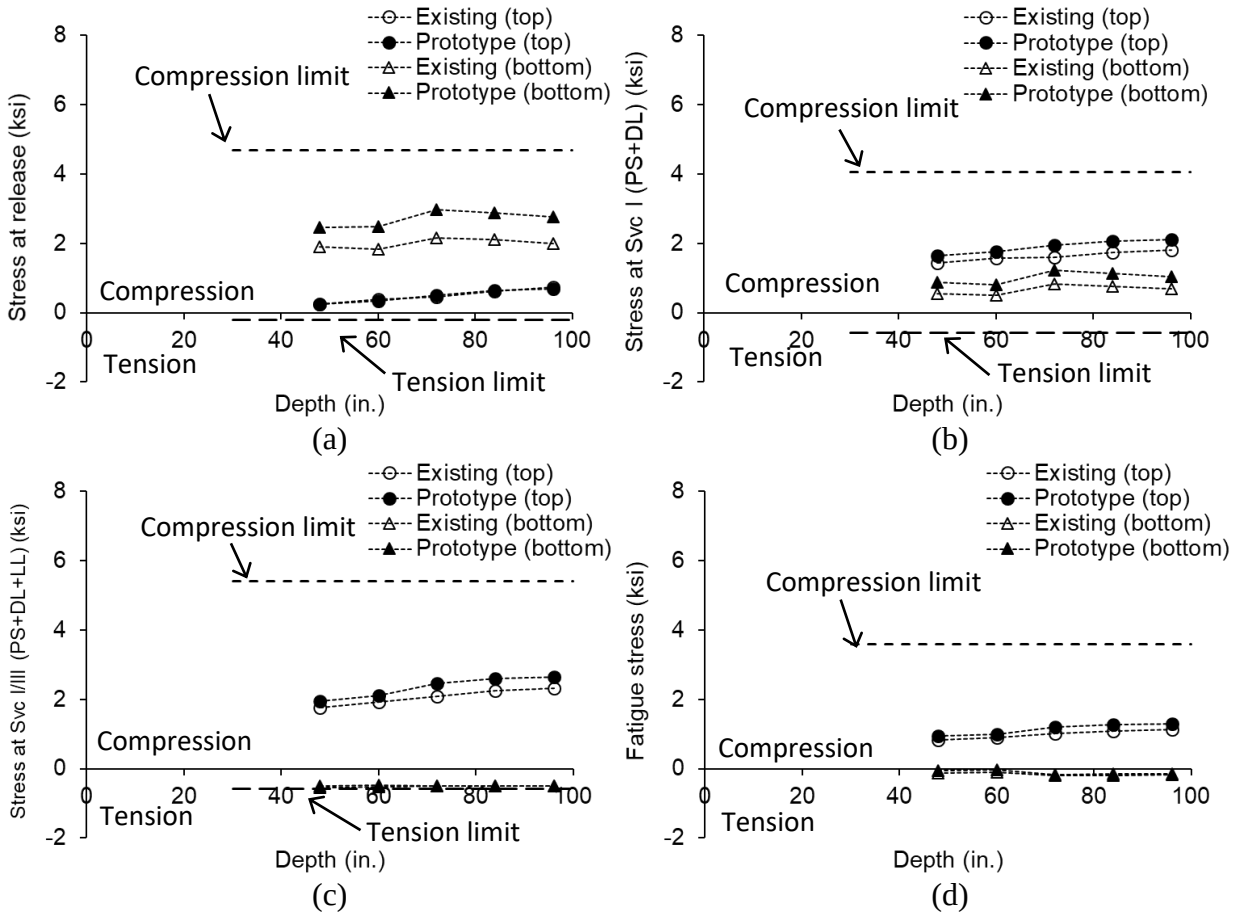

Fig. 59. Stress variation for four lanes with four girders- interior girder: (a) release; (b) Service I (PS+DL); (c) Service I/III (PS+DL+LL); (d) fatigue

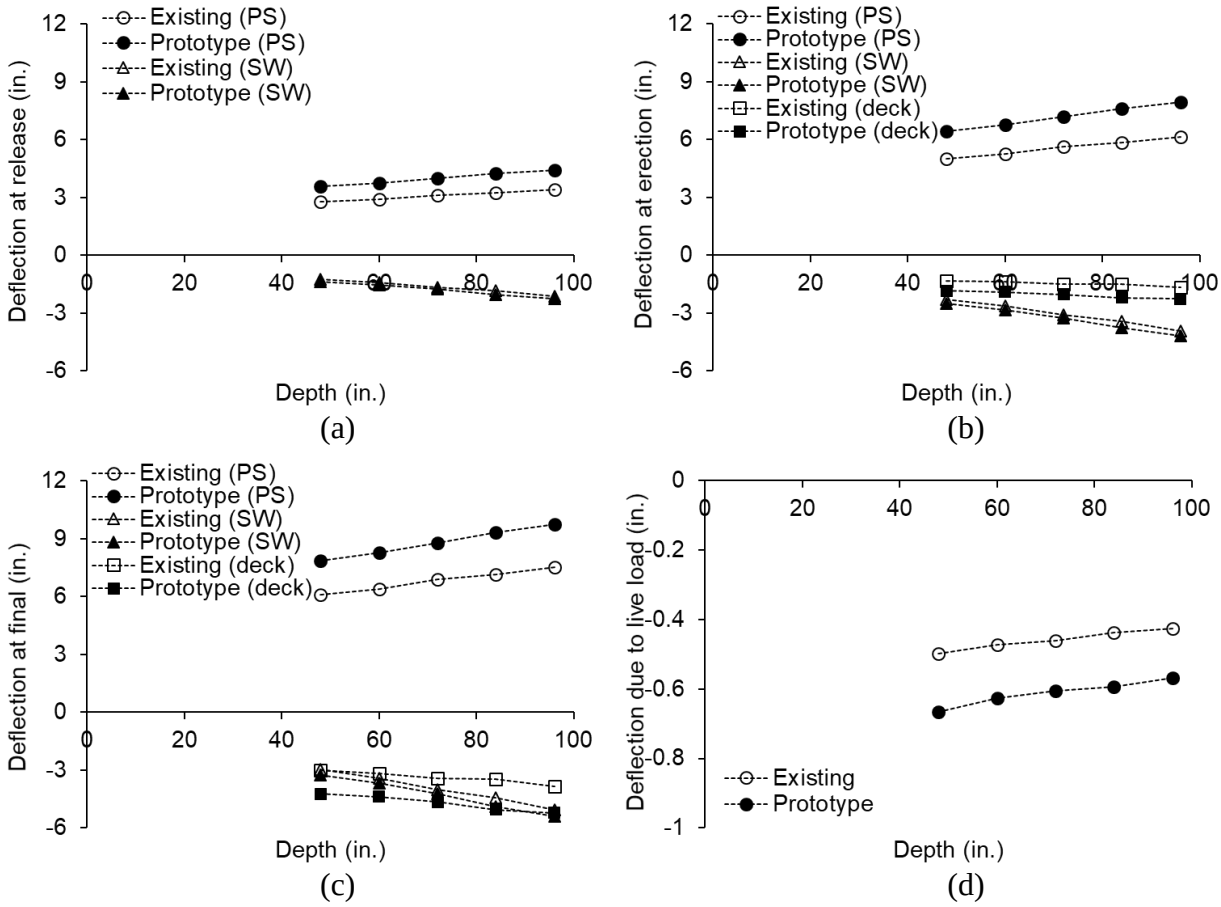

Fig. 60. Deflection for one lane with one girder: (a) release; (b) erection; (c) final; (d) due to live load

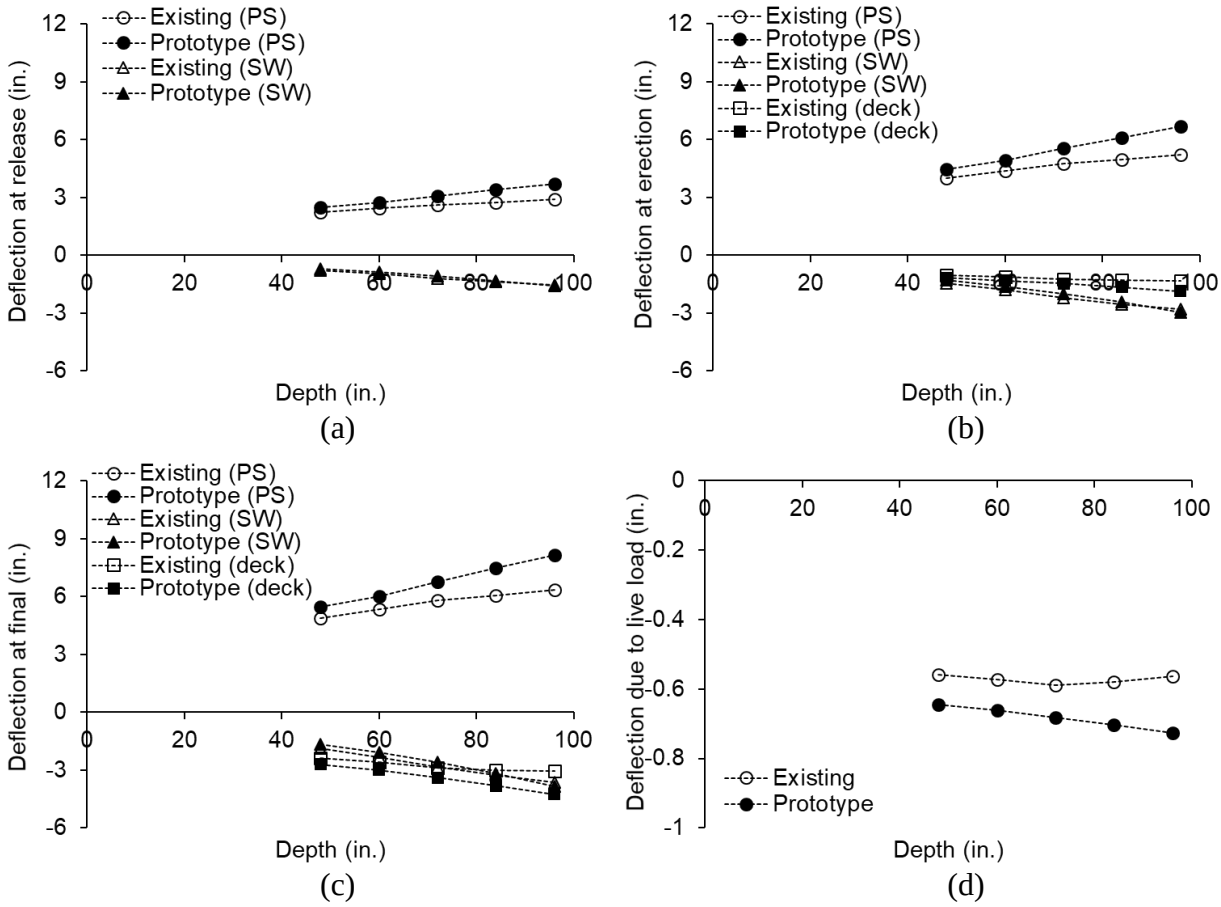

Fig. 61. Deflection for two lanes with two girders: (a) release; (b) erection; (c) final; (d) due to live load

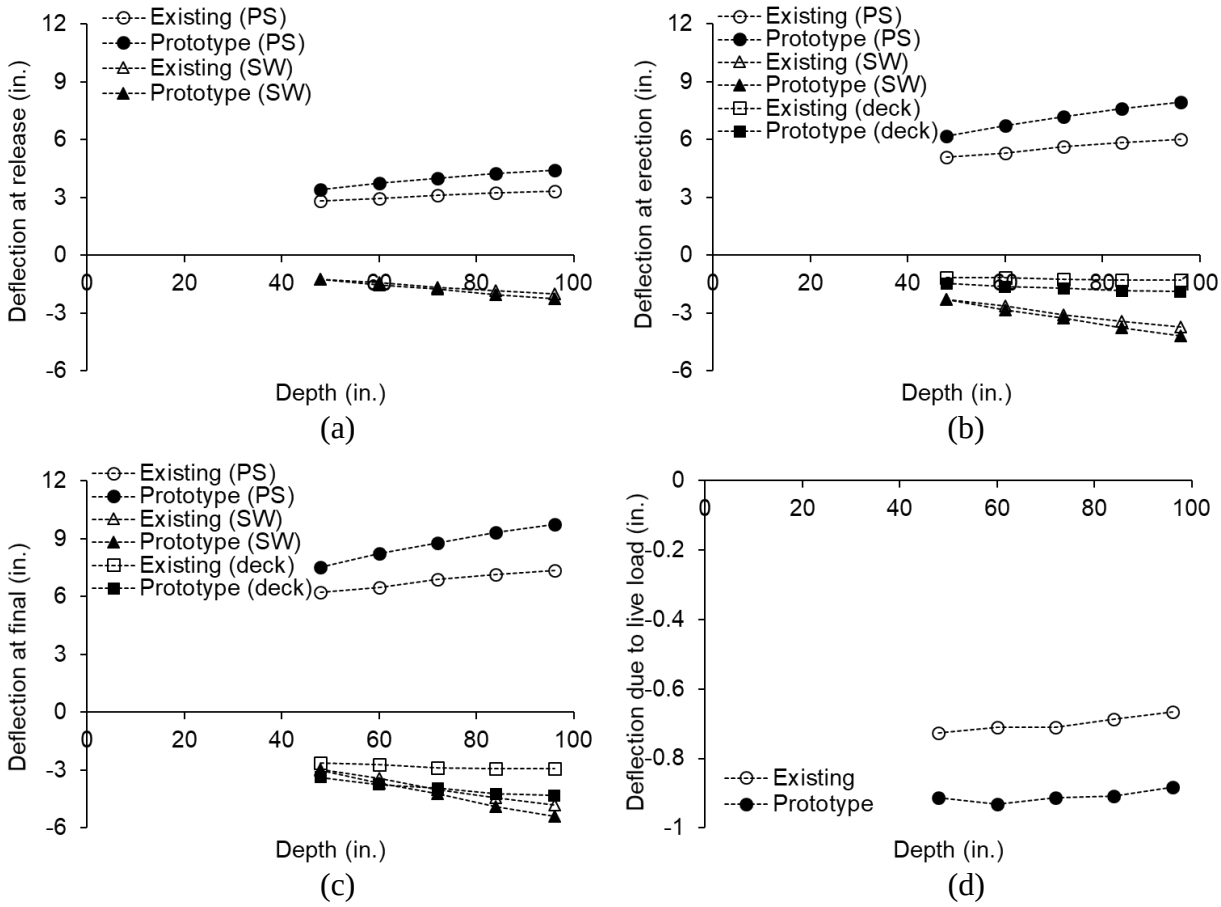

Fig. 62. Deflection for two lanes with three girders- exterior girder: (a) release; (b) erection; (c) final; (d) due to live load

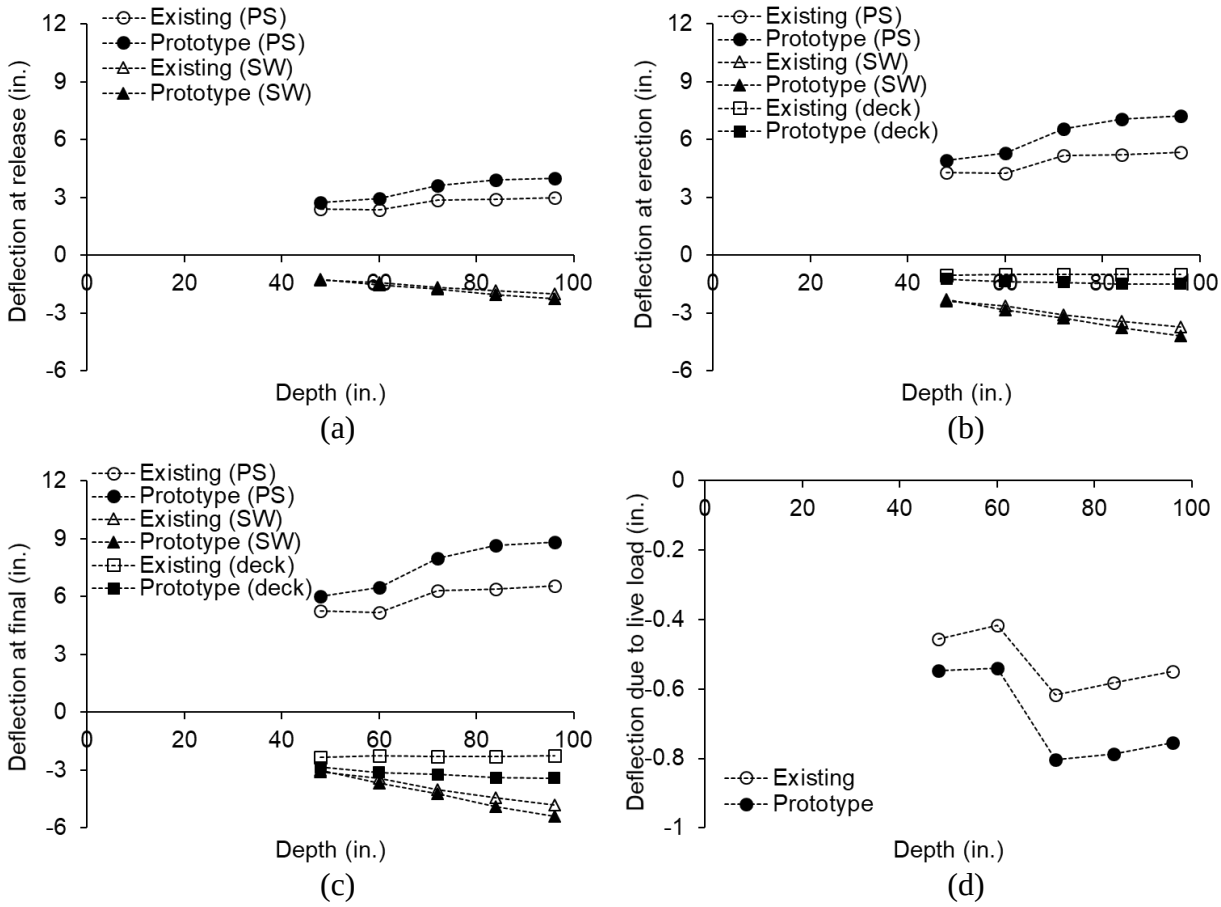

Fig. 63. Deflection for two lanes with three girders- interior girder: (a) release; (b) erection; (c) final; (d) due to live load

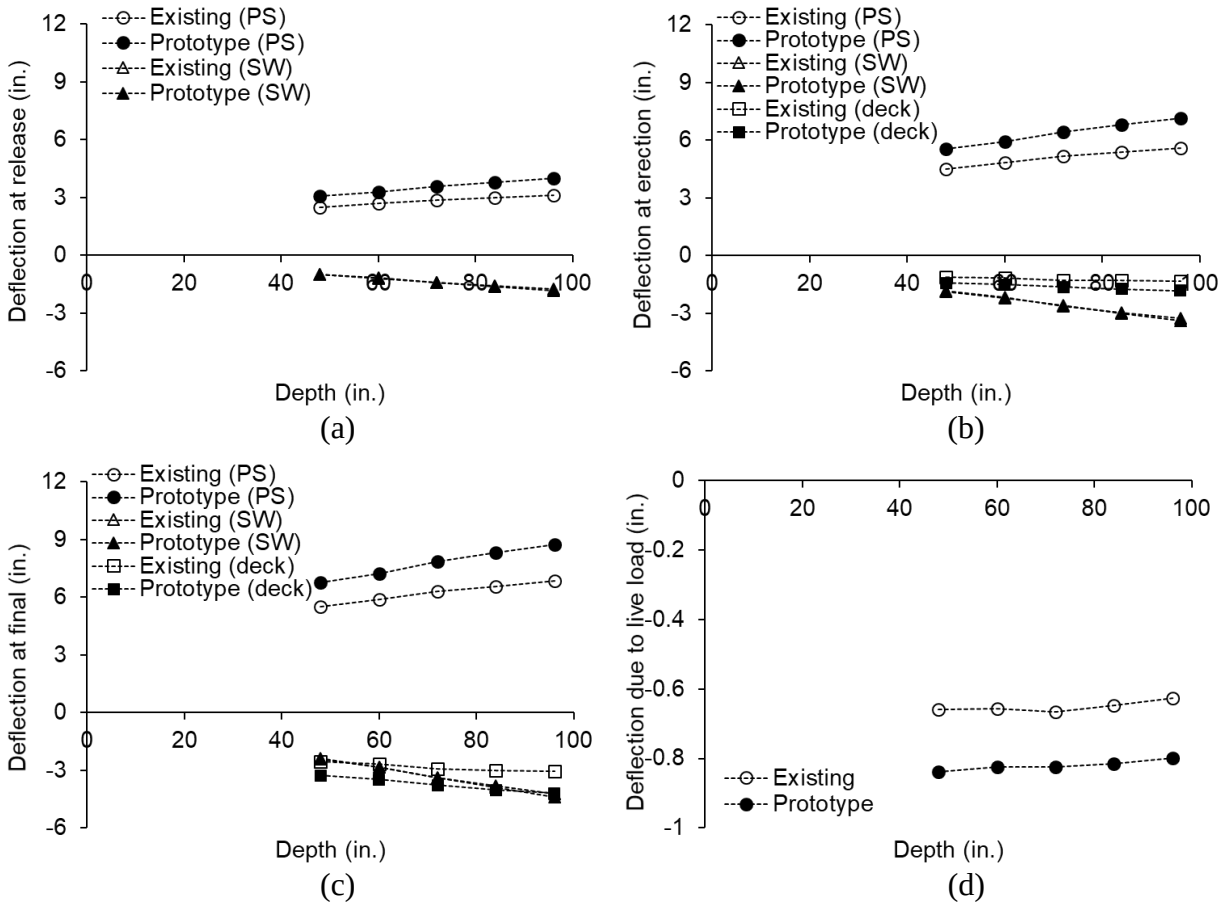

Fig. 64. Deflection for three lanes with three girders- exterior girder: (a) release; (b) erection; (c) final; (d) due to live load

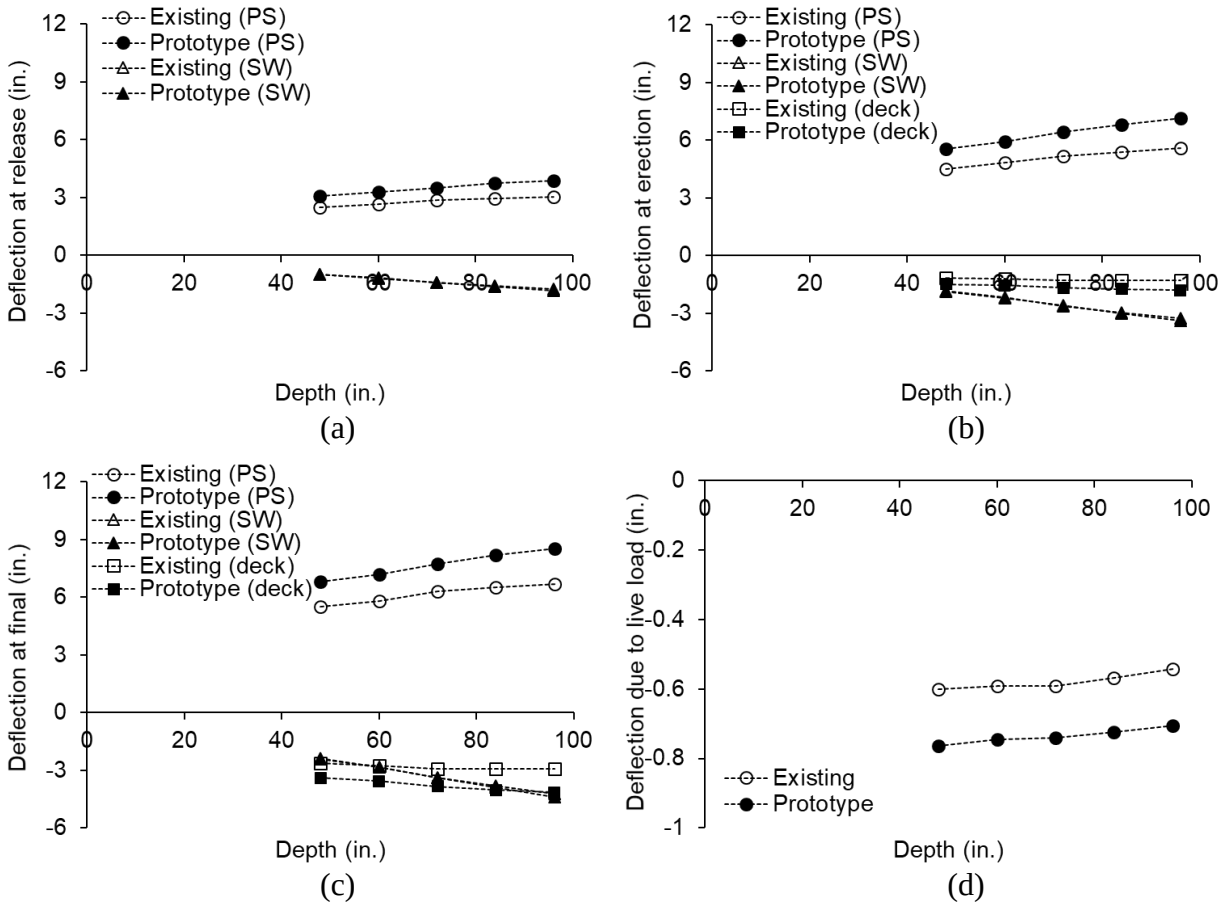

Fig. 65. Deflection for three lanes with three girders- interior girder: (a) release; (b) erection; (c) final; (d) due to live load

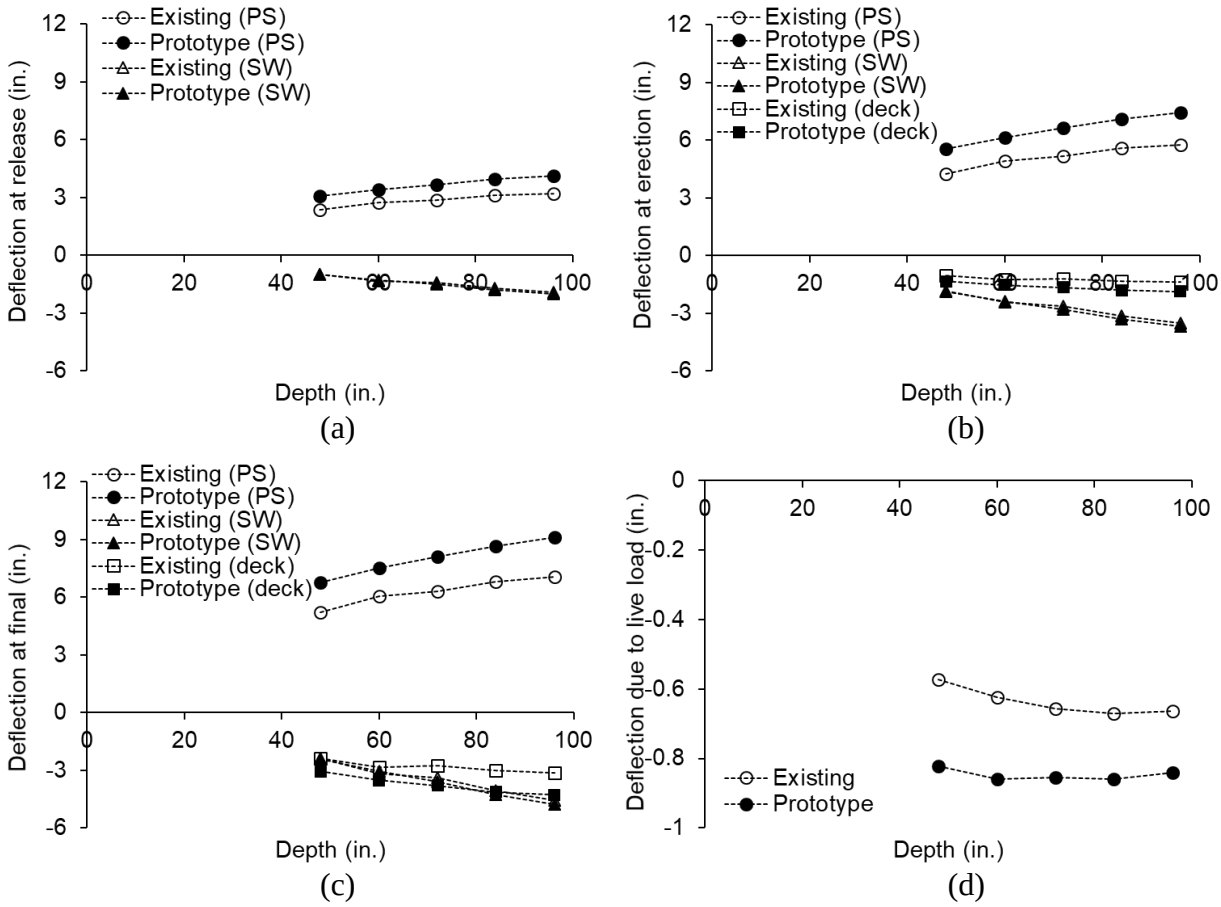

Fig. 66. Deflection for four lanes with four girders- exterior girder: (a) release; (b) erection; (c) final; (d) due to live load

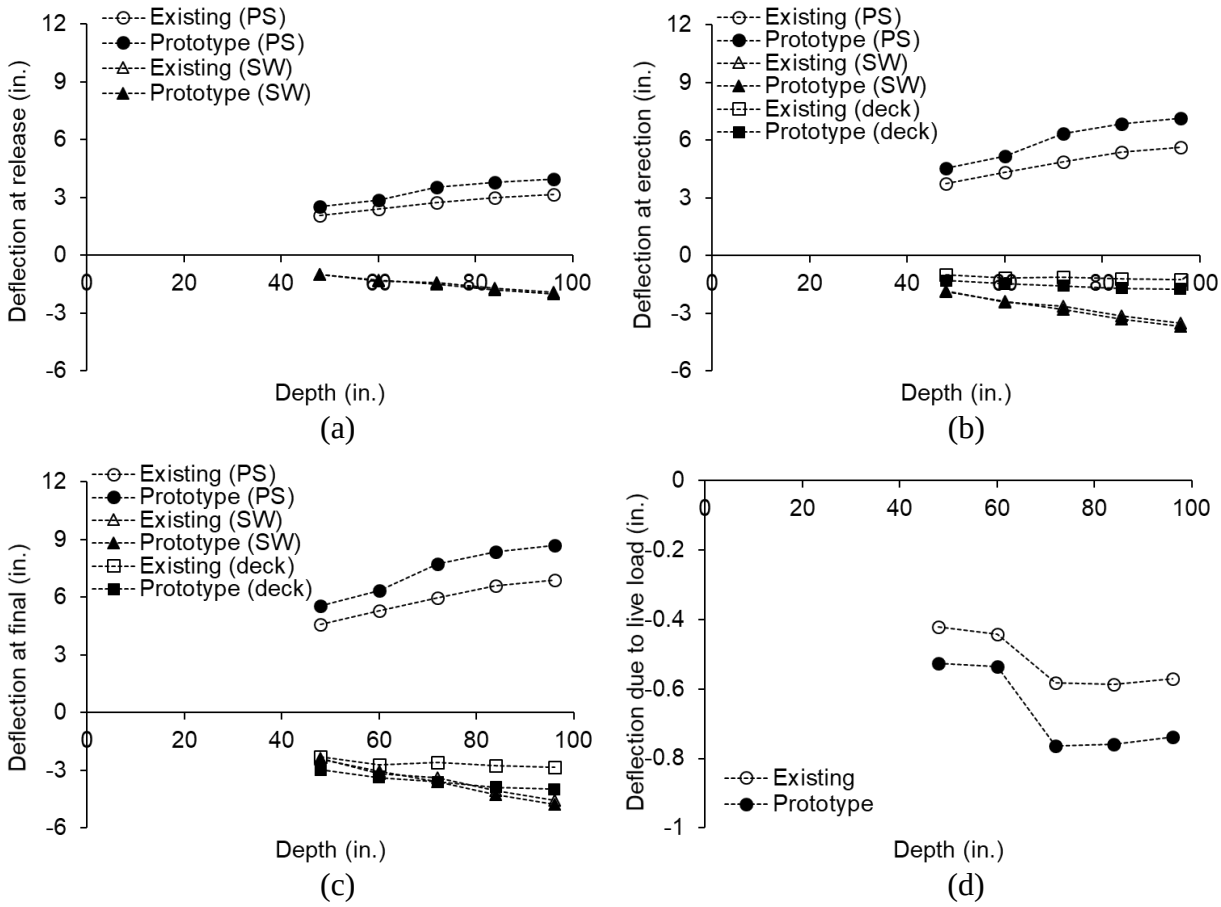

Fig. 67. Deflection for four lanes with four girders- interior girder: (a) release; (b) erection; (c) final; (d) due to live load

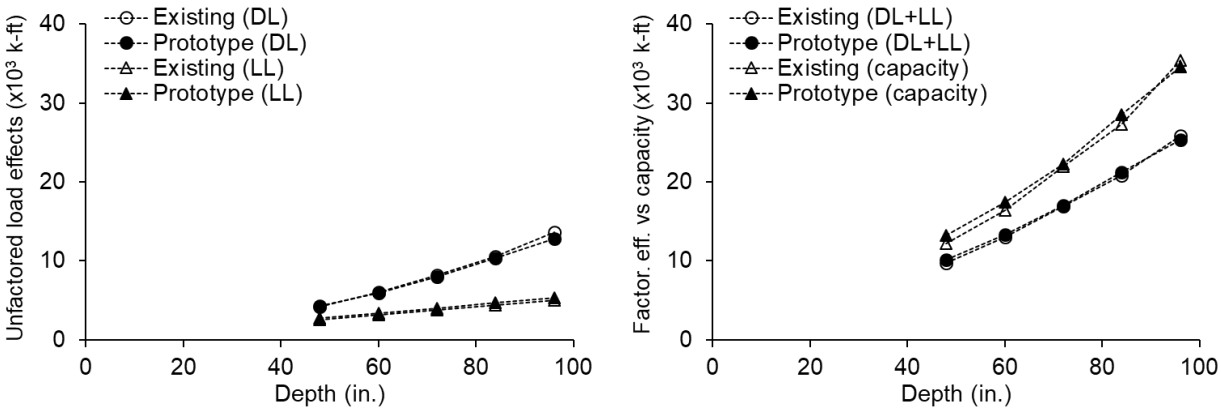

Fig. 68. Ultimate limit state with one land and one girder: (a) unfactored load effects; (b) factored load effects versus capacity

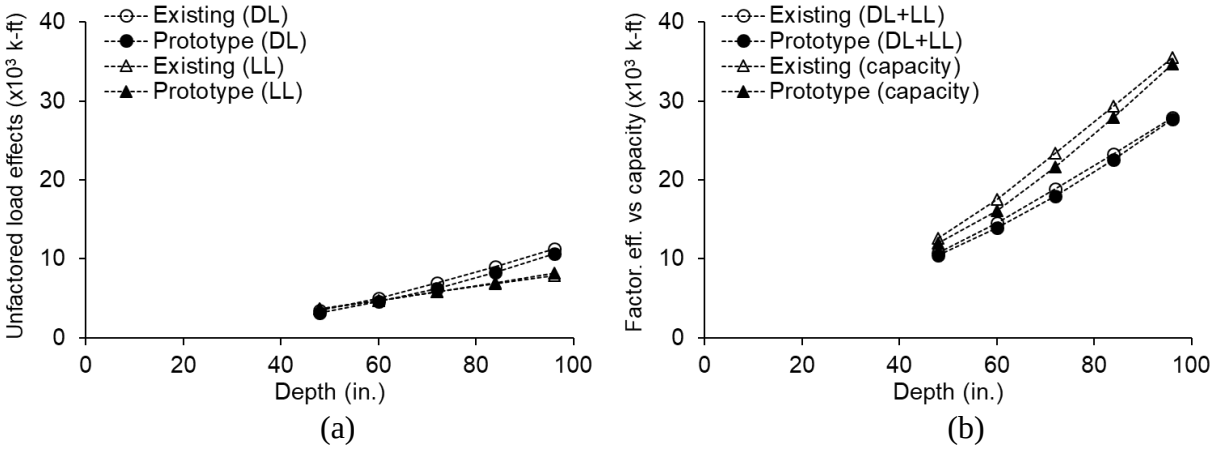

Fig. 69. Ultimate limit state with two lanes and two girders: (a) unfactored load effects; (b) factored load effects versus capacity

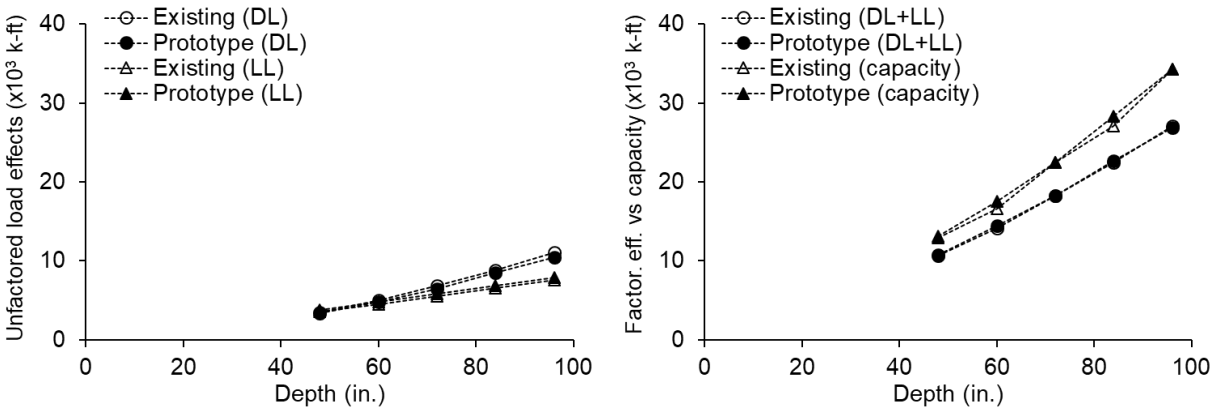

Fig. 70. Ultimate limit state for two lanes with three girders- exterior girder: (a) unfactored load effects; (b) factored load effects versus capacity

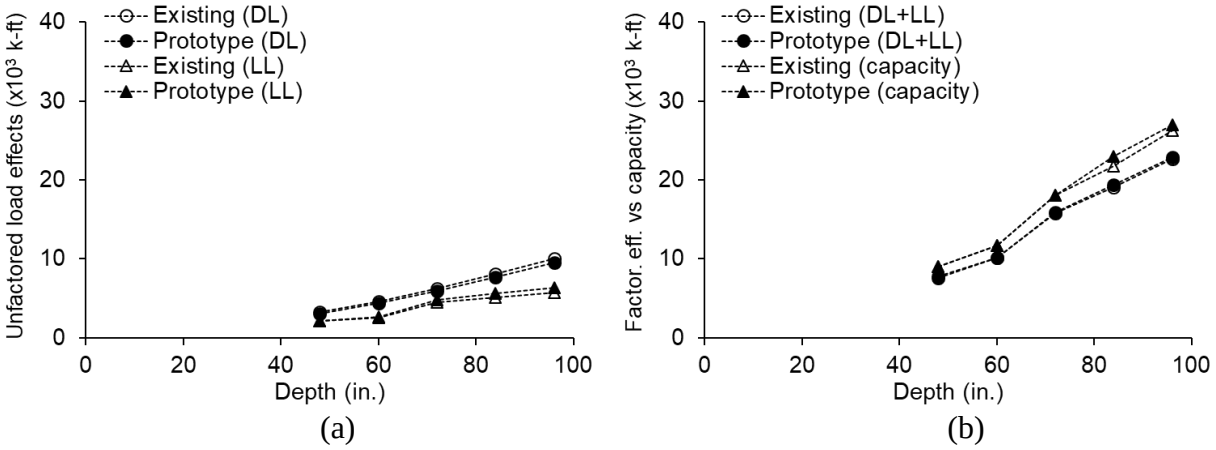

Fig. 71. Ultimate limit state for two lanes with three girders- interior girder: (a) unfactored load effects; (b) factored load effects versus capacity

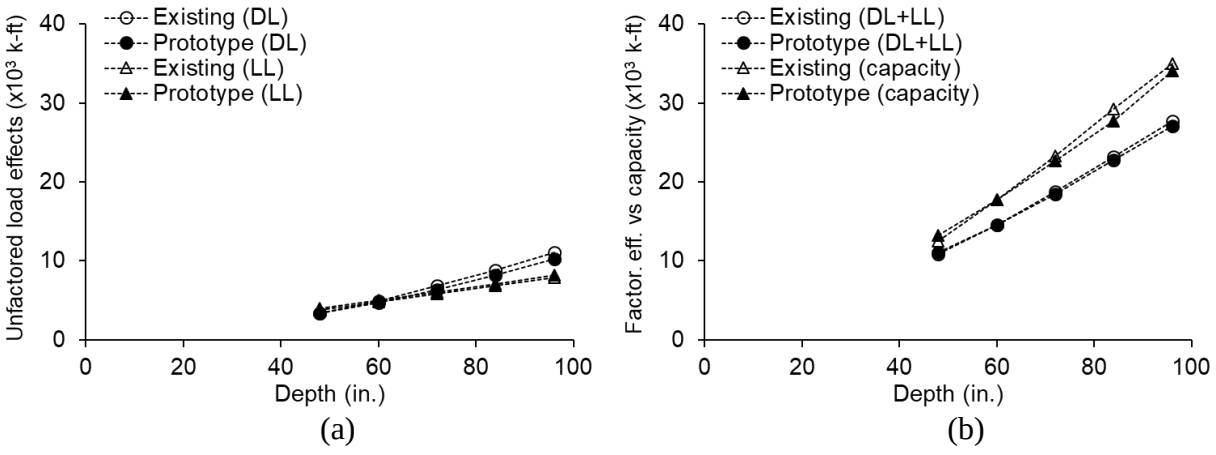

Fig. 72. Ultimate limit state for three lanes with three girders- exterior girder: (a) unfactored load effects; (b) factored load effects versus capacity

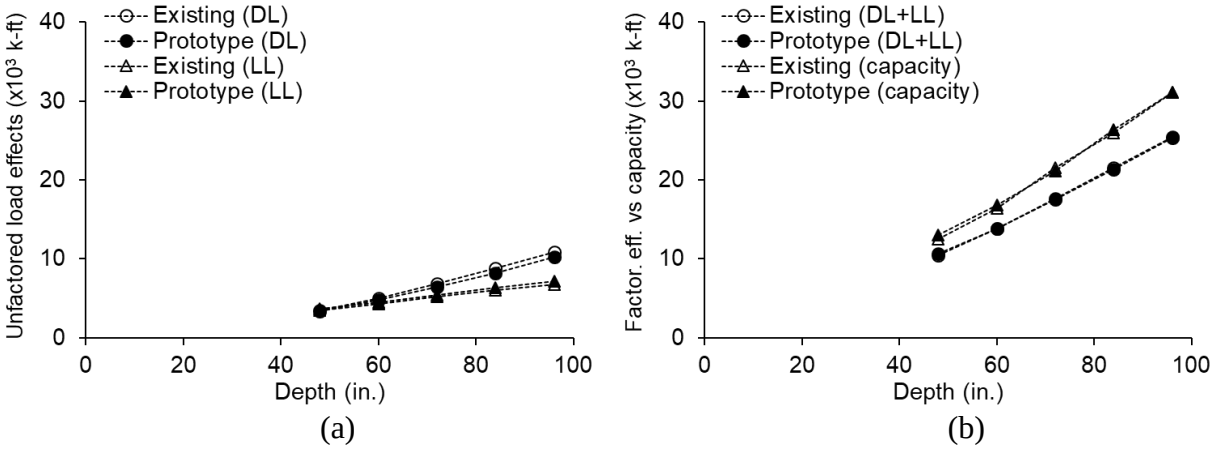

Fig. 73. Ultimate limit state for three lanes with three girders- interior girder: (a) unfactored load effects; (b) factored load effects versus capacity

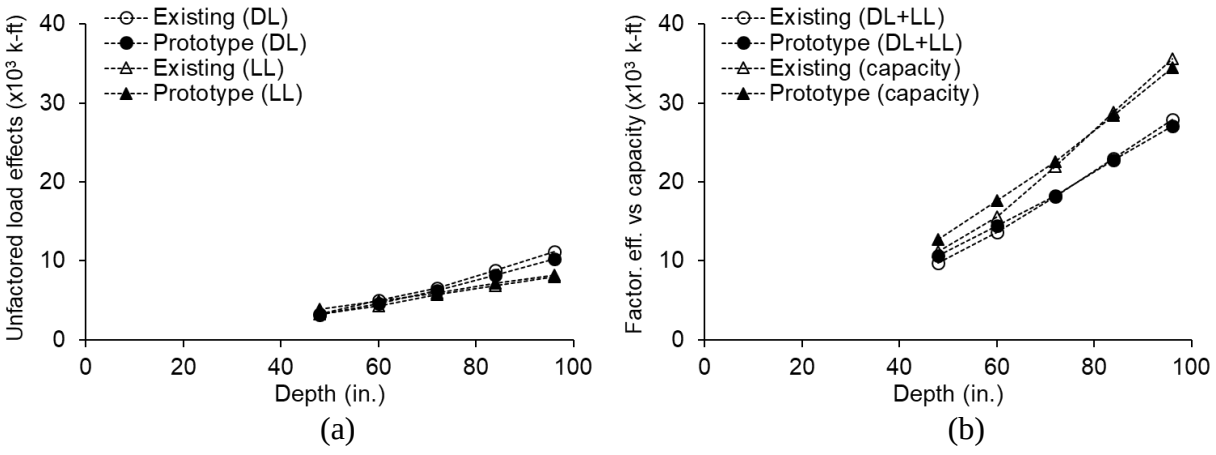

Fig. 74. Ultimate limit state for four lanes with four girders- exterior girder: (a) unfactored load effects; (b) factored load effects versus capacity

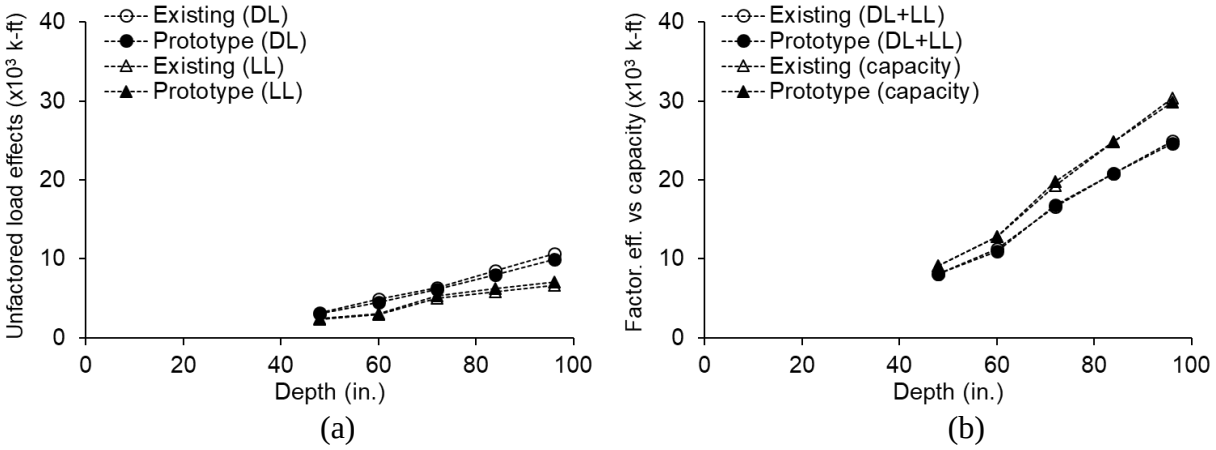

Fig. 75. Ultimate limit state for four lanes with four girders- interior girder: (a) unfactored load effects; (b) factored load effects versus capacity

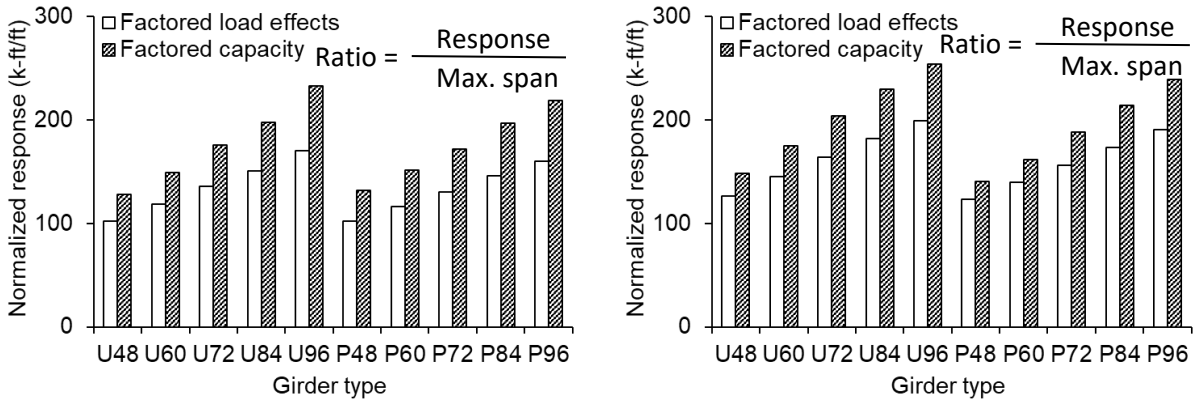

Fig. 76. Normalized factored response for one and two girders with considering span length: (a) one land with one girder; (b) two lanes with two girders

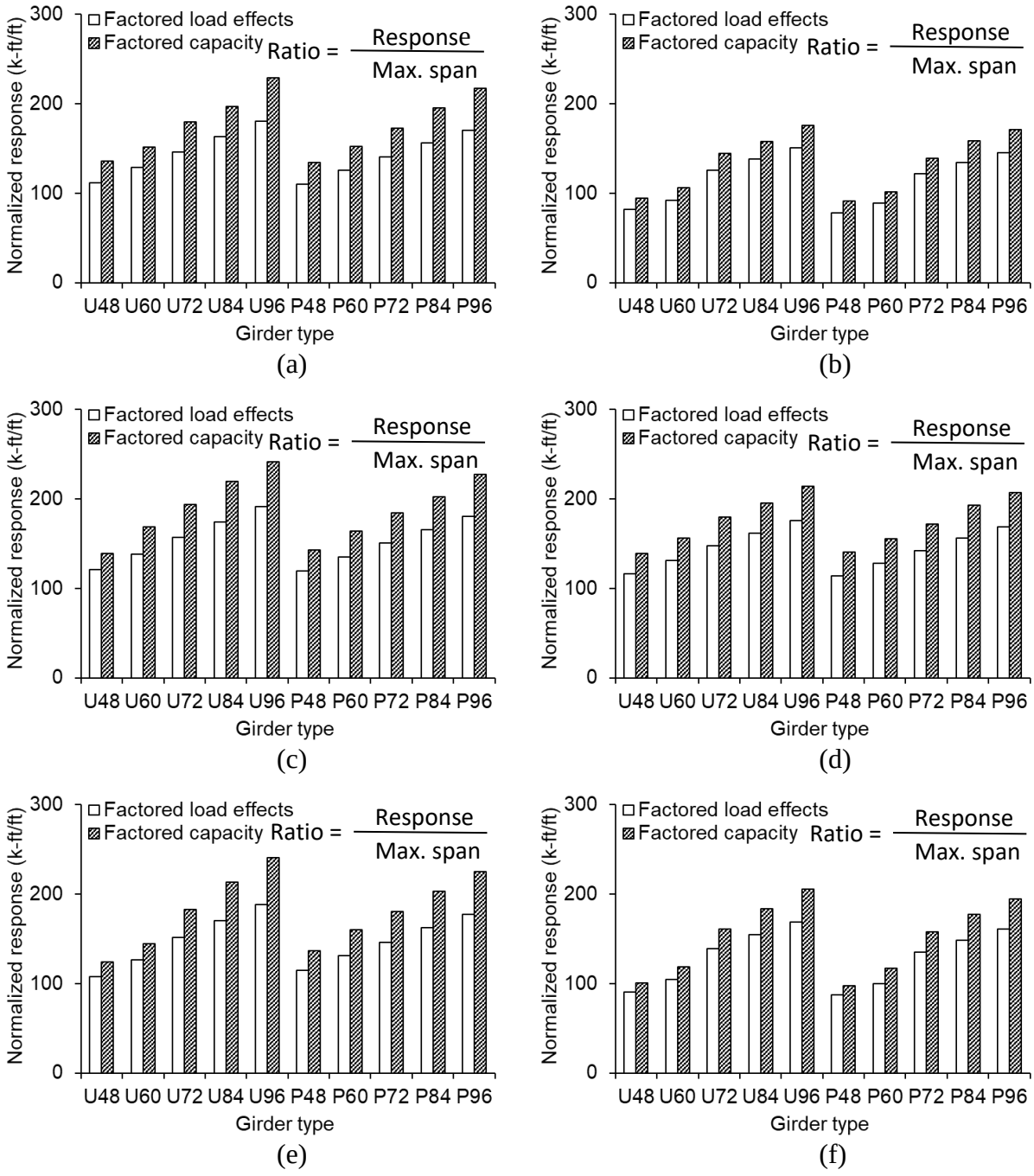

Fig. 77. Normalized factored response for three and four girders with considering span length: (a) two lanes with three girders- exterior girder; (b) two lanes with three girders- interior girder; (c) three lanes with three girders- exterior girder; (d) three lanes with three girders- interior girder; (e) four lanes with four girders- exterior girder; (f) four lanes with four girders- interior girder

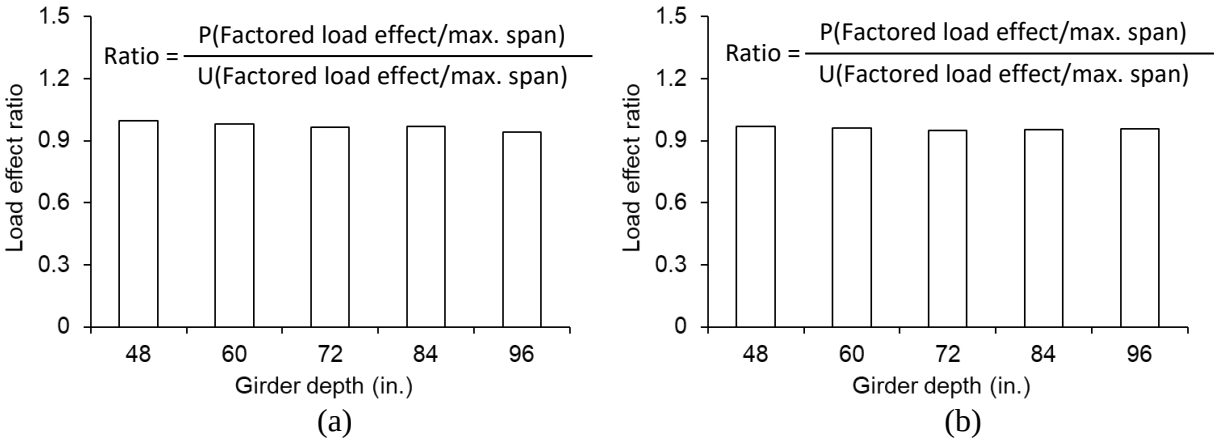

Fig. 78. Load effect ratio for one and two girders with considering span length: (a) one land with one girder; (b) two lanes with two girders

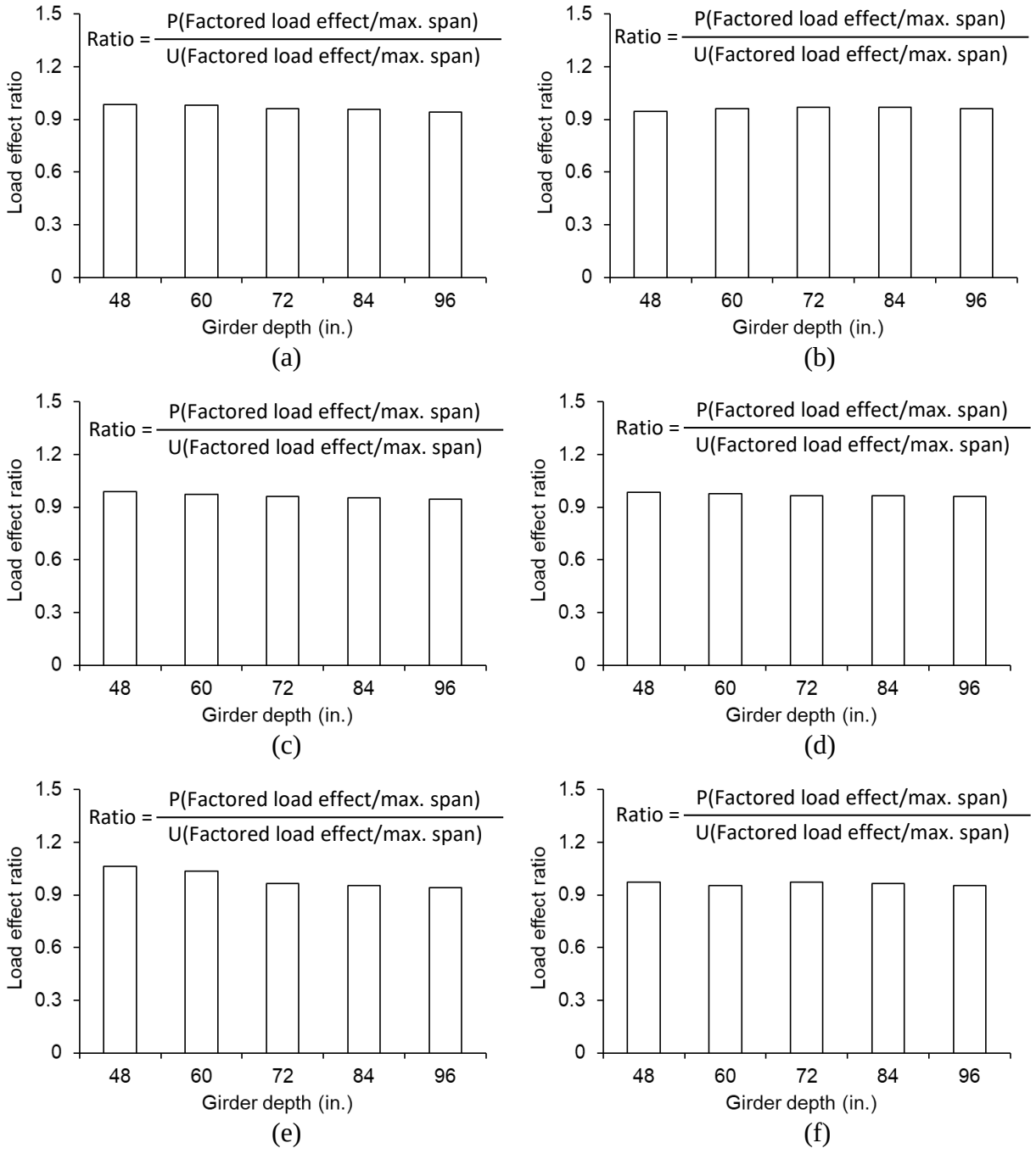

Fig. 79. Load effect ratio for three and four girders with considering span length: (a) two lanes with three girders- exterior girder; (b) two lanes with three girders- interior girder; (c) three lanes with three girders- exterior girder; (d) three lanes with three girders- interior girder; (e) four lanes with four girders- exterior girder; (f) four lanes with four girders- interior girder

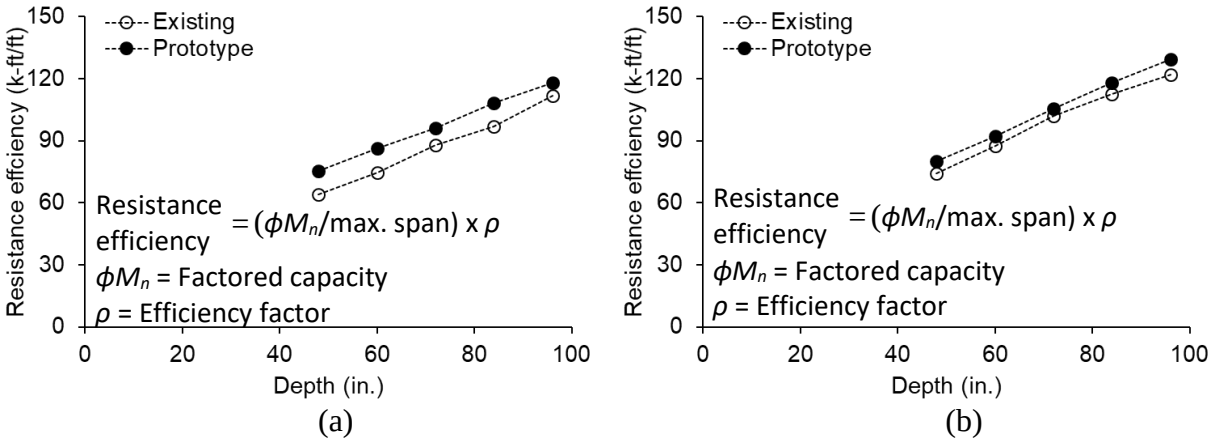

Fig. 80. Resistance efficiency for one and two girders with considering span length: (a) one land with one girder; (b) two lanes with two girders

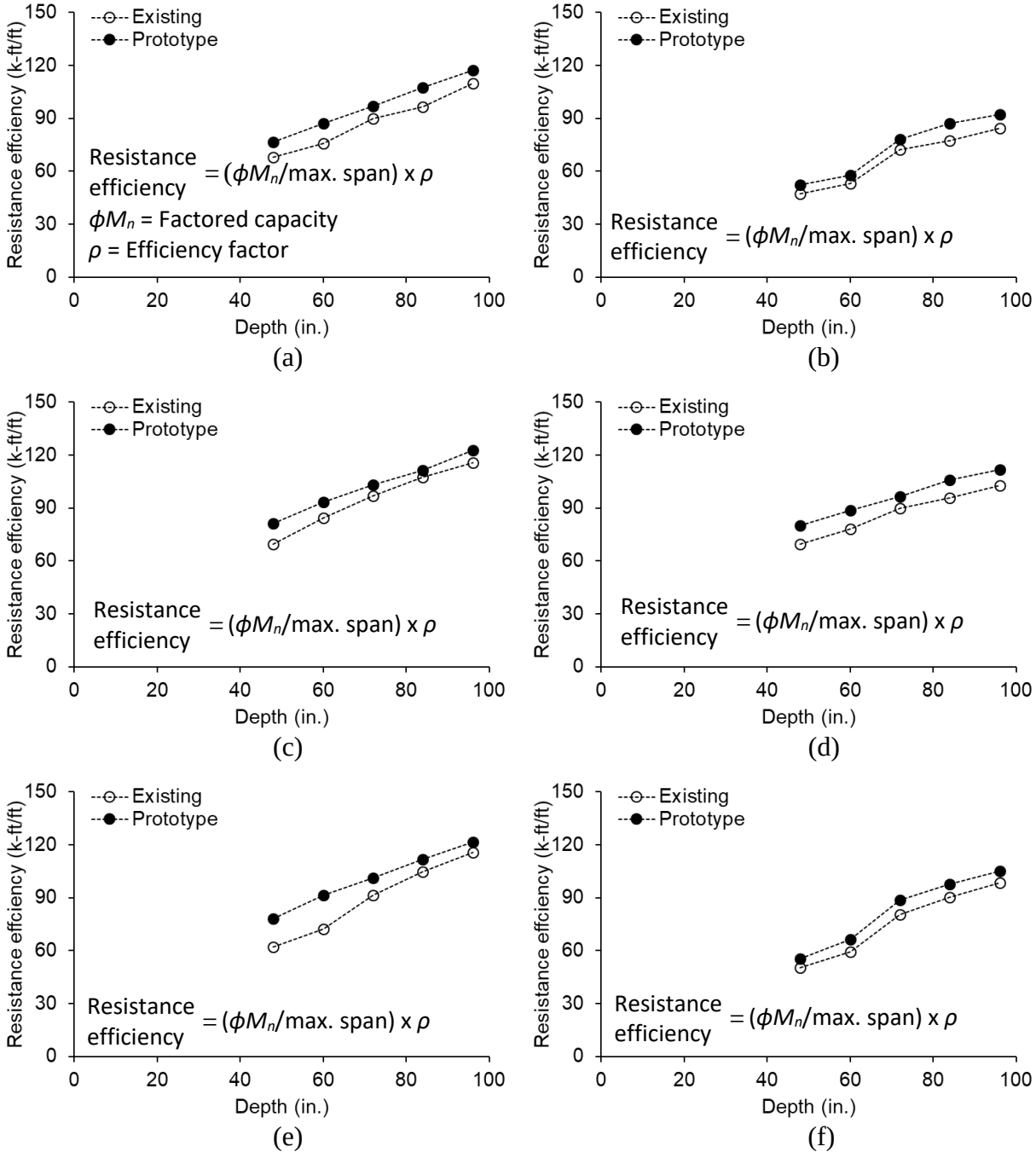

Fig. 81. Resistance efficiency for three and four girders with considering span length: (a) two lanes with three girders- exterior girder; (b) two lanes with three girders- interior girder; (c) three lanes with three girders- exterior girder; (d) three lanes with three girders- interior girder; (e) four lanes with four girders- exterior girder; (f) four lanes with four girders- interior girder

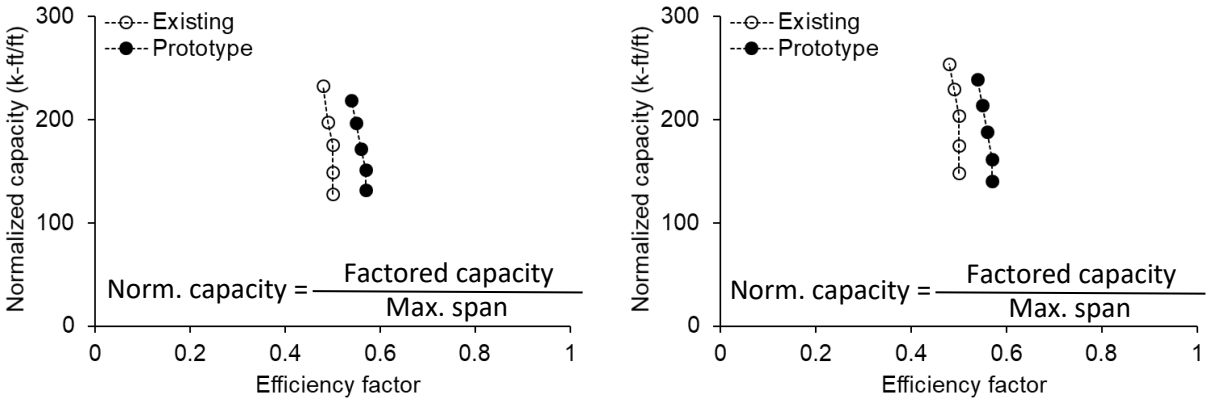

Fig. 82. Capacity vs. efficiency factor for one and two girders with considering span length: (a) one land with one girder; (b) two lanes with two girders

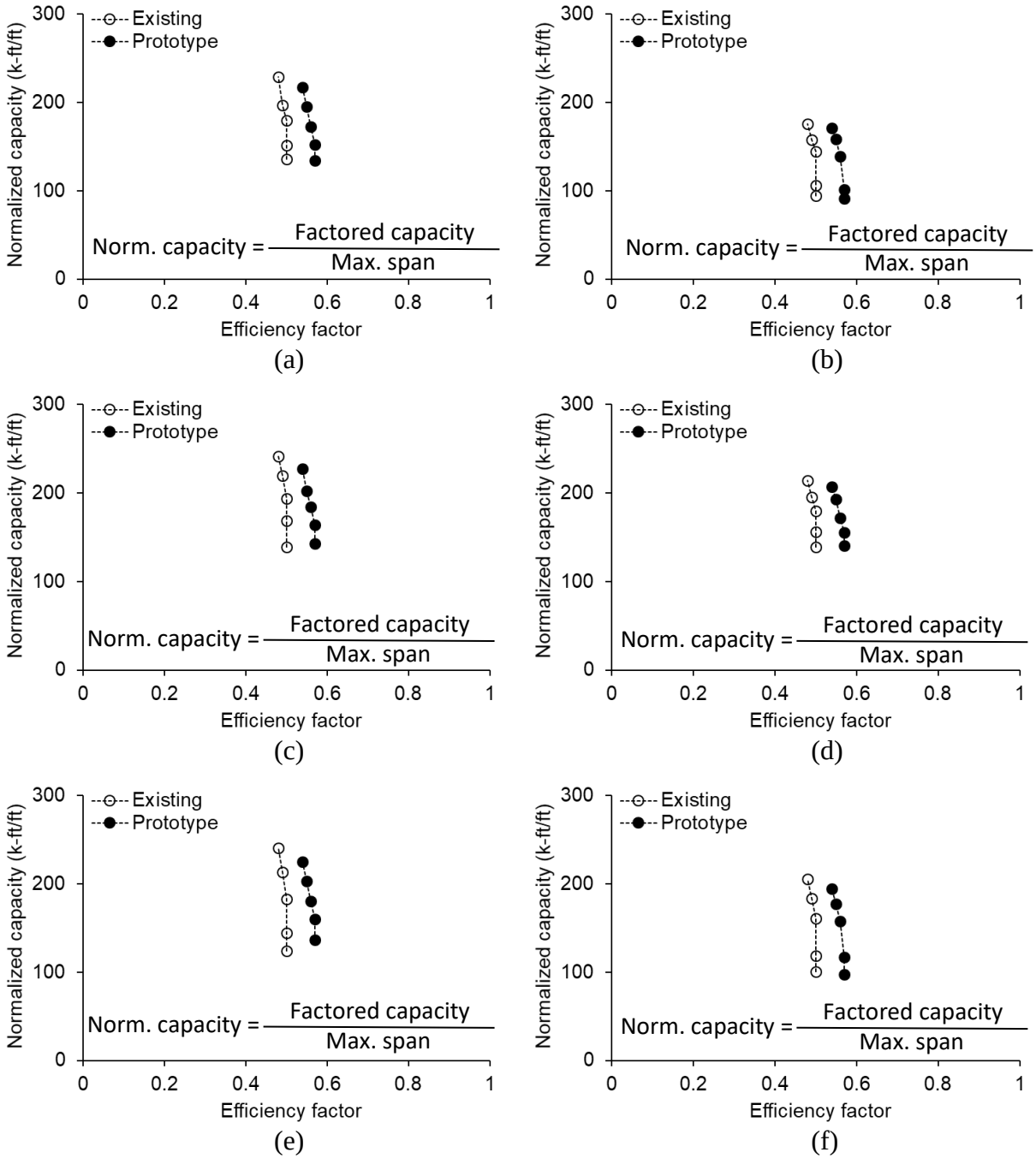

Fig. 83. Capacity vs. efficiency factor for three and four girders with considering span length: (a) two lanes with three girders- exterior girder; (b) two lanes with three girders- interior girder; (c) three lanes with three girders- exterior girder; (d) three lanes with three girders- interior girder; (e) four lanes with four girders- exterior girder; (f) four lanes with four girders- interior girder

5. Simplified Girder Sections Considering Constructability

5.1. Simplified Section

According to the request of the Colorado Department of Transportation, the prototype section was simplified to enhance constructability. The haunches at the web-flange intersections (V10 in Fig. 32(a)) were minimized, and the bilinear exterior webs were changed to straight lines, as in the case of the existing B618-U girder. Figure 84 renders the simplified version of the prototype girder. Even if these minute adjustments did not alter the structural functionality of the girders, subsidiary tasks were undertaken to elucidate potential concerns about geometric stability.

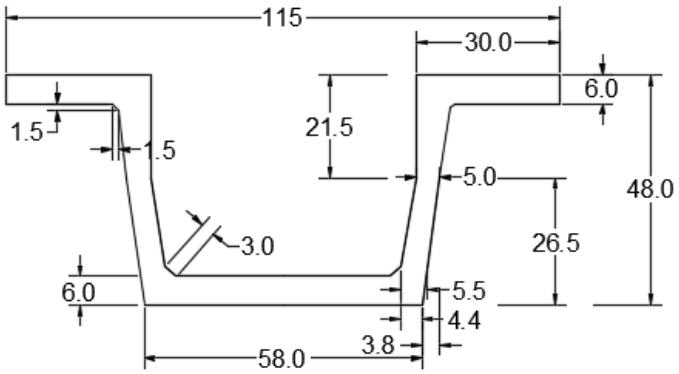

Fig. 84. Simplified section for construction convenience

5.2. Buckling Analysis

To account for the influence of the revised section, eigenbuckling analysis was performed using the commercial finite element package, ANSYS. For comparison, the existing, prototype, and simplified configurations were modeled with a variable web thickness from 5 in. to 10 in. along with a segmental length of 3.3 ft (selecting a web size for pre- and post-tensioning is at the discretion of CDOT). The elastic modulus and Poisson's ratio of the concrete (f'_c = 9,000 psi) were E_c = 5,400 ksi and ν = 0.2, respectively. Three-dimensional concrete elements (SOLID 65), consisting of eight nodes and three degrees of freedom at a node, were formulated to represent the girder shapes (Fig. 85(a)). The steel strands were not included owing to their insignificant contribution to the cross-sectional stiffness of the girders (Okumus et al. 2012). The upper flanges of the meshed sections were constrained in the horizontal directions for the presence of a concrete deck in constructed bridges, and the bottom of the sections was fully restrained (i.e., all translational degrees of freedom were fixed as supported by bearing plates in the field). After imposing these boundary conditions, loads were applied on the upper flanges (V2 in Fig. 32(a)) to compress the webs. Subsequently, the eigenvalues of the sections' first modes were extracted by the Block Lanczos algorithm (Saini et al. 2021) to calculate the buckling load of each girder.

The occurrence of buckling was consistent within the top-third region of the webs throughout the girder shapes (Fig. 85(b)) and thicknesses (Fig. 85(c)). Notwithstanding the similar conformation, the critical loads of the individual sections differed noticeably (Fig. 85(d)). The prototype girders buckled at 33,984 kips to 62,932 kips, linking with a web thickness of 5 in. to 10 in.; contrarily, the simplified girders showed lower loads from 9,121 kips to 36,464 kips. For the existing girders (web thicknesses of 5 in., 7.5. in. and 10 in. are allowed by the transportation agency), the average buckling load was 13.0% and 65.9% greater than those of the prototype and simplified girders (Fig. 85(e)). Overall, the buckling capacities of the existing and prototype girders were comparable; however, when the simplified girder series is erected, internal diaphragms or bracings should be placed at support points to address stability issues.

5.2. Torsional Resistance

The torsional rigidity (GJ) of the sections was appraised to ensure the lateral stability of the girders, where G is the shear modulus of the concrete and J is the section's polar moment of inertia (Table 17). The shear modulus was gained from elastic theory ($G = E_c/\{2(1 + \nu)\}$). The rigidity of the prototype and simplified sections was alike with an average difference of 1.8%, whereas the response slope of the existing section was lower than that of others (Fig. 86(a)). As such, the torsional performance of the existing section was better at a web thickness of 5 in., virtually identical at 7.5 in., and worse at 10 in. when compared with the performance of the prototype and simplified sections (Fig. 86(b)).

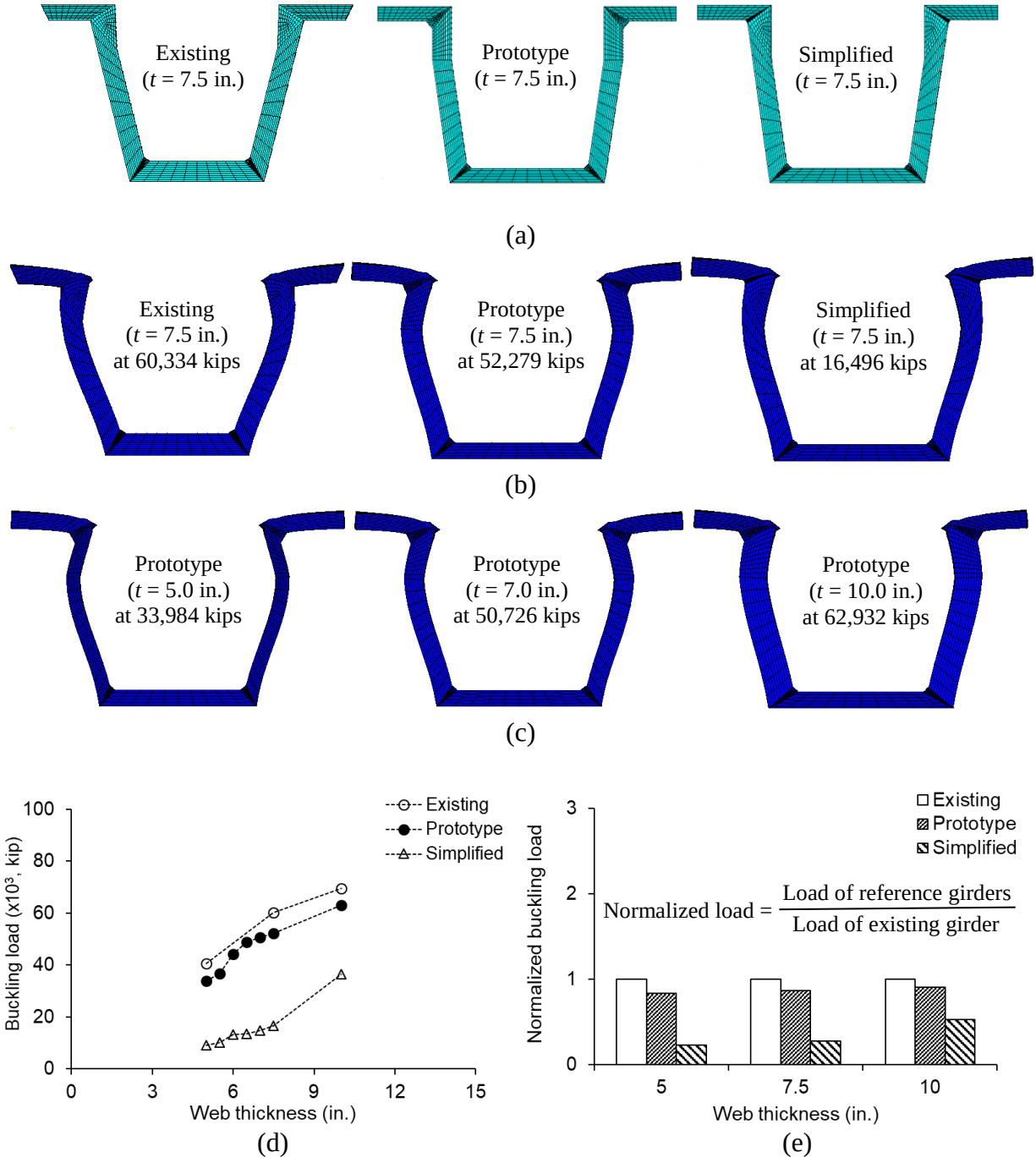

Fig. 85. Buckling of tub girders at a depth of 72 in.: (a) developed models; (b) buckled shapes with girder type; (c) buckled shapes with web thickness; (d) buckling load; (e) normalized comparison

Table 17. Polar moment of inertia

Girder type	Web thickness (in.)	Polar moment of inertia (in.^{4})
B618-U (H = 72 in.)	5	2,652,410
	7.5	3,075,240
	10	3,446,470
Prototype (H = 72 in.)	5	2,431,987
	5.5	2,603,440
	6	2,707,595
	6.5	2,812,627
	7	2,919,654
	7.5	3,022,898
	10	3,604,800
Simplified (H = 72 in.)	5	2,463,420
	5.5	2,654,403
	6	2,759,748
	6.5	2,865,931
	7	2,974,102
	7.5	3,078,435
	10	3,666,160

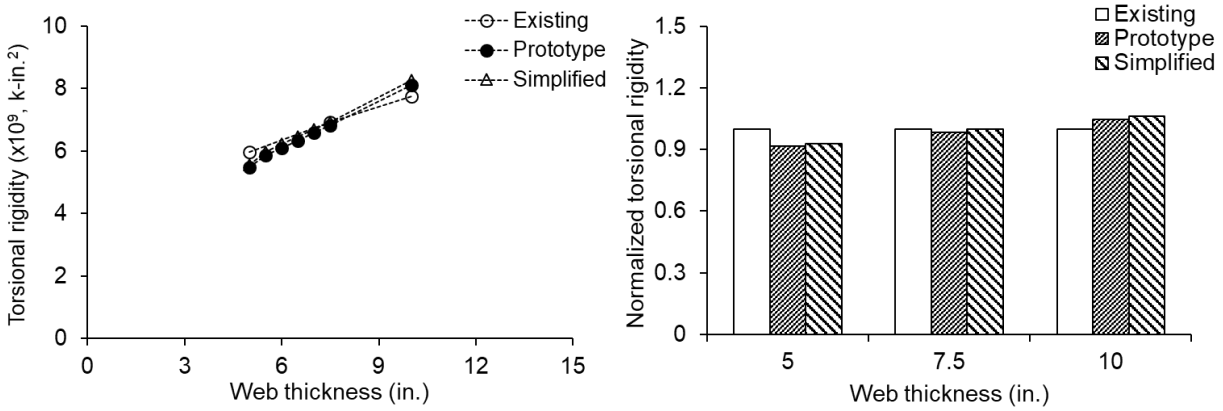

(a) (b)

Fig. 86. Torsional resistance of girders at a depth of 72 in.: (a) torsional rigidity; (b) normalized torsional rigidity

5.3. Cost Benefit Analysis

Pursuant to the tabulated guidelines of the Florida Department of Transportation (FDOT 2022), the cost of the three girders was estimated. It is important to note that this section is intended to assess the financial attributes of these girders, rather than to provide absolute budgetary information that is not acquirable from local precasters. The one-lane bridge supported by one girder (Fig. 42(a)) was set to the default, which minimized interactions between multiple girders, and the number of steel strands coupled with the depth of the girders mentioned earlier were applied. The average cost of typical tub girders was \$89.1/ft^2 per unit length with material and labor expenses except for the contribution of manufacturing facilities, equivalent to \$0.59/lb. Figure 87(a) relates the depth of the prototype girders to projected costs. The cost gap between t_{web} = 5 in. and 10 in. increased as the section became deeper. Hence, for pretensioning application, a web thickness of less than t_{web} = 7.5 in. should first be considered; similarly, when post-tensioning is planned, t_{web} = 7.5 in. is suggested unless t_{web} = 10 in. is imperative for structural reasons. Described in Fig. 87(b) are the average costs of the three girder types. The B618-U girders were 4.2% and 2.4% more expensive than the prototype and simplified girders per foot, respectively. If a span of 150 ft is to be designed with the prototype and simplified girders, the owner may save over \$6,108 and \$3,566, respectively, per girder.

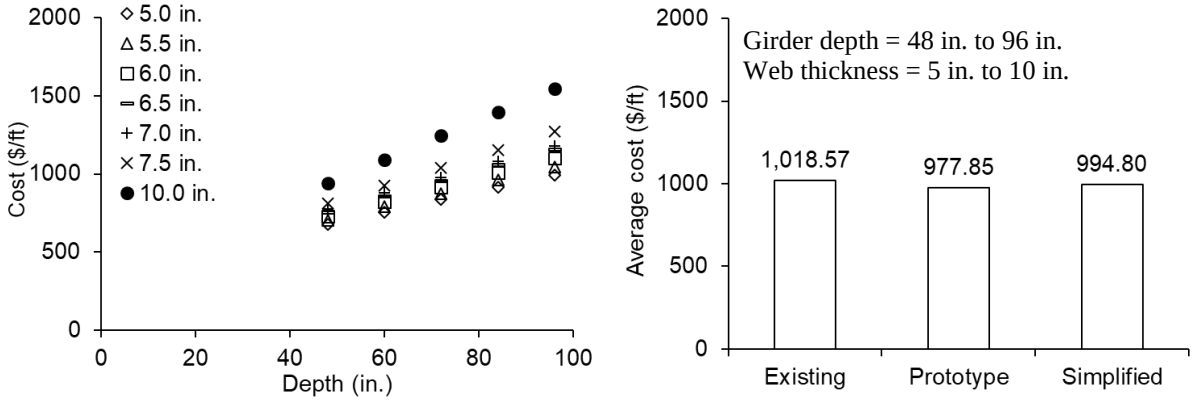

Fig. 87. Cost estimate: (a) prototype; (b) average

6. Use of 0.7 in. Steel Strands for B618-U Girders

Although 0.7 in. strands are not prevalently employed in Colorado at this time, there will be a transition from 0.6 in. to 0.7 in. in the future, similar to the occasion of 0.5 in. to 0.6 in. Comparative research was thus conducted to assess the performance of the existing B618-U girder series incorporating 0.6 in. and 0.7 in. strands. As illustrated in Fig. 88(a), the girders with 0.7 in. accomplished 12.6% longer spans relative to those with 0.6 in. with 4.4% less steel strands (Fig. 88(b)), on average. The average stresses of the girders with the 0.7 in. strands were generally higher due to the increased magnitude of prestressing force (Fig. 89), and the AASHTO requirements were satisfied. The extended span length of the girders with the 0.7 in. strands raised deflections (Fig. 90), particularly evident under the prestressing (PS in Figs. 90(a) through (c)) and live load (Fig. 90(d)) conditions. On the flexural capacity of the girders, an average improvement of 30.3% was noticed with the 0.7 in. strands (Fig. 91). Figures 92 to 113 demonstrate the specific responses of all girder cases with the 0.6 in. and 0.7 in. strands. While the use of 0.7 in. strands is beneficial from a structural point of view, further investigations are necessary for the implementation of this nontraditional strand size in the field, as delineated in Sec. 1.4.

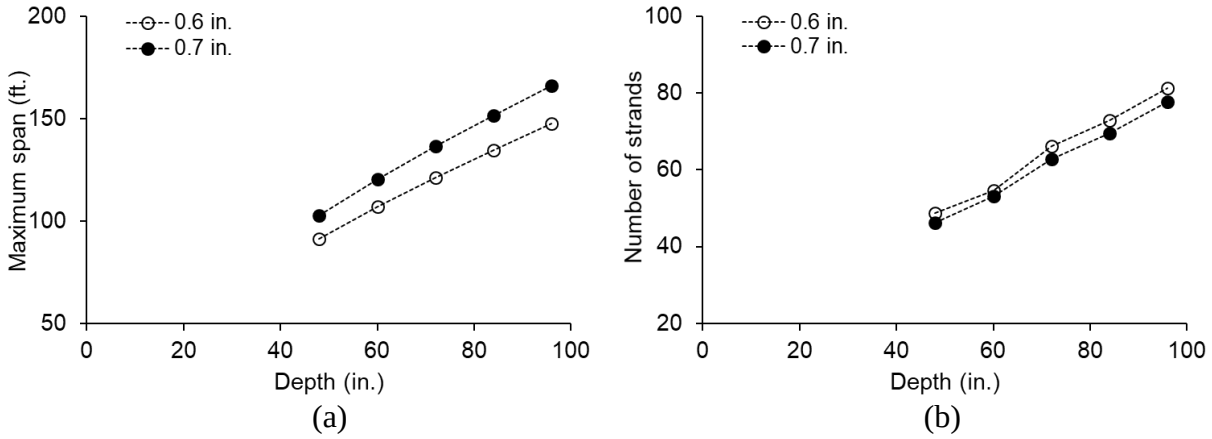

Fig. 88. Average configuration of girders: (a) maximum achievable span; (b) number of strands

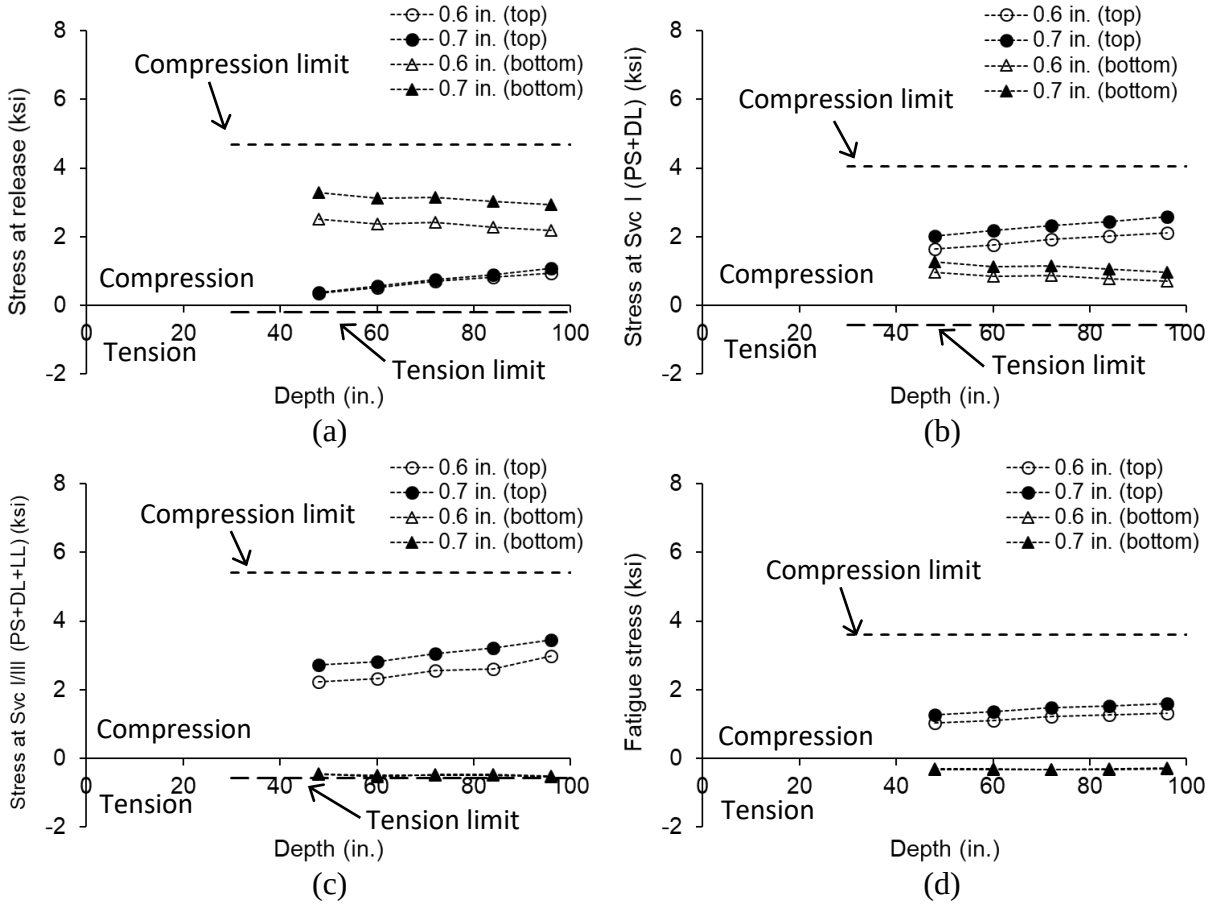

Fig. 89. Average stress variation: (a) release; (b) Service I (PS+DL); (c) Service I/III (PS+DL+LL); (d) fatigue

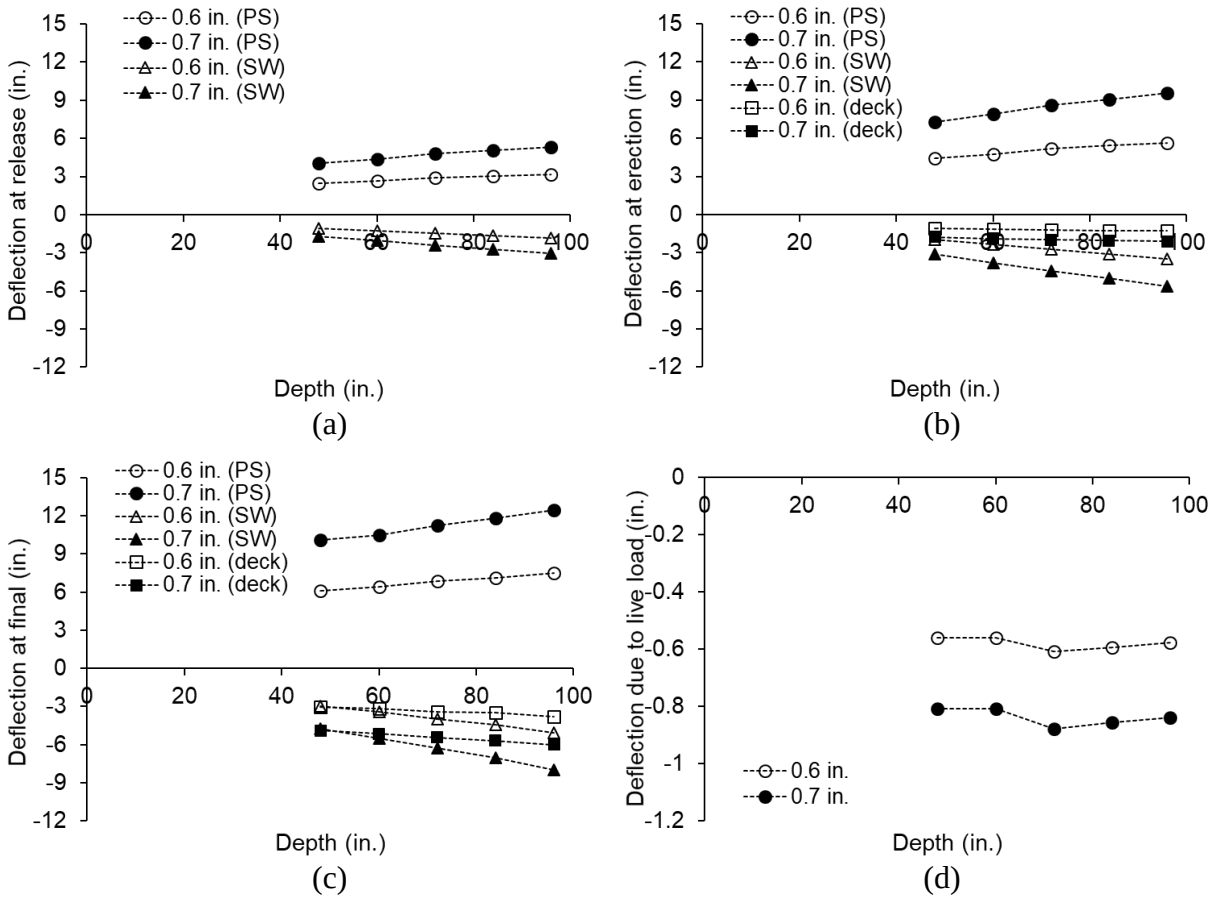

Fig. 90. Average deflection: (a) release; (b) erection; (c) final; (d) due to live load

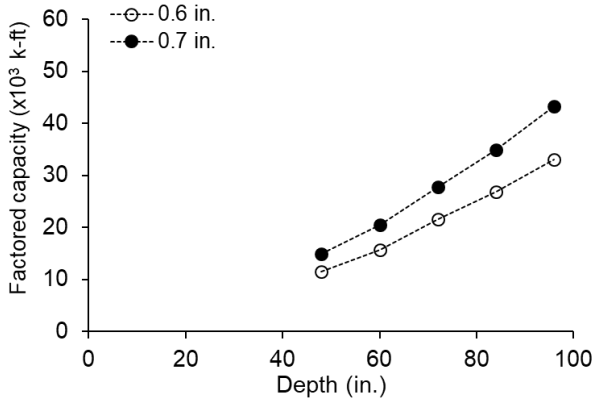

Fig. 91. Average flexural capacity at midspan

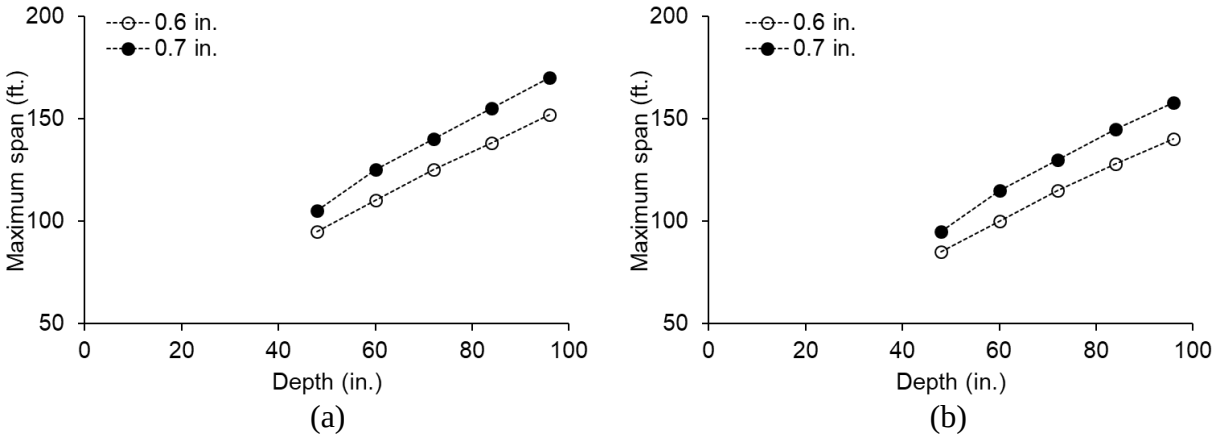

Fig. 92. Maximum achievable span length for one and two girders: (a) one lane with one girder; (b) two lanes with two girders

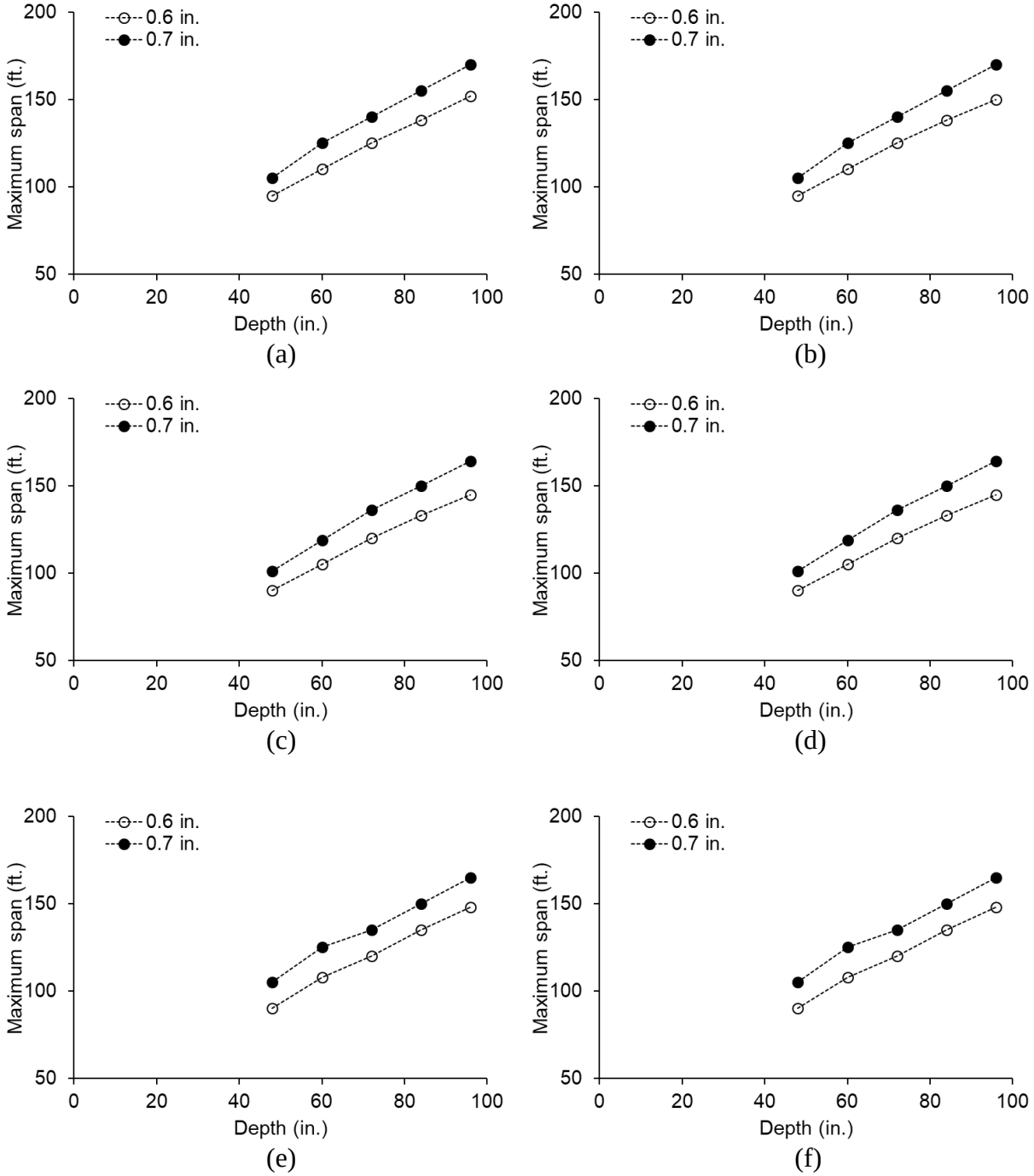

Fig. 93. Maximum achievable span length for three and four girders: (a) two lanes with three girders for exterior girder; (b) two lanes with three girders for interior girder; (c) three lanes with three girders for exterior girder; (d) three lanes with three girders for interior girder; (e) four lanes with four girders for exterior girder; (f) four lanes with four girders for interior girder

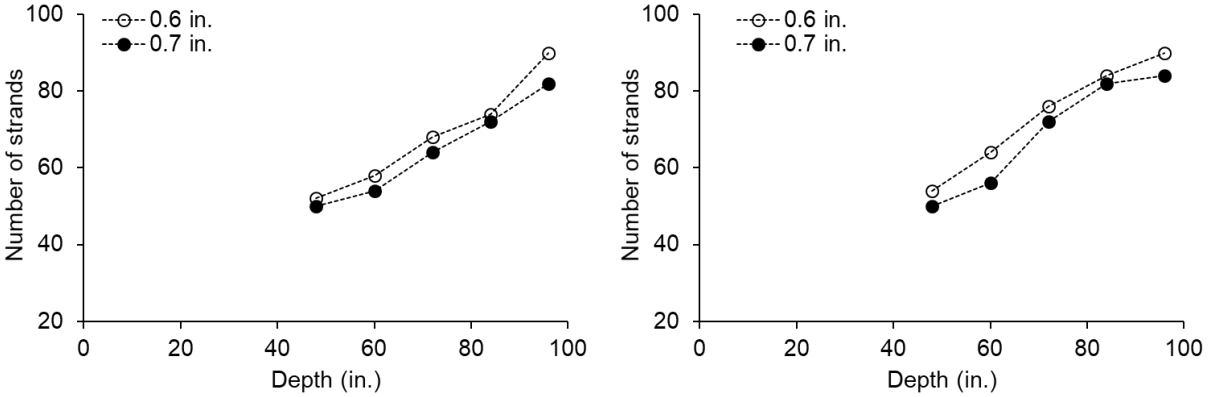

Fig. 94. Number of strands for one and two girders: (a) one lane with one girder; (b) two lanes with two girders

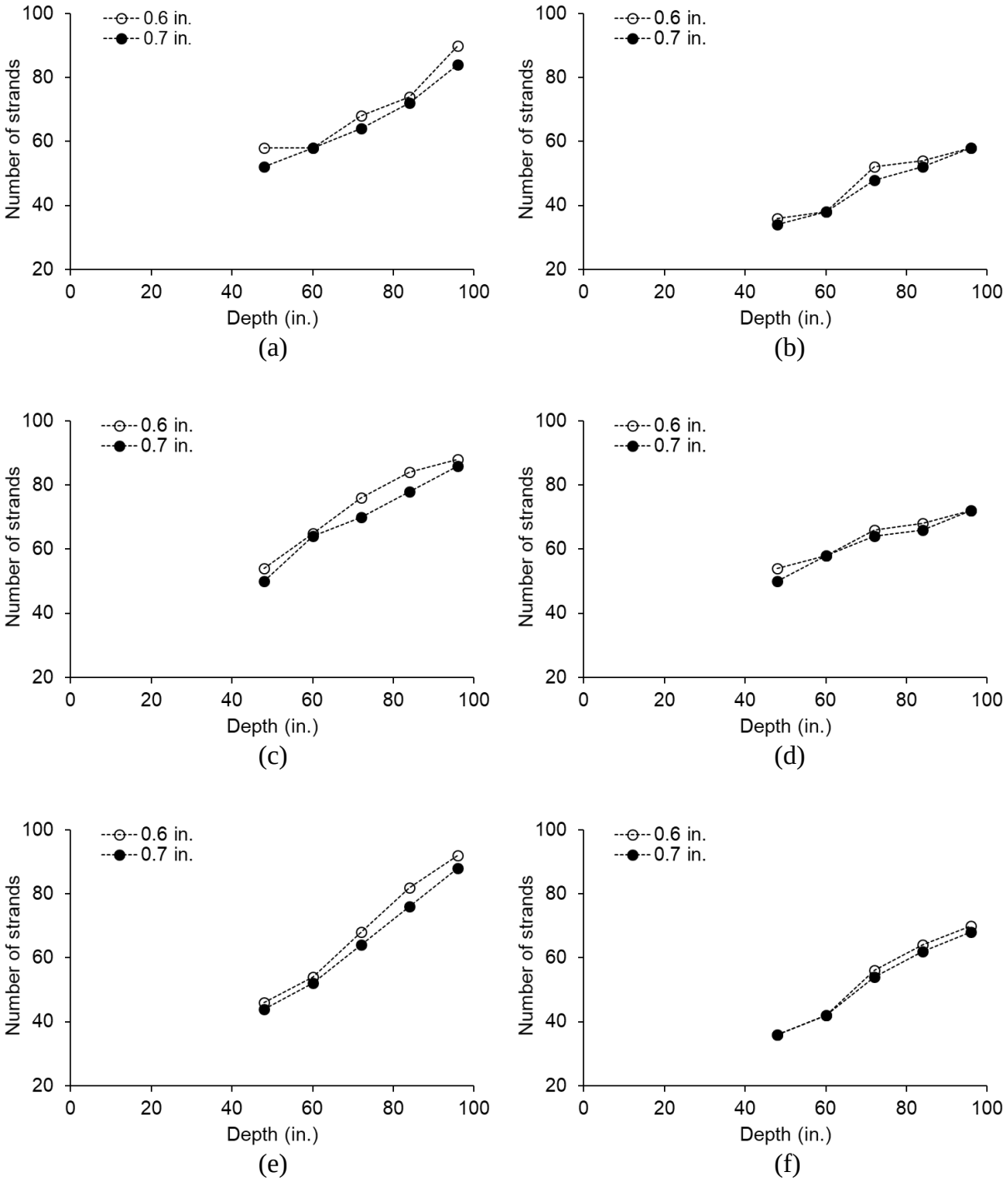

Fig. 95. Number of strands for three and four girders: (a) two lanes with three girders for exterior girder; (b) two lanes with three girders for interior girder; (c) three lanes with three girders for exterior girder; (d) three lanes with three girders for interior girder; (e) four lanes with four girders for exterior girder; (f) four lanes with four girders for interior girder

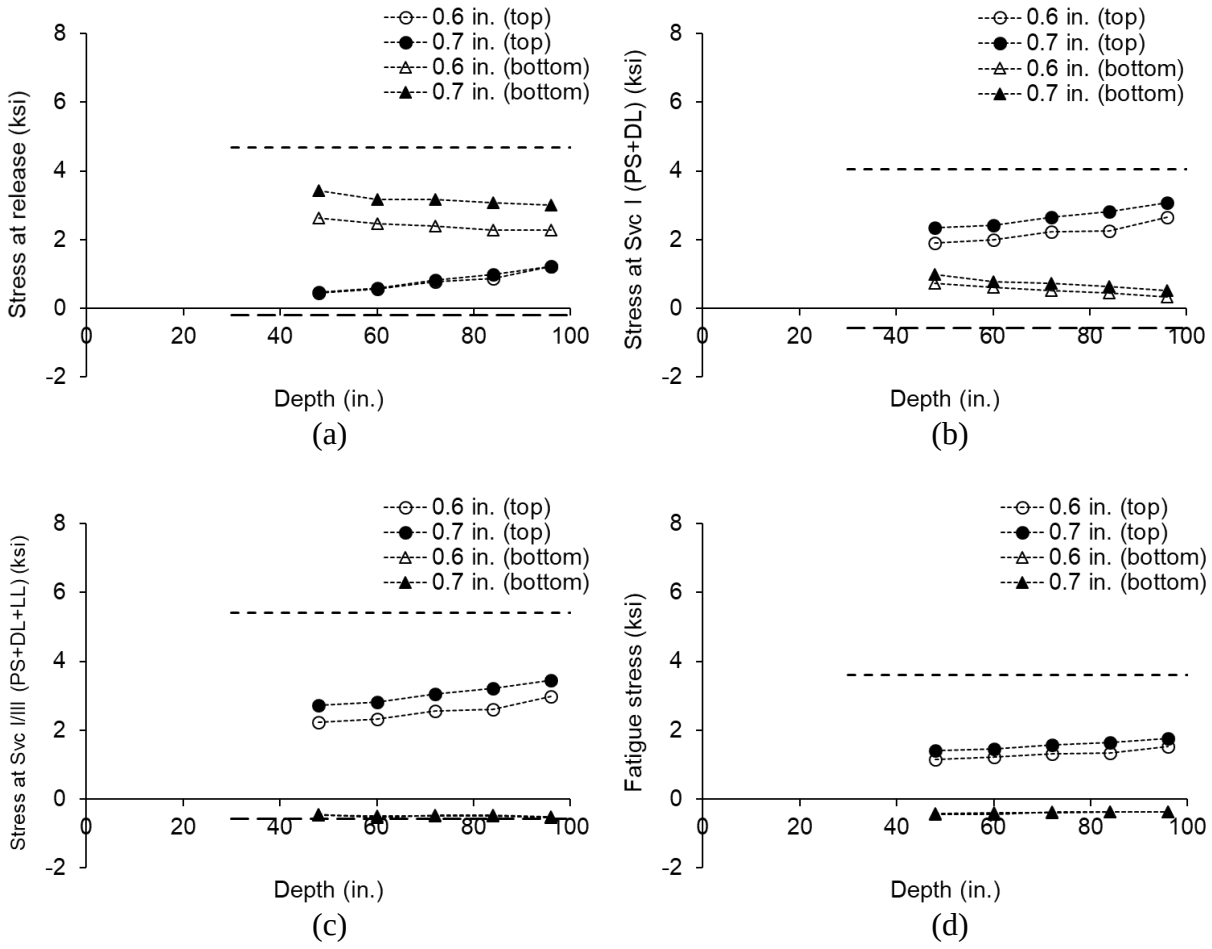

Fig. 96. Stress variation for one lane with one girder: (a) release; (b) Service I (PS+DL); (c) Service I/III (PS+DL+LL); (d) fatigue

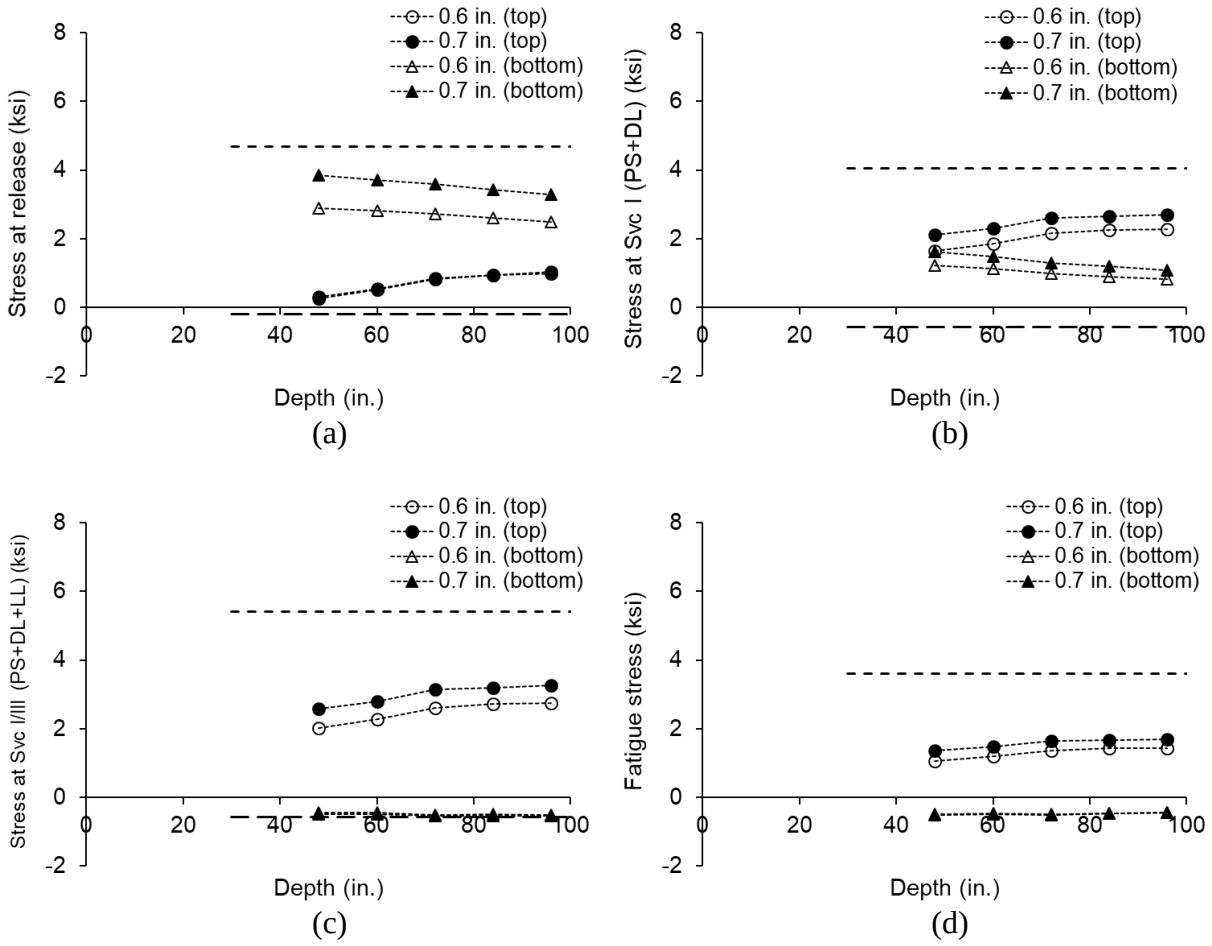

Fig. 97. Stress variation for two lanes with two girders: (a) release; (b) Service I (PS+DL); (c) Service I/III (PS+DL+LL); (d) fatigue

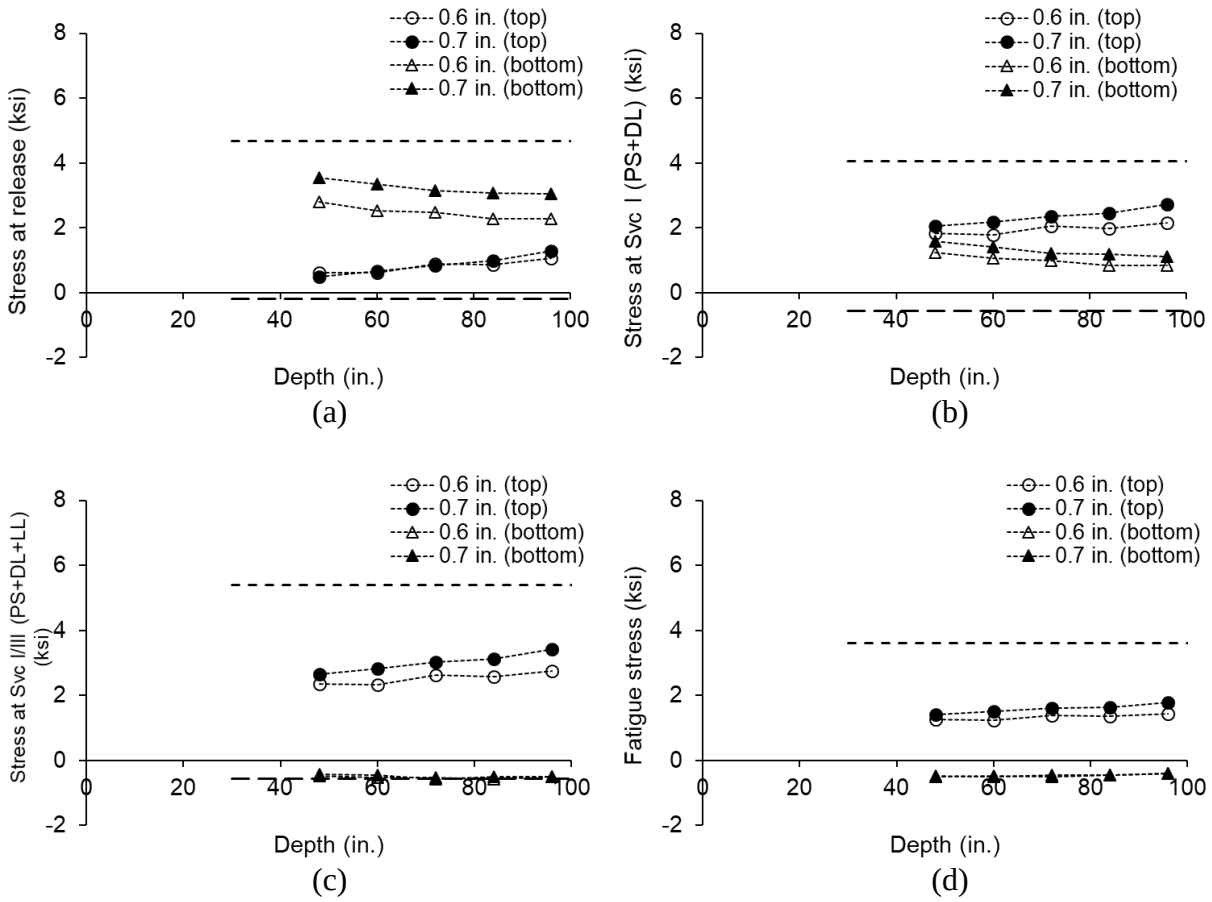

Fig. 98. Stress variation for two lanes with three girders- exterior girder: (a) release; (b) Service I (PS+DL); (c) Service I/III (PS+DL+LL); (d) fatigue

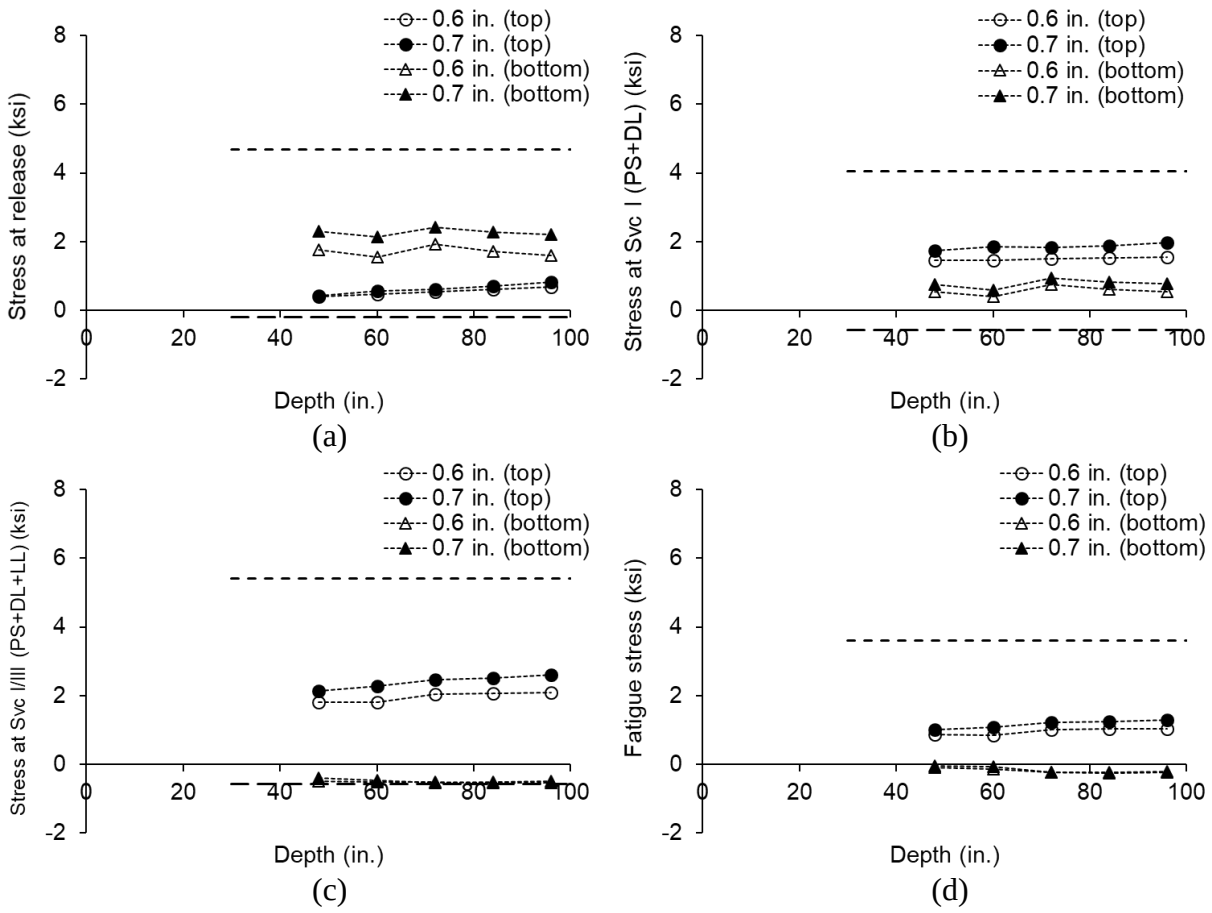

Fig. 99. Stress variation for two lanes with three girders- interior girder: (a) release; (b) Service I (PS+DL); (c) Service I/III (PS+DL+LL); (d) fatigue

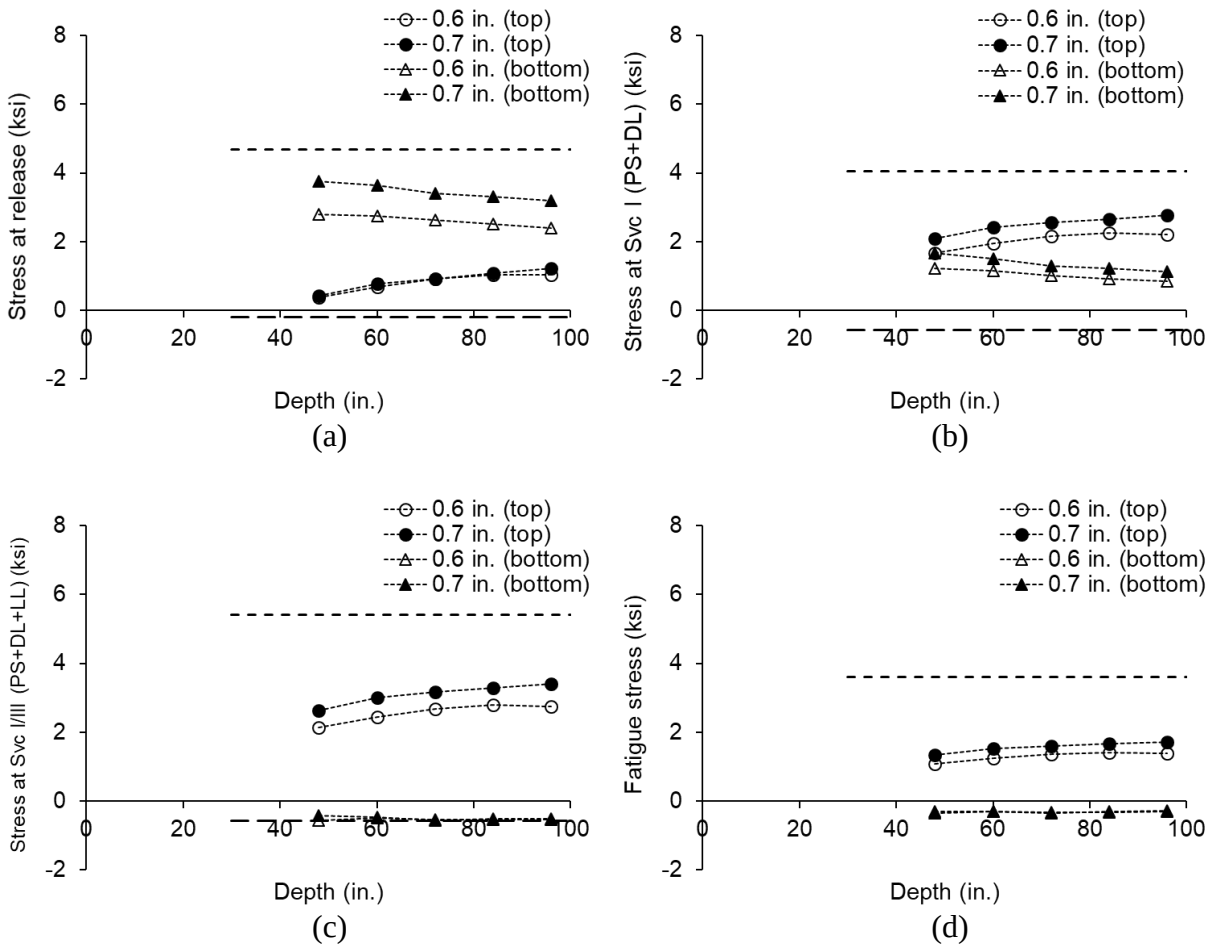

Fig. 100. Stress variation for three lanes with three girders- exterior girder: (a) release; (b) Service I (PS+DL); (c) Service I/III (PS+DL+LL); (d) fatigue

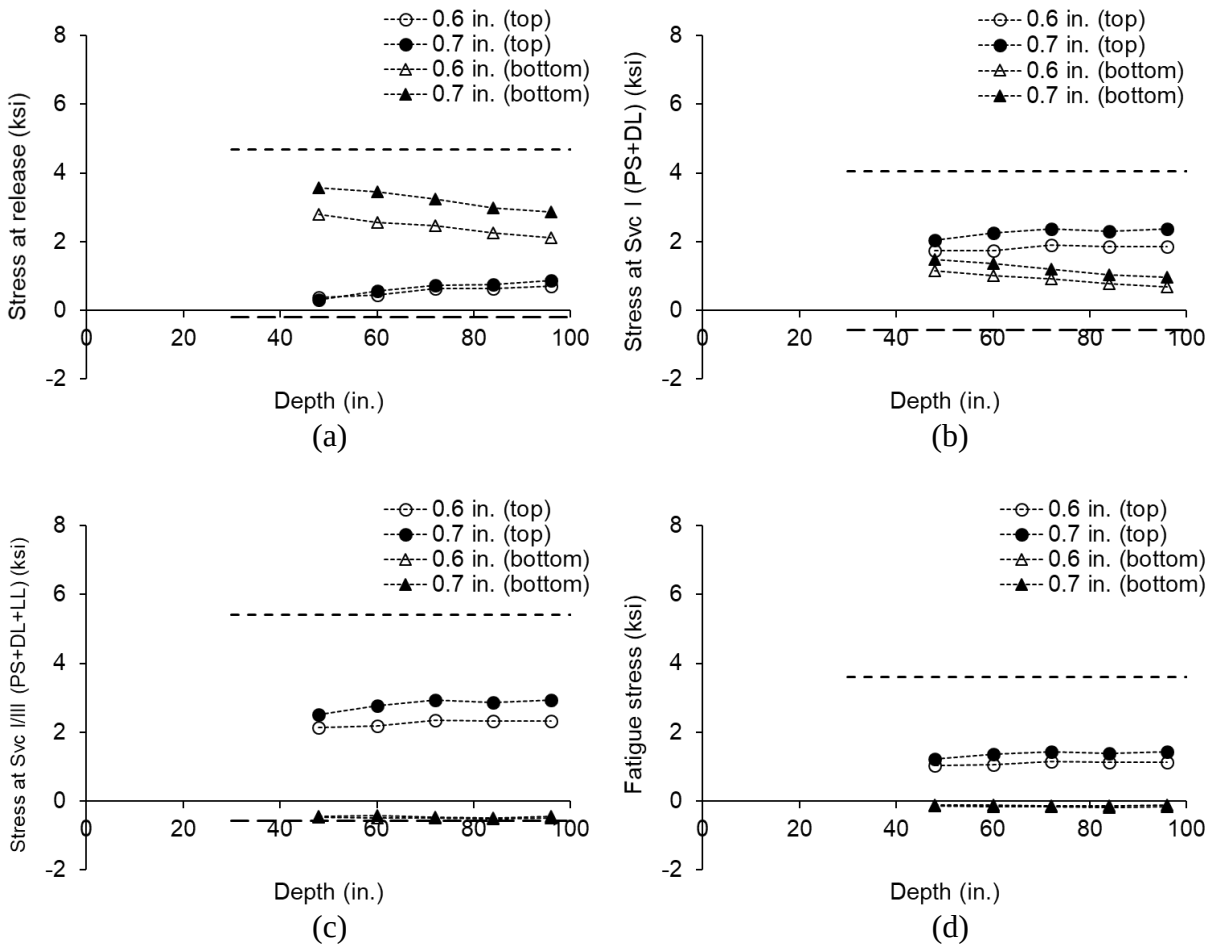

Fig. 101. Stress variation for three lanes with three girders- interior girder: (a) release; (b) Service I (PS+DL); (c) Service I/III (PS+DL+LL); (d) fatigue

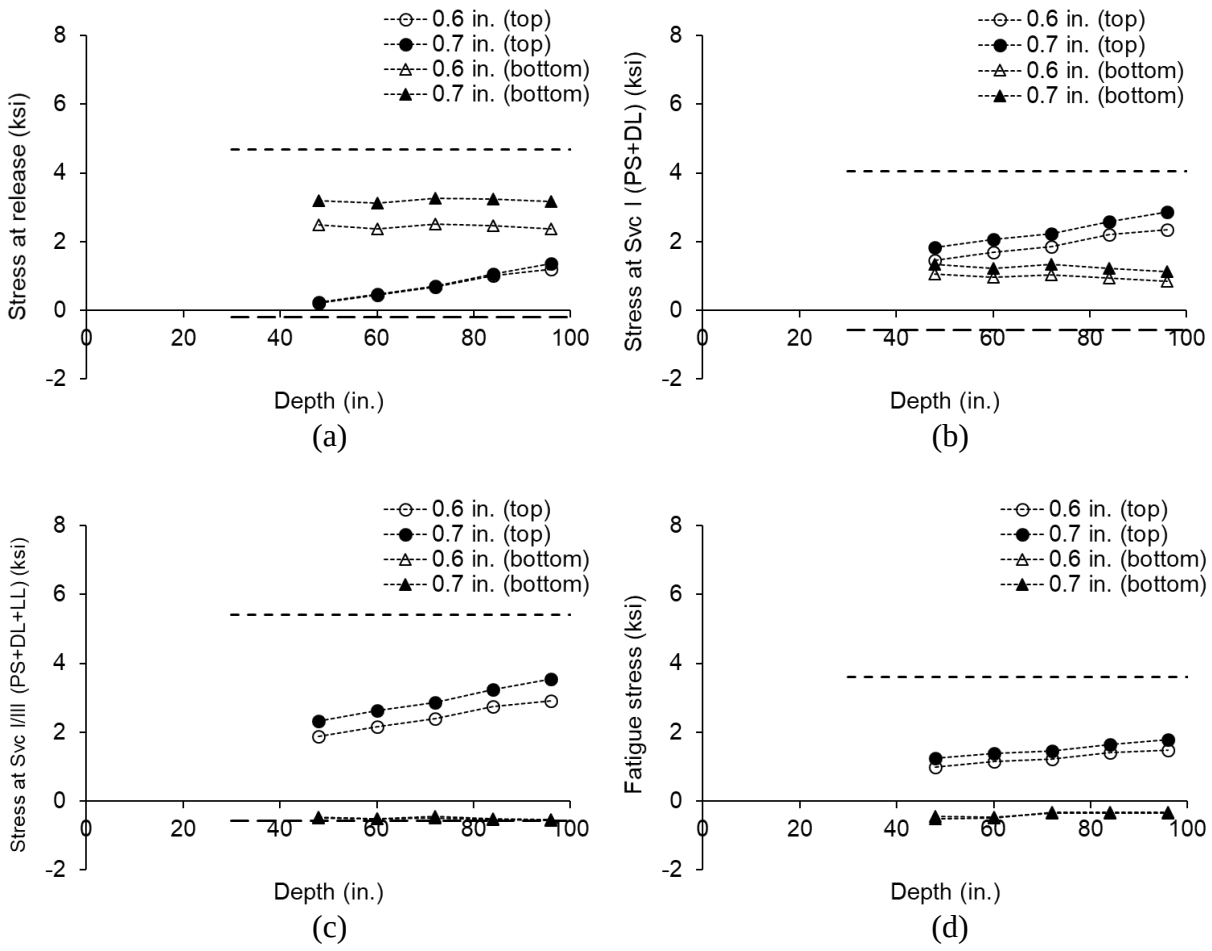

Fig. 102. Stress variation for four lanes with four girders- exterior girder: (a) release; (b) Service I (PS+DL); (c) Service I/III (PS+DL+LL); (d) fatigue

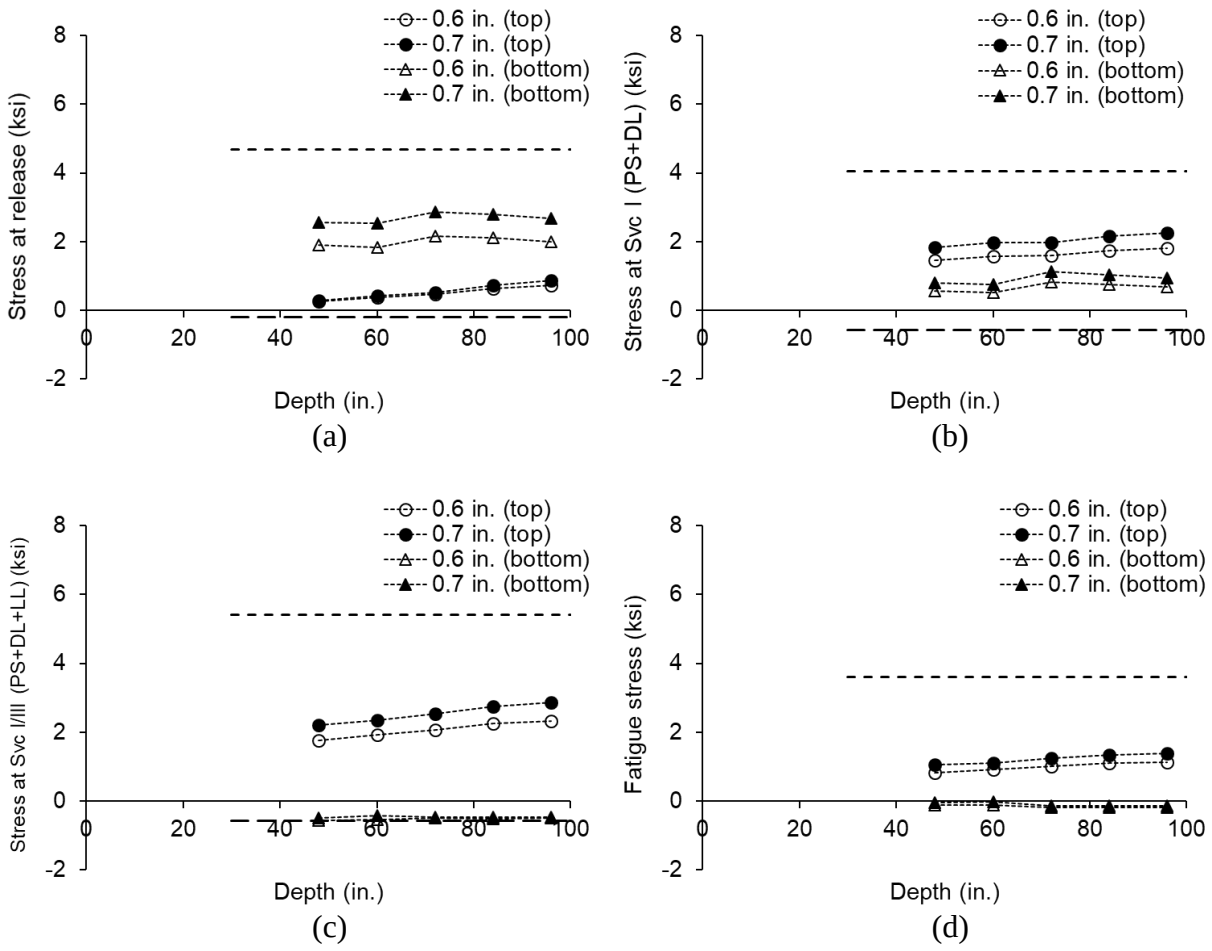

Fig. 103. Stress variation for four lanes with four girders- interior girder: (a) release; (b) Service I (PS+DL); (c) Service I/III (PS+DL+LL); (d) fatigue

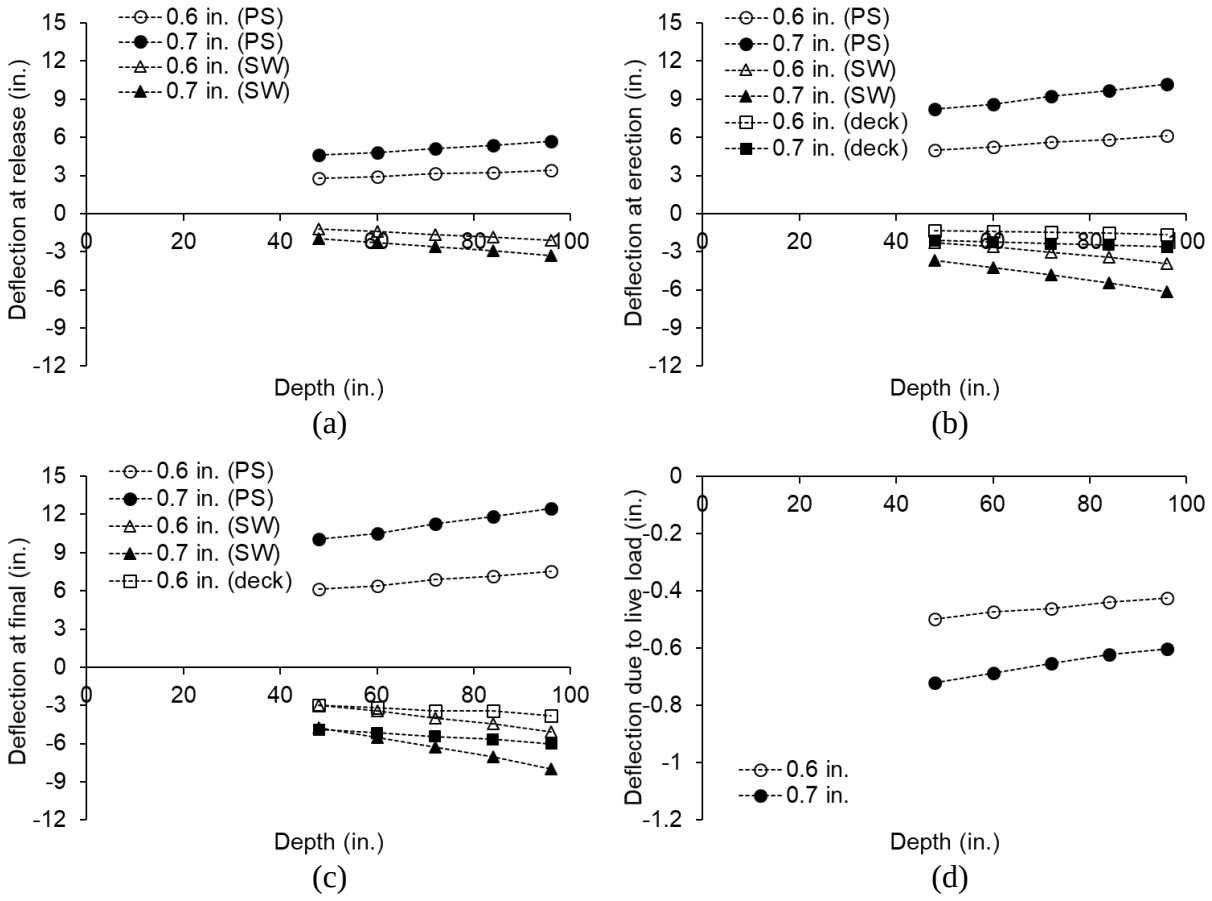

Fig. 104. Deflection for one lane with one girder: (a) release; (b) erection; (c) final; (d) due to live load

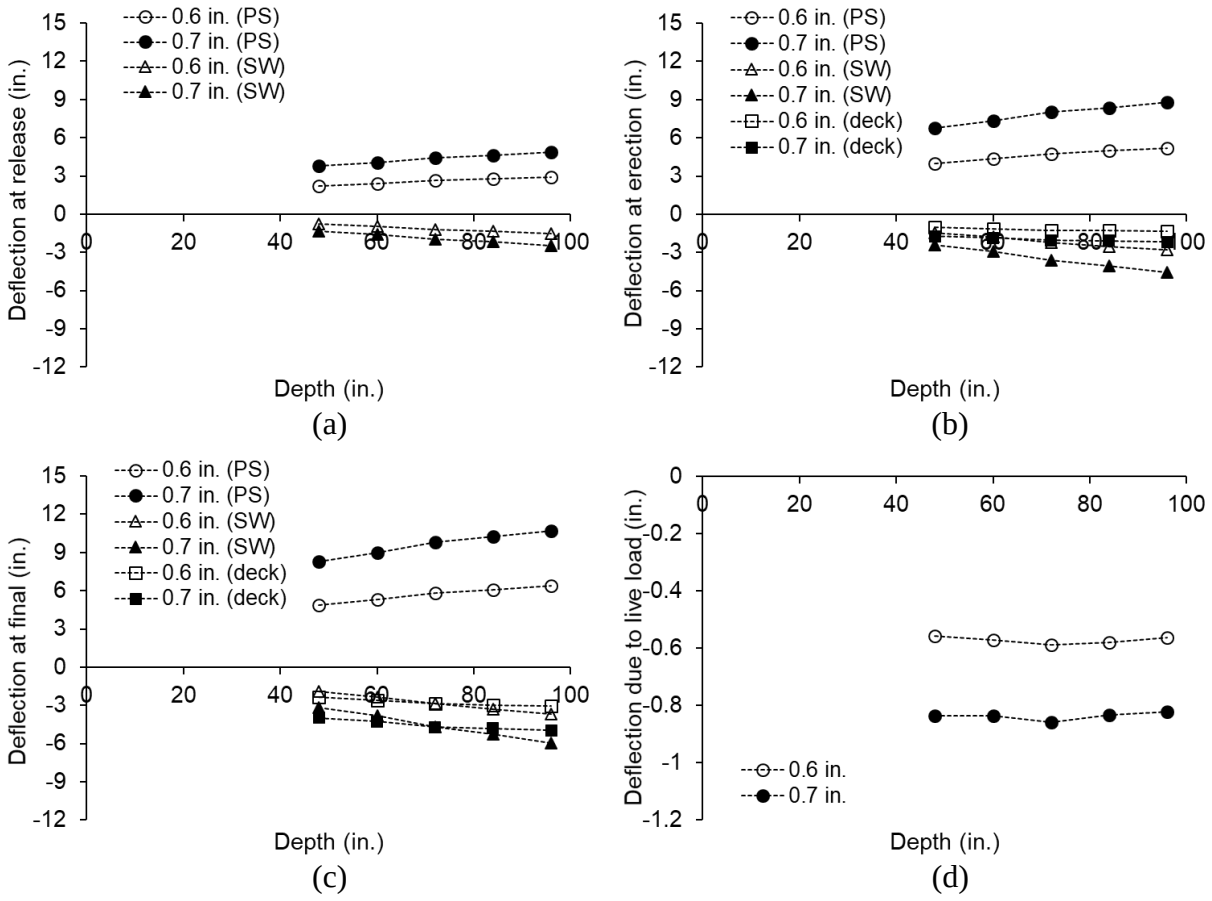

Fig. 105. Deflection for two lanes with two girders: (a) release; (b) erection; (c) final; (d) due to live load

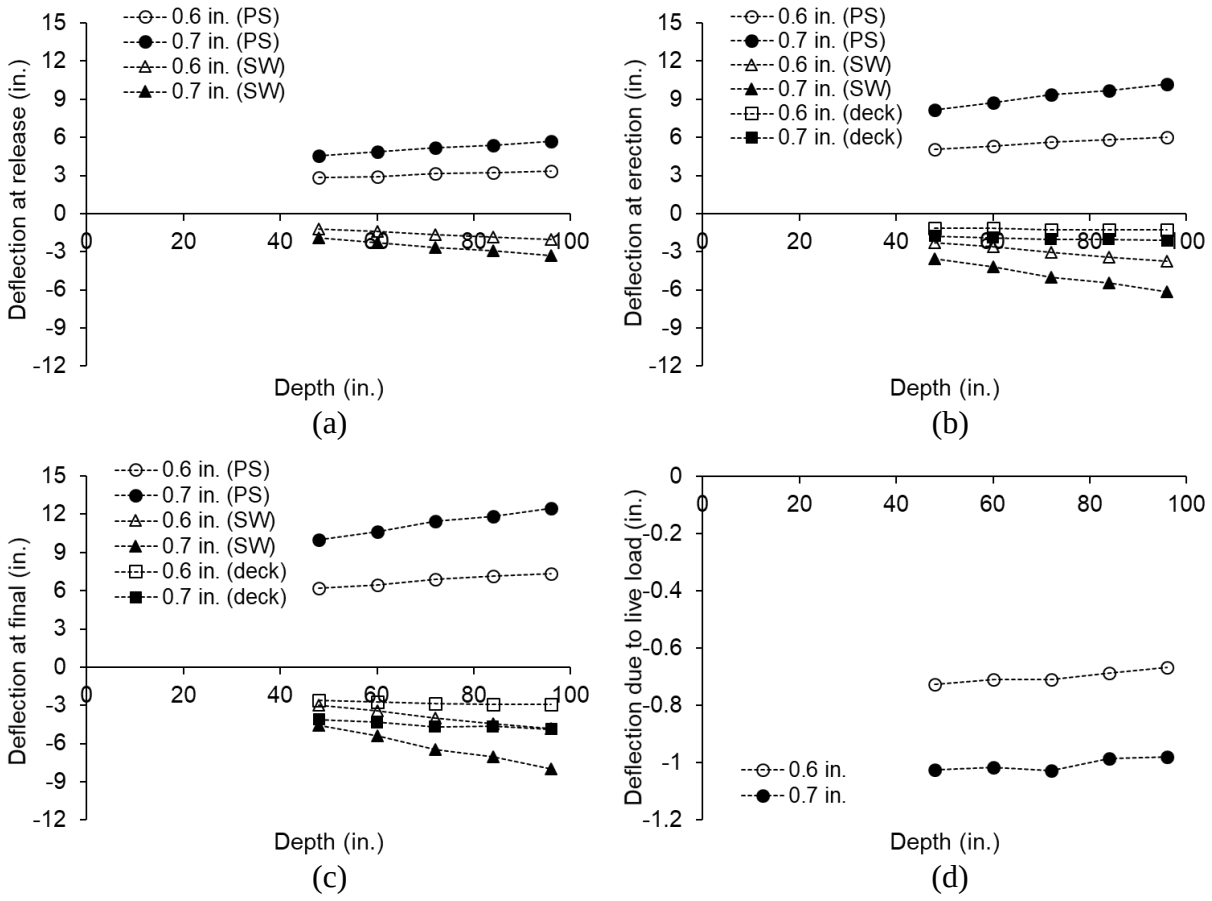

Fig. 106. Deflection for two lanes with three girders- exterior girder: (a) release; (b) erection; (c) final; (d) due to live load

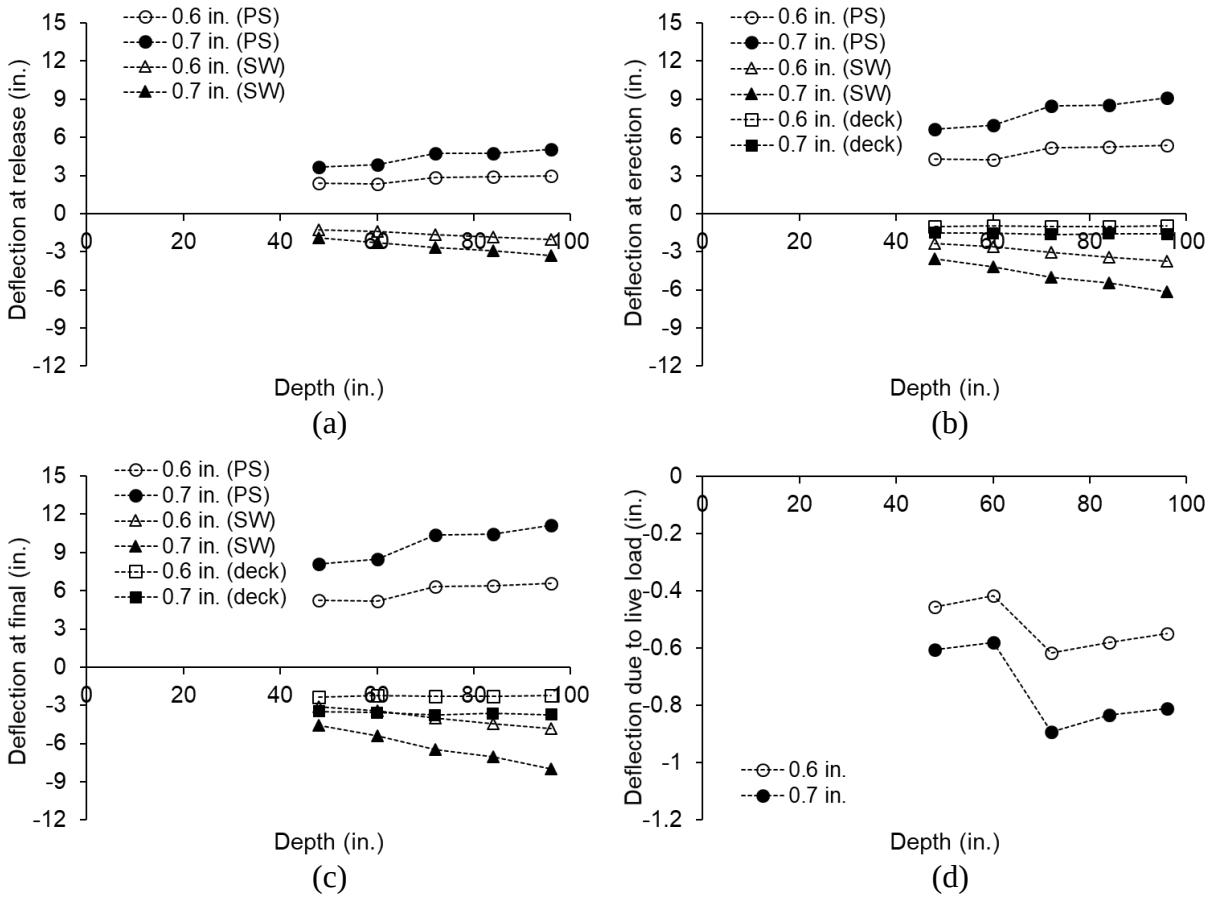

Fig. 107. Deflection for two lanes with three girders- interior girder: (a) release; (b) erection; (c) final; (d) due to live load

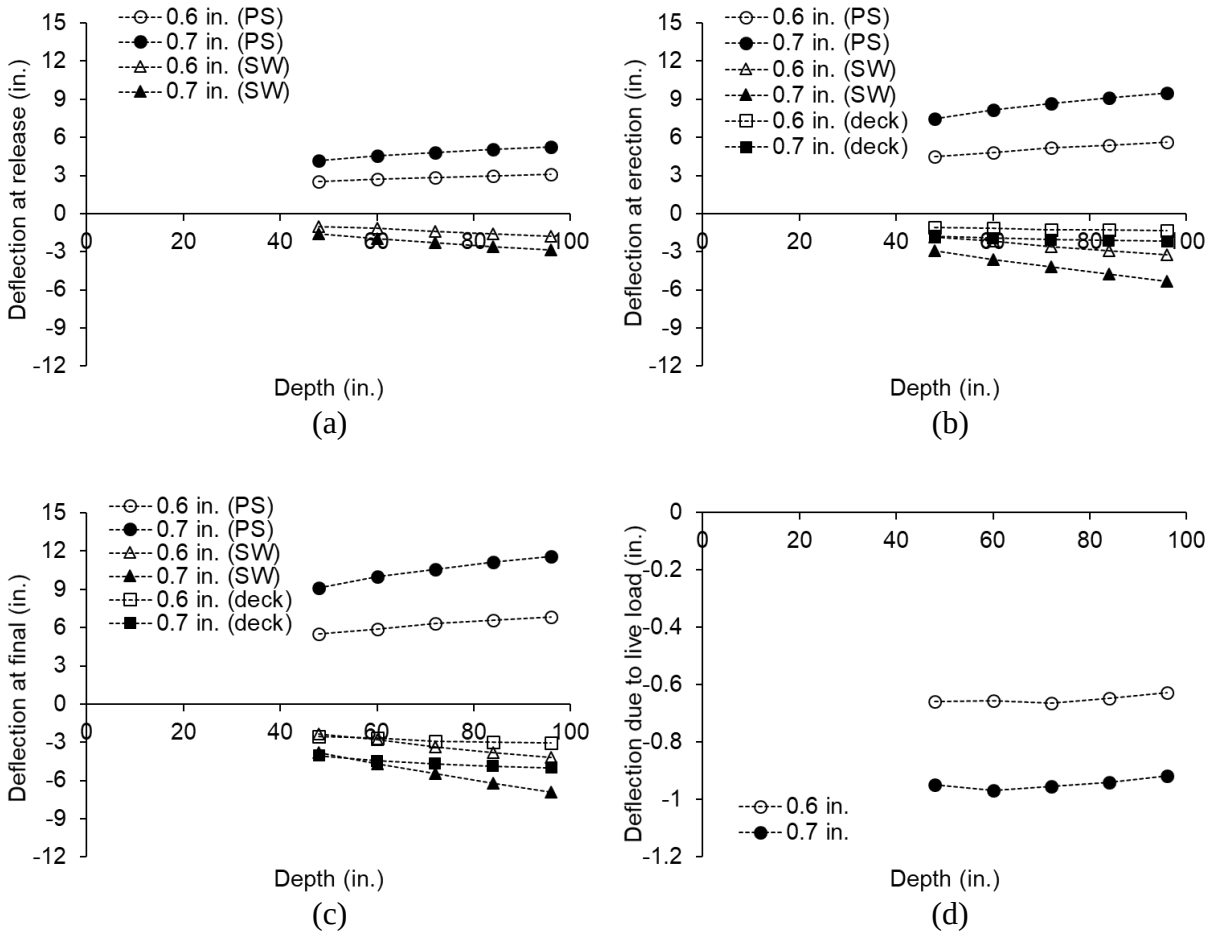

Fig. 108. Deflection for three lanes with three girders- exterior girder: (a) release; (b) erection; (c) final; (d) due to live load

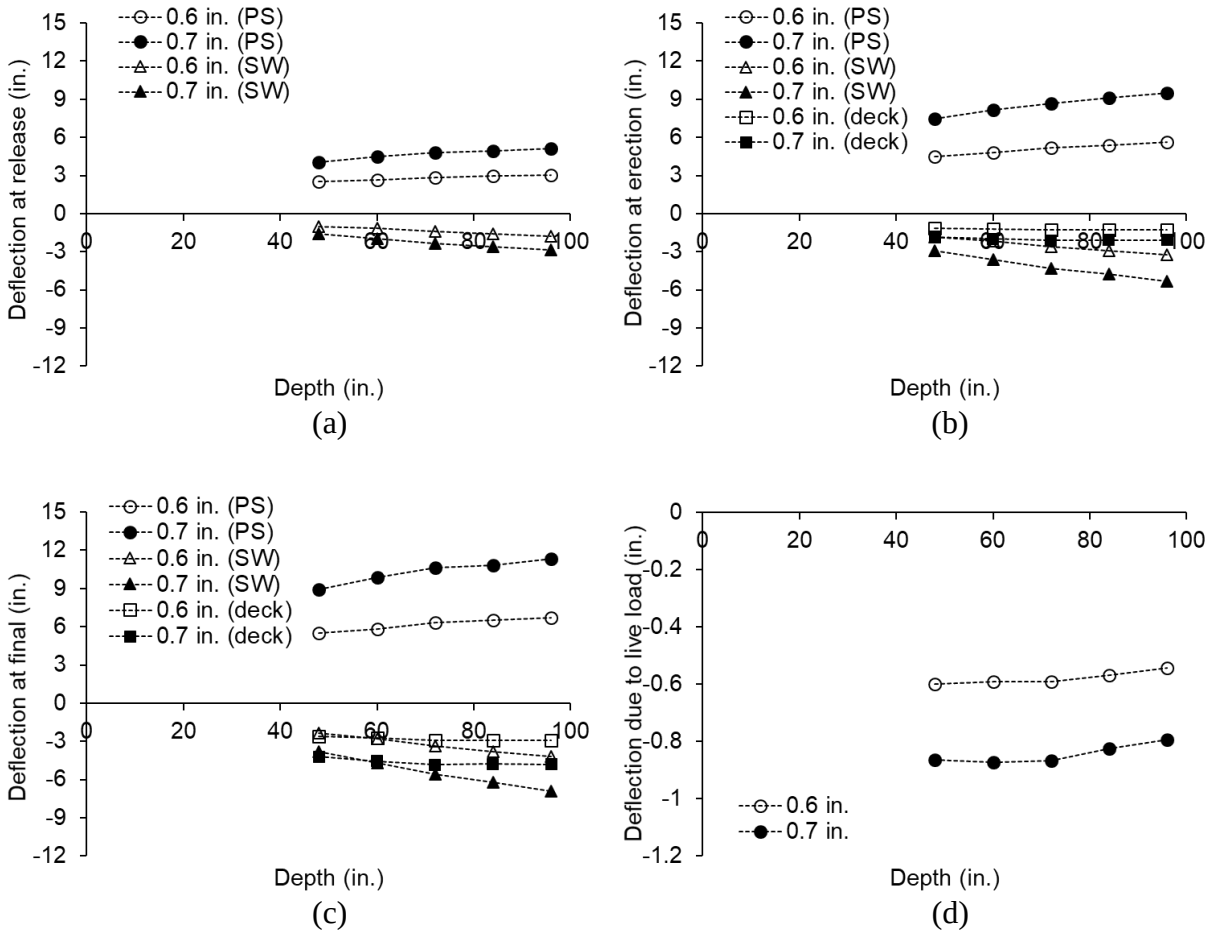

Fig. 109. Deflection for three lanes with three girders- interior girder: (a) release; (b) erection; (c) final; (d) due to live load

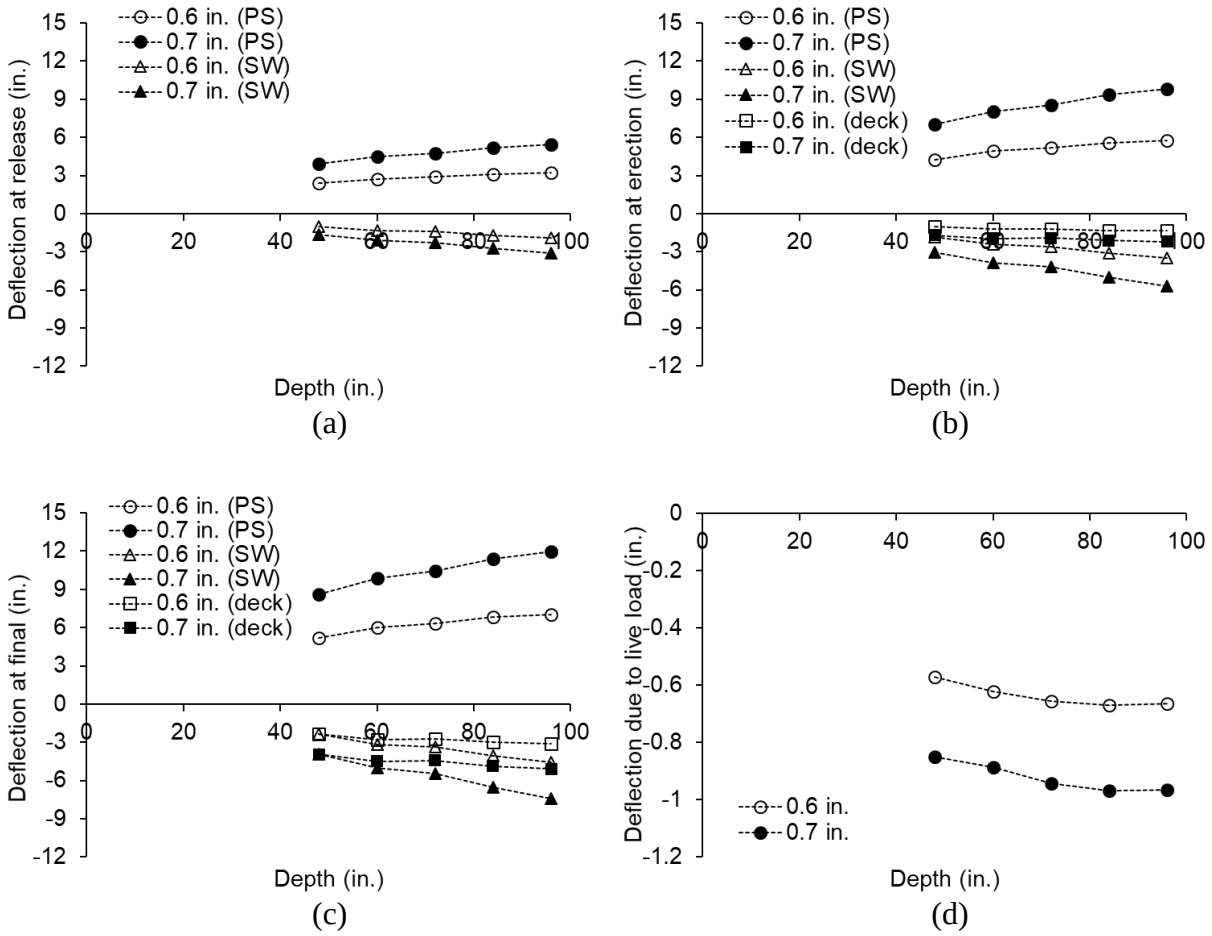

Fig. 110. Deflection for four lanes with four girders- exterior girder: (a) release; (b) erection; (c) final; (d) due to live load

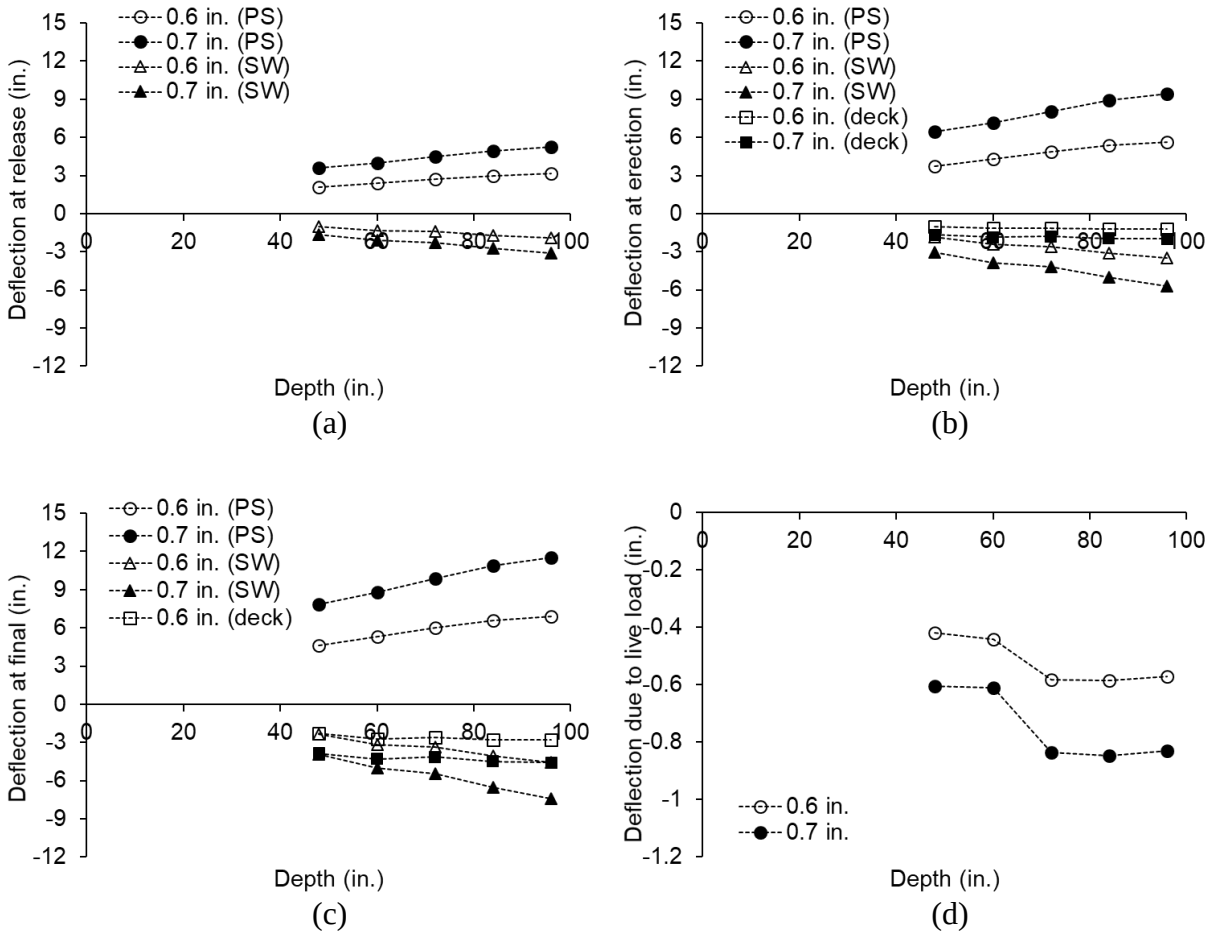

Fig. 111. Deflection for four lanes with four girders- interior girder: (a) release; (b) erection; (c) final; (d) due to live load

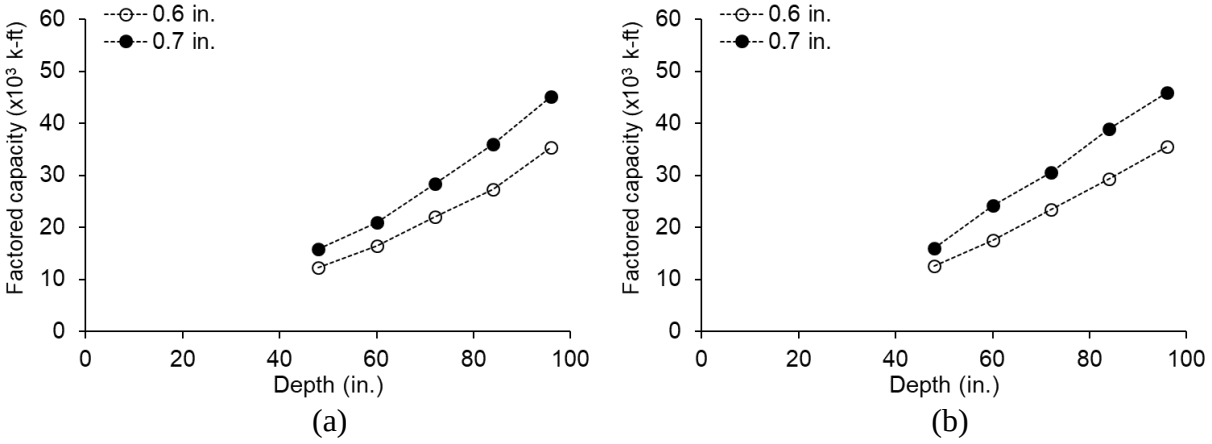

Fig. 112. Flexural capacity at midspan: (a) one lane with one girder; (b) two lanes with two girders

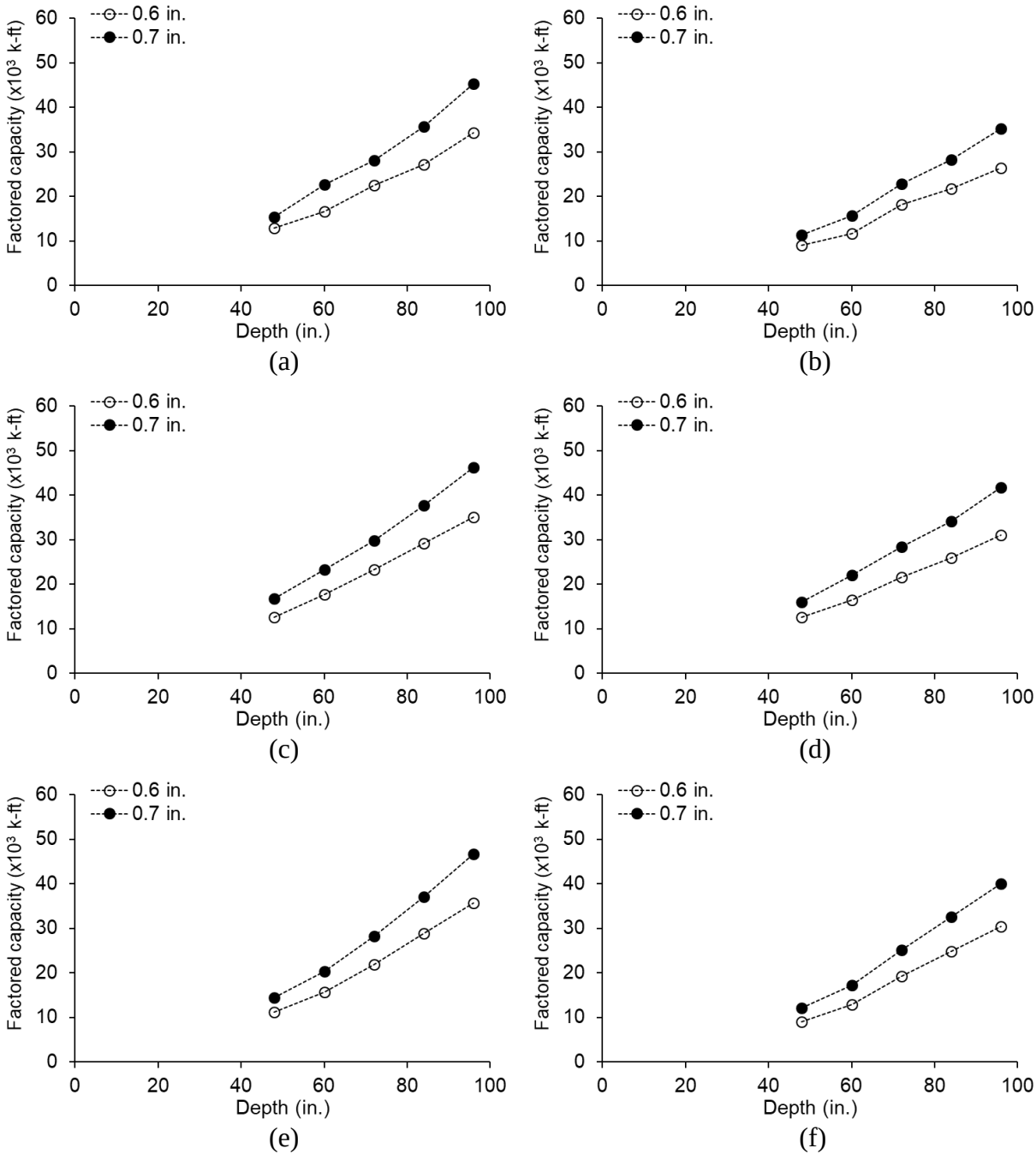

Fig. 113. Flexural capacity at midspan: (a) two lanes with three girders for exterior girder; (b) two lanes with three girders for interior girder; (c) three lanes with three girders for exterior girder; (d) three lanes with three girders for interior girder; (e) four lanes with four girders for exterior girder; (f) four lanes with four girders for interior girder

7. Summary and Conclusions

This report has discussed three major aspects that were related to the development of tub girders for prestressed concrete bridges complying with LRFD: i) a literature review, ii) an assessment of existing and proposed girders, and iii) parametric investigations. In addition, the use of 0.7 in. strands was elaborated for the B618-U girders. The first part of the report provided a holistic overview of prestressed concrete tub girders for highway bridges. The geometric configuration and reinforcing schemes of the girders dominated the performance of a superstructure. Both pretensioning and post-tensioning were applicable in practice. Several decking methods were proposed and implemented. The distribution of live load was studied in line with an evaluation of the existing AASHTO equations. The majority of research concerning end zone cracking was empirical and inconsistent contents were documented. Findings from the literature review are as follows:

- Due to the many advantages and favorable functionality, tub girders have been broadly used for bridge construction in the United States. As far as Colorado is concerned, the B618-U series were developed in the 1990s and CDOT was one of the first to pioneer curved tub girders. Nonetheless, limited endeavors were made to enhance the performance of the sections and, thus, an update should be made to satisfy the contemporary requirements of LRFD with structurally efficient sections.
- The behavior of tub girders is controlled by several parameters (e.g., geometric properties, prestressing schemes, and in-situ splice). Diaphragms may be required to enhance the stability of the open-section girders against torsional stress. A couple of end block options are available in skewed tub girders to address curing heat and delayed ettringite formation. The geometric details of tub girders vary from agency to agency; accordingly, an appraisal is needed to investigate the structural efficiency of existing girders. So informed, parameters influencing the efficiency of tub girders can be identified and will be considered when developing a new girder series for Colorado's bridge structures.
- Across the nation, the strand size of 0.5 in. and 0.6 in. is utilized for prestressing concrete girders. Harping and debonding techniques are performed to reduce stress levels near the end of the girders. Early efforts encompassed the application of 0.7 in. strands, whereas generalized design information was not yet developed. For the adoption of 0.7 in. strands,

research is indispensable to check the applicability of current design specifications and to propose new provisions. Precasters' facilities should be examined as well.

- Tub girders are post-tensioned and spliced on site to accomplish continuities, which will benefit the superstructure system. Before planning a post-tensioning scheme, the designer should evaluate span length, girder spacing, self-weight, maintenance, stability, and life cycle costs. The loss of prestress may be estimated according to AASHTO LRFD BDS (AASHTO 2020). Splicing redistributes bending moments and improves serviceability.
- Full- and partial-depth decks are used for tub girders. Cast-in-place concrete is conventional, while precast panels offer a number of advantages as regards construction time, quality, and costs. After placing decks, a composite system is achieved and thus the tub girders act like closed boxes. Overhangs extend the space of the deck, while their length should be determined within a range that does not cause excessive deflections and distortional stresses.
- The interaction among the deck, girders, and secondary structural members of tub girders results in uneven live load distributions. The position and number of vehicles govern the magnitude of distribution factors. The empirically calibrated distribution factors of AASHTO LRFD BDS (AASHTO 2020) are convenient for preliminary design, whereas refined factors attained from finite element modeling provide accurate live loads. The shear distribution factors of AASHTO LRFDS BDS are recommended to be recalibrated for tub girders.
- End zone cracking is a problem that remains unsolved. The splitting and bursting cracks of prestressed concrete girders frequently occur. Design approaches were based on experience and their applicability is largely unknown; consequently, discrepancies exist in the bridge engineering community. Extensive endeavors should be expended to ameliorate practice guidelines.

The second part of the report has explored the development of new prestressed concrete tub girders in Colorado. To begin with, the strength and weakness of existing state girders (35 types taken from six transportation agencies across the United States) were evaluated. Analytical and computational approaches were then utilized to quantify the structural efficiency of Colorado's B618-U series. Through a mathematical algorithm, an optimized girder section was identified

and its practical significance was appraised with a strand diameter of ϕ = 0.5 in., 0.6 in., and 0.7 in. at a compressive concrete strength of f'_c = 9 ksi, 10 ksi, and 11 ksi. The applicability of proposed prototype girders was investigated in the context of AASHTO LRFD BDS (AASHTO 2020), covering the serviceability and ultimate limit states. To comprehend the practicality of the prototype girders, five bridge superstructures were designed and their behavior was studied. The prototype sections were simplified for the sake of constructability by modifying haunches and bilinear exterior web lines. The production costs of the girders were estimated and monetary benefits were discussed for the prototype and simplified girders. The following conclusions are drawn:

- Among the existing tub girders, the Texas and Florida ones showed higher efficiency than others. The unit weight of the Colorado girders was heavier, which could unfavorably raise the dead load of a bridge system; accordingly, the weight of B618-U was recommended to be lowered to meet the range of the Florida and Washington girders.
- Relative to the B618-U girders, the optimized section enhanced the efficiency by up to 12.9% with a reduction in unit weight (kips/ft) as low as 22.3%. The 5-in. web thickness of the prototype girder with a strand diameter of ϕ = 0.5 in. and 0.6 in. maintained stress levels below the limits of AASHTO LRFD BDS (AASHTO 2020), while a wider web thickness of t_{web} = 6.6 in. was necessary for ϕ = 0.7 in.
- Parametric analysis of the one- to four-lane superstructures indicated that the prototype girders enabled longer spans and greater resistance efficiency in comparison with the B618-U girders without increasing the number of steel strands.
- The buckling-critical zone of all tub girders was located within the top-third region of the webs. The buckling load of the prototype with t_{web} = 5 in. to 10 in. was tantamount to that of B618-U, while the stability of the simplified sections did not reach those levels and the use of bracing elements was recommended. On the torsional rigidity of these three girders, there was no notable difference.
- The performance of the B618-U girders with the 0.7 in. strands outperformed that of the girders with the 0.6 in. strands in the matter of span length and flexural capacity. In spite of such satisfactory responses, follow-up research is suggested to clarify the general applicability of AASHTO LRFD BDS (AASHTO 2020) when the enlarged strands are adopted.

8. References

AASHTO. 2020. AASHTO LRFD Bridge Design Specification (9th edition), American Association of State Highway and Transportation Officials, Washington, D.C.

ACI. 2019. Building Code Requirements for Structural Concrete (ACI 318-19), American Concrete Institute, Farmington Hills, MI.

Alawneh, M., Tadros, M., and Morcous, G. 2016. Innovative system for curved precast posttensioned concrete I-girder and U-girder bridges, Journal of Bridge Engineering, 21(11), 04016076.

ASTM. 2018. Standard specifications for low-relaxation, seven-wire steel strand for prestressed concrete (ASTM A416), ASTM International, West Conshohocken, PA.

Baker, T., Saiidi, M.S., Nakashoji, B., Bingle, J., Moore, T., and Khaleghi, B. 2018. Precast concrete spliced-girder bridge in Washington State using superelastic materials in bridge columns to improve seismic resiliency: from research to practice, PCI Journal, 63(1), 57-71.

Bakht, B. and Jaeger, L. G. 1992. Ultimate load test of slab-on-girder bridge, Journal of Structural Engineering, 118(6), 1608-1624.

Ball, P.D. 2019. The use of 0.7-in. prestressing strand in various bridge girder types, MS Thesis, University of Cincinnati, Cincinnati, OH.

Barrios, A.O. 1994. Behavior of high strength concrete pretensioned girders during transfer of prestressing forces, MS Thesis, University of Texas, Austin, TX.

Bichop, E.D. 1962. Continuity connection for precast prestressed concrete bridges, ACI Journal, 585-599.

Caroland, W.B., Depp, D., Janssen, H.H., and Spaans, L. 1992. Spliced segmental prestressed concrete I-beams for Shelby Creek Bridge, PCI Journal, 37(5), 22-33.

CDOT. 2020. Bridge design manual, Colorado Department of Transportation, Denver, CO.

Cruz, P.J.S. and Wisniewski, D. 2004. Ave River Bridge- a major precast prestressed concrete U-girder bridge in Portugal, PCI Journal, 49(4), 72-86.

Dang, C.N., Floyd, R.W., Hale, W.M., and Marti-Vargas, J. R. 2016. Spacing requirements of 0.7 in. (18 mm) diameter prestressing strands, PCI Journal, 61(1), 70-87.

Duan, L. and Chen, K. 2014. Posttensioned prestressed concrete girder bridges, Bridge Engineering handbook (second edition), 51-89.

Dunkman, D.A. 2009. Bursting and spalling in pretensioned U-beams, MSE Thesis, University of Texas, Austin, TX.

Eamon, C. D. and Nowak, A. S. 2002. Effects of edge-stiffening elements and diaphragms on bridge resistance and load distribution, Journal of Bridge Engineering, 7(5), 258-266.

FDOT. 2020. Index 450-210 series Florida-U beams, Florida Department of Transportation, Tallahassee, FL.

FDOT. 2022. Bridge development report (BDR) cost estimate, Florida Department of Transportation, Tallahassee, FL.

Ficenec, J.A., Kneip, S.D., Tadros, M.K., and Fischer, L.G. 1993. Prestressed spliced I-girders: Tenth Street Viaduct project, Lincoln, Nebraska, PCI Journal, 38(5), 38-48.

Gergely, P., Sozen, M.A., and Siess, C.P. 1963. The effect of reinforcement on anchorage zone cracks in prestressed concrete members, University of Illinois Structural Research Series No. 271.

Holombo, J., Prietley, M.J.N., Seible, F.S. 2000. Continuity of precast prestressed spliced-girder bridges under seismic loads, PCI Journal, 45(2), 40-63.

Hovell, C., Avendano, A., Moore, A., Dunkman, D., Bayrak, O., and Jirsa, J. 2013. Structural performance of Texas U-beams at prestress transfer and under shear-critical loads, Final Report, FHWA/TX-13/0-5831-2, University of Texas, Austin, TX.

Huang, D. and Shahawy, M. 2005. Analysis of tensile stresses in transfer zone of prestressed concrete U-beams, Transportation Research Record, 1928, 134-141.

Hueste, M.B.D., Mander, J.B., and Parkar, A.S. 2012. Continuous prestressed concrete girder bridges volume 1: literature review and preliminary designs, Report 0-6651-1, Texas Transportation Institute, College Station, TX.

Hughs, E. and Idriss, R. 2006. Live-load distribution factors for prestressed concrete, spread box-girder bridge, Journal of Bridge Engineering, 11(5), 573-581.

Itani, R.Y. and Galbraith, R.L. 1986. Design of prestressed concrete girders without end blocks, WSDOT Report WA-RD 81, Washington Department of Transportation, Olympia, WA.

Janssen, H.H. and Spaans, L. 1994. Record span spliced bulb-tee girders used in Highland View Bridge, PCI Journal, 39(1), 12-19.

Kim, J.R., Kwak, H.-G., and Kim, B.-S. 2019. Design equation to evaluate bursting forces at the end zone of post-tensioned members, Computers and Concrete, 24(5), 423-436.

Kim, Y.J. 2017. Prestressed concrete plant in Colorado, Professional Visit, Denver, CO.

Kim, Y.J., Tanovic, R., and Wight, R.G. 2009. Recent advances in performance evaluation and flexural response of existing bridges, Journal of Performance of Constructed Facilities, 23(3), 190-200.

Lasdon, L.S., Fox, R.L., and Ratner, M.W. 1973. Nonlinear optimization using the Generalized Reduced Gradient method, Technical Memorandum No. 325, National technical Information Service, US Department of Commerce, Springfield, VA.

Lounis, Z., Mirza, M.S., and Cohn, M.Z. 1997. Segmental and conventional precast prestressed concrete I-bridge girders, Journal of Bridge Engineering, 2(3), 73-82.

Ma, J. and Low, S.-G. 2014. Precast-pretensioned concrete girder bridges, Bridge Engineering handbook (second edition), 1-49.

Marshall, W.T. and Mattock, A.H. 1962. Control of horizontal cracking in the ends of pretensioned preestressed concrete girders, PCI Journal, 7(10), 56-75.

McMullen, M.L., Elkaissi, J.I., and Leonard, M.A. 2008. Long-span precast U-girders in Colorado, ASPIRE, 2(4), 64-66.

MDOT. 2013. Michigan bridge design manual, Lansing, MI

Miller, R.A., Castrodale, R.W., Mirmiran, A., and Hastak, M. 2004. Connection of simple span precast concrete girders for continuity, NCHRP Report 519, Transportation Research Board, Washington, D.C.

Monzon, E.V., Itani, A.M., and Reno, M. 2014. Horizontally curved girder bridges, Bridge Engineering handbook (second edition), 259-281.

Morcous, G., Assad, S., Hatami, A., and Tadros, M.K. 2014. Implementation of 0.7 in. diameter strands at 2.0 × 2.0 in. spacing in pretensioned bridge girders, PCI Journal, 59(3), 145-158.

Mott, R. and Diaz, M.A. 2010. Distribution factors for short-haul vehicular loads on prestressed concrete open box beam (U-beam) bridges, Practice Periodical on Structural Design and Construction, 15(2), 101-108.

Nawy, E.G. 2006. Prestressed concrete: a fundamental approach, Prentice Hall, Upper Saddle River, NJ

Newhouse, C.D., Roberts-Wollmann, C.L., and Cousins, T.E. 2005. Development of an optimized continuity diaphragm for new PCBT girders, Report No. FHWA/VRTC 06-CR3, Virginia Transportation Research Council.

Nickas, W.N. 2004. Change to structures design guidelines: prestressed beams (FDOT Bulletin C04-01), Florida Department of Transportation, Tallahassee, FL.

NJDOT. 2016. Design manual for bridges and structures (sixth edition), New Jersey Department of Transportation, Trenton, NJ

Noisternig, J.F. and Jungwirth, D. 1996. Design and analysis of anchoring system for a carbon fiber composite cable." Proc., 2nd Intl. Conf. on Advanced Composite Materials in Bridges and Structures (ACMBS-2), 935-942.

Nutt, R.V., Schamber, R.A., and Zokaie, T. 1988. Distribution of wheel loads on highway bridges (NCHRP 12-26), Transportation Research Board, Washington, D.C.

O'Callaghan, M.R. and Bayrak, O. 2008. Tensile stresses in the end regions of pretensioned I-beams at release, Technical Report No. IAC-88-5DD1A003-1, Texas Department of Transportation, Austin, TX.

Okumus, P., Oliva, M.G., and Becker, S. 2012. Nonlinear finite element modeling of cracking at ends of pretensioned bridge girders, Engineering Structures, 40, 267-275.

Pantelides, C.P., Saxey, B.W., and Reaveley, L.D. 2007. Post-tensioned tendon losses in a spliced-girder bridge, part 1: field measurements, PCI Journal, 52(3), 44-56.

PCI. 1985. Fabrication and shipment cracks in precast or prestressed beams and columns, PCI Journal, 30(3), 2-27.

PCI. 2017. PCI design handbook, Precast/Prestressed Concrete Institute, Chicago, IL.

Petty, G. 2019. Assessment of live load distribution characteristics of press-brake-formed tub girder superstructures, MS Thesis, Marshall University, Huntington, WV.

Rabbat, B.G. and Russell, H.G. 1982. Optimized sections for precast prestressed bridge girders, PCI Journal, 27(4), 88-104.

Ralls, M.L., Ybanez, L., and Panak, J.J. 1993. The new Texas U-beam bridges: an aesthetic and economical design solution, PCI Journal, 38(5), 20-29.

Reese, G. and Neckas, W.N. 2010. Development of spliced precast U-beam bridge construction, Precast/Prestressed Concrete Institute, Chicago, IL.

Saindon, K.C. and McMullen, M.L. 2010. Curved precast prestressed concrete bridge girder systems, Structures Congress, 51-58.

Saini, H.S., Sayal, R., Govardhan, A., and Buyya, R. 2021. Innovations in computer science and engineering, Springer Nature, Singapore.

Salazar, J., Yousefpour, H., Katz, A., Abyaneh, R.A., Kim, H.S., Garber, D., Hrynyk, T., and Bayrak, O. 2017. Benefits of using 0.7 in. (18 mm) diameter strands in precast, pretensioned girders: a parametric investigation, PCI Journal, 62(6), 59-75.

Samaan, M., Sennah, K., and Kennedy, J. B. 2005. Distribution factors for curved continuous composite box-girder bridges, Journal of Bridge Engineering, 10(6), 678-692.

Sarles, D. and Itani, R.Y. 1984. Effect of end blocks on anchorage zone stresses in prestressed concrete girders, PCI Journal, 29(6), 100-114.

Shen, J. 2014. Concrete decks, Bridge Engineering handbook (second edition), 573-588.

Sun, C. 2004. High performance concrete bridge stringer system, PhD Dissertation, University of Nebraska, Lincoln, NE.

Tadros, M.K. and Baishya, M.C. 1998. Rapid replacement of bridge decks (NCHRP Report 407), Transportation Research Board, Washington, D.C.

Tadros, M.K., Badie, S.S., and Tuan, C.Y. 2010. Evaluation and repair procedures for precast/prestressed concrete girders with longitudinal cracking in the web (NCHRP Report 654), Transportation Research Board, Washington, D.C.

Tarhini, K.M. and Frederick, G.R., 1992. Wheel load distribution in I-girder highway bridges, Journal of Structural Engineering, 118(5), 1285-1294.

Theryo, T.S. 2014. Segmental concrete bridges, Bridge Engineering handbook (second edition), 91-170.

Tuan, C.Y., Yehia, S.A., Jongpitaksseel, N., and Tadros, M.K. 2004. End zone reinforcement for pretensioned concrete girders, PCI Journal, 49(3), 68-82.

TxDOT. 2006. Bridge division standard drawings: English prestressed concrete U-beam standards, Texas Department of Transportation, Austin, TX.

Wilensky, U. and Rand, W. 2015. An introduction to agent-based modeling, The MIT Press, Boston, MA.

Yoo, C.H., Kang, J., and Kim, K. 2015. Stresses due to distortion on horizontally curved tub-girders, Engineering Structures, 87, 70-85.

Yuan, A. 2019. Model derivation and validation of spalling-force calculations for prestressed concrete bridge girder ends based on a modified G-S model, Journal of Bridge Engineering, 24(3), 04018122.

Zhang, J., Hou, D., Zhao, J., Shen, S., and Horpibulsuk, S. 2020. Experimental evaluation of strut-and-tie model of anchorage zone in posttensioned concrete structures," Journal of Testing and Evaluation, 48(1), 390-408

Zokaie, T., Osterkamp, T.A., and Imbsen, R.A. 1991. Distribution of wheel loads on highway bridges, NCHRP Report 12-26, Transportation Research Board, Washington, D.C.

Zokaie, T. 2000. AASHTO-LRFD live load distribution specifications, Journal of Bridge Engineering, 5(2), 131-138.